SWIM – Sensing with Independent Micro-Swimmers

Ethan W. Schaler, Ph.D. (P.I.)
Azadeh Ansari, Ph.D.
Samuel Howell, Ph.D.
Hyeong Jae Lee, Ph.D.
Miles Smith, Ph.D.

with additional technical inputs from

Adarsh Rajguru
Luis Phillip Tosi, Ph.D.
Zhijian (Chris) Hao
Jea Du Kim

E.W. Schaler is with the Jet Propulsion Laboratory, California Institute of Technology, M/S 82-110, 4800 Oak Grove Drive, Pasadena, CA, USA, 91101
E-mail: ethan.w.schaler@jpl.nasa.gov
Website: https://www-robotics.jpl.nasa.gov/people/Ethan Schaler/
A. Ansari, Z. Hao, and J.D. Kim are with the Georgia Institute of Technology
S. Howell, H.J. Lee, M. Smith, A. Rajguru, and L. Tosi are with the Jet Propulsion Laboratory, California Institute of Technology

ABSTRACT

The next decades of space exploration will focus on Ocean Worlds – especially Enceladus, Europa, and Titan – whose liquid oceans beneath kilometers of icy crust are some of the most likely locations beyond Earth to harbor life. To access these aquatic environments, NASA is developing and maturing numerous ocean-access mission concepts, including the Scientific Exploration Subsurface Access Mechanism for Europa (SESAME) class of thermo-mechanical drilling robots. We propose developing SWIM – Sensing with Independent Micro-swimmers – to dramatically expand the capabilities of SESAME-class ocean-access robotic missions and significantly increase their likelihood of detecting evidence of habitability / biomarkers / life once they reach the ocean-ice interface.

The SWIM system consists of cm-scale, swimming micro-robots (micro-swimmers) equipped with MEMS sensors, propelled by miniature actuators, and wirelessly controlled with ultrasound waves. The micro-swimmers are deployed individually or as a swarm from a single SESAME robot mothercraft, which has limited mobility once reaching / anchoring at the ocean-ice interface. SWIM enables active sampling of ocean water beyond the reach of the SESAME robot (increasing the chances of detecting biomarkers), as well as temporally- and spatially-distributed measurement of desired ocean properties, habitability metrics, and potential biomarkers (infeasible with a single robot). Together these capabilities will enable scientists to better characterize / understand the alien ocean's composition and habitability on NASA's first ocean-access mission.

In this Phase 1 Report, we establish the fundamental feasibility of operating SWIM robots wirelessly at multi-meter distances from a robotic mothercraft through 2 Major Tasks:

Building a Science Traceability Matrix focused on focused on science goals for a NASA SESAME-class robotic mission at the ocean-ice interface.

Performing a Micro-Swimmer Design Trade Study to determine the appropriate robot designs / sizes to use available science instruments at the intended exploration ranges and under the expected sub-surface ocean conditions. It will focus on 4 key miniaturized subsystems: scientific instruments (MEMS sensors, spectrometers, cameras), actuators (ultrasound, piezo-electric, motors), communication (ultrasound), and power (batteries, energy harvesters).

ACKNOWLEDGEMENTS

The authors would like to thank the NASA Innovative Advanced Concepts (NIAC) program office for the opportunity to conduct this Phase I study, as well as the technical contributions from a number of Subject Matter Experts at JPL, NASA, Georgia Institute of Technology, and beyond. Specific thanks to Patrick McGarey (for guidance on tethers), John-Paul Jones (for guidance on batteries), and Jacob Izraelevitz (for guidance on underwater robot vehicle forms).

We are also extremely grateful for the positive public response / feedback to our work on SWIM, including when presenting at the 2021 NIAC Symposium and independent outreach / inquiries made to learn more about SWIM or share information about SWIM with a broader audience.

The research was carried out at the Jet Propulsion Laboratory, California Institute of Technology, under a contract with the National Aeronautics and Space Administration (80NM0018D0004).

CONTENTS

LIST OF FIGURES

LIST OF TABLES

1 INTRODUCTION

The discovery of subsurface liquid water beneath solid ice sheets on Europa, Enceladus, and Ceres has galvanized the search for extraterrestrial life and guided the latest Decadal Survey for Planetary Sciences / Astrobiology [1]–[4], the NASA Roadmap to Ocean Worlds [5], and ongoing mission development for Europa Clipper [6], Europa Lander, and SESAME [7]. The ultimate science goal is to penetrate these ice-sheets and explore the subsurface ocean: a single robot mothercraft would be able to evaluate large ocean volumes for habitability / biomarkers by deploying a swarm of micro-swimmers (10-1000 cm^3-scale robots with mm-scale components), equipped with MEMS sensors and remotely controlled via ultrasound (Fig. 1.1). MEMS sensors enable the swarm to collect simultaneous, distributed measurements of spatial / temporal variations in ocean properties (redox gradients, biogenic elements, salinity, density, etc.) at ocean-ice interfaces, in open water, and around theorized hydrothermal vents [5] – enabling scientists to better understand the alien ocean's composition and habitability. Overall, the envisioned micro-swimmer swarm enables untethered exploration and distributed in-situ measurements in a large ocean volume in order to significantly increase the likelihood of detecting evidence of habitability / life.

NASA / JPL are investigating multiple viable spacecraft technologies for subsurface ocean access on icy moons, including cryobots like PRIME (a radioisotope-powered penetrator probe) [8]–[11]. Access to the subsurface ocean by melting / boring through the ice is extremely challenging, and imposes significant size / shape constraints on the spacecraft: streamlined body, with small cross-sections and limited in-ocean mobility. The miniaturized design of our proposed swimming micro-robot enables ~50 robots, each 60-75 cm^3 in volume, to stow away on the larger robotic spacecraft, before being deployed to perform directed scouting / scientific measurements in locations inaccessible or hazardous to the larger robot. Recent advancements in microfabrication and additive manufacturing will aid in realizing micro-robot swarms for extraterrestrial exploration; however, robust sensing and autonomy, especially in hostile, unexplored environments, remain the largest hurdles to overcome.

1.1 SWIM Concept Overview

SWIM System Design – We propose building swimming micro-robots at ~100 cm^3 size-scale (see Fig. 1.1) that can be deployed individually or in swarms from a cryobot mothership to rapidly scout locations of interest for detailed analysis and / or perform scientifically-valuable measurements in locations the cryobot is unable to access. Operating under Europan ocean conditions imposes unique engineering / environmental / science mission requirements for SWIM robots – some of which are outlined in Table 3.2, and discussed in Section 3.2 – as well as significant planetary protection requirements that we are aware of

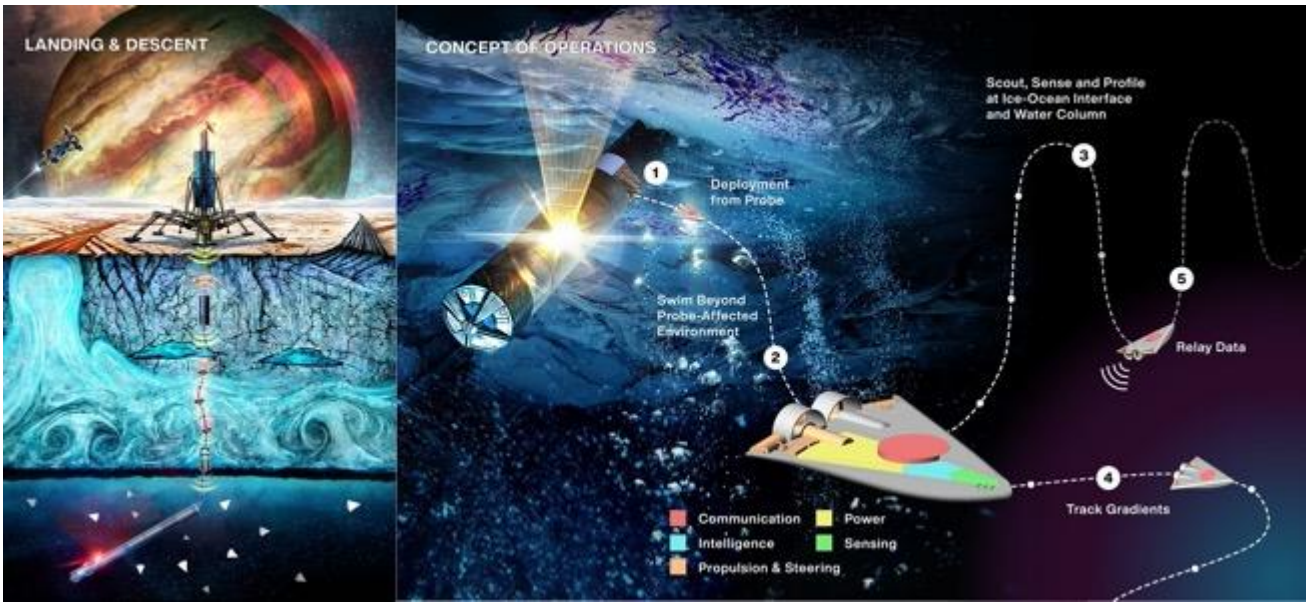

Fig. 1.1: SWIM concept of operations, including lander / ocean-access cryobot (left) and deployed micro-swimmers (right) with independent propulsion, sensing and two-way communication to the cryobot mothercraft.

but are not covered in Phase I. The individual micro-swimmers will share 5 key subsystems within a 3D-printable chassis. The subsystem design spaces are extremely broad, so a trade study in Phase I identified preferred technologies, and the majority of specific component selection will be left to future work:

Propulsion / Steering – ultrasound-powered fins / legs [12], electricity-powered fins (via PZT [13], solenoids [14], motors [15], etc.), or motor-powered propellers

Sensing – MEMS redox [16], dissolved oxygen [16], pH [16], pressure [17], temperature [18], [19], conductivity / salinity [20], and IMU [19] sensors have ∼4 mm^2 form-factors, while miniature multi-spectral cameras and mass spectrometers are in development [21]–[23]

Communication – wireless ultrasound [24], optical, or RF [25]; cryobot uses active transmission / micro-swimmers use passive (backscattering), active, or a mesh network

Power – onboard energy storage (battery / capacitor), energy harvesting (e.g. via wireless ultrasound / PZT [24], [26]), or a hybrid system with energy storage / wireless recharging

Compute – sliding scale from analog-only circuitry (directly coupling sensors / actuators to comms. for fully remotecontrolled micro-swimmers), to radiation-tolerant micro-controllers [27], to a radiation-hardened FPGA / CPU.

Individual robots are designed to operate for ∼2 hours, and use staggered deployments to collect data at multiple times over a diurnal cycle. A Tether is also viable on larger-scale micro-swimmers, and was explored in Phase I. Tethers can offer advantages – sourcing (abundant) cryobot power, providing reliable 2-way comms., and providing a mechanical link to retain robots in unexpectedly high ocean currents – but also present challenges (e.g. entanglement risks) for multi-robot operations. Since the ideal micro-swimmer size / quantity was not immediately obvious, we compared the science and mobility capabilities of designs ranging from thousands of ∼1 cm-scale robots to scores of ∼100 cm^3-scale robots to five or fewer 1000 cm^3-scale robots. Science requirements also refined our focus to platforms that provide Exploration Ranges of 5-100 meters beyond the mothercraft, and Operational Durations that let us collect data multiple times across the 85 hr diurnal cycle.

SWIM Innovation – The goal of SWIM is to demonstrate autonomous, untethered, swimming micro-robots that are 1-3 orders of magnitude smaller than conventional scientific ROVs / AUVs, while maintaining sufficient instrument / mobility / communication capabilities to operate in Europan ocean conditions and collect scientifically-valuable data.

Similar to NASA's success with miniature satellites (MarCO cubesats), rovers (PUFFER [28]), and helicopters (Ingenuity [29]), miniaturization allows SWIM to carry scores of robots within a limited payload volume. This in turn enables new science missions where simple robot swarms (operating in large numbers but reduced individual capability) conduct simultaneous, distributed scientific measurements over a large ocean volume. Such behavior increases scientifically-valuable measurements of ocean habitability and the likelihood of finding extant biomarkers, but is unachievable (or substantially slower) if performed by a single, conventional robot.

SWIM will achieve these capabilities by combining state-of-the-art technologies to produce rugged swimming robots that (1) use reliable actuation, control, and communication mechanisms, (2) use the latest advances in MEMS sensor development and integration, and (3) provide mission risk-reduction through massive robot redundancy and very low unit cost.

1.2 SWIM Mission Context

The coming decades of planetary science and astrobiology will turn to Ocean Worlds – Europa, Enceladus, and Titan – whose liquid oceans beneath kilometers of icy crust contain environments thought to be the most likely locations beyond Earth to harbor life within our Solar System [2]:

1) **Ice / Ocean Interfaces –** the boundary at which surface nutrients meet a starved ocean
2) **Open Water –** mapping temperature and salinity to aid in understanding ice-ocean exchange
3) **Ocean Floor –** water-rock interactions may provide the chemical energy for life

The NASA Roadmap to Ocean Worlds [5] recommends first characterizing oceans (e.g. salinity, density, composition, currents), then assessing each environment for habitability (e.g. temporal / spatial variation of energy sources, redox gradients, and biogenic / organic compounds), and finally exploring for signs of life (e.g. niches of habitability, biomarkers).

To this end, NASA / JPL are developing and maturing numerous ocean-access mission concepts, including the Scientific Exploration Subsurface Access Mechanism for Europa (SESAME) [7] class of thermo-mechanical drilling robots, whose stated goal is to:

> "Identify ice penetration systems capable of facilitating the detection of evidence of life by providing access to liquid water located 100s of meters to 10s of kilometers below the surface of the ice." [7]

NASA JPL is developing the Probe Using Radioisotopes for Icy Moons Exploration (PRIME) cryobot concept (Fig. 1.2) [8]–[11]. PRIME is a streamlined robot (~3.5 m long, ~23-25 cm diameter with a ~28-40 L scientific payload volume) capable of penetrating thick planetary ice shells via "passive melting using a multi-kilowatt heat source; active melting using water jetting; and heated mechanical cutting and drilling," before anchoring at the ice-ocean interface and partially emerging into the sub-surface ocean [11]. Cryobot mass and volume constraints prohibit the implementation of an in-water mobility system, so PRIME's onboard science instruments are limited to analyzing melt water (during descent) and ocean water (once anchored) that flows past the vehicle. SWIM provides a path to mobility of key instrument payloads within the PRIME architecture and concept of operations, which extends the cryobot mission capabilities while leveraging the results of PRIME's multi-program, multi-year concept (see Table 3.2).

The primary tethered communications channel provides up to 1 kbps baseline data rates for science, and a redundant freespace RF and acoustic communications system can maintain a threshold data rate of 100 bps. The system is electrically rich due to an overabundance of thermal power used for melting, and considers a 10 orbit (~30 Earth day) ocean mission, limited by transmitted data volume. The cryobot is capable of onboard science and GNC autonomy.

Cryobot missions using a Radioisotope Power System (RPS) must also contend with ~10 kW of continuously-generated thermal power. RPSs are critical for descending through the ice, but cannot be safely ejected or disabled once the cryobot reaches the ocean. Pressures of 25-50 MPa at the ice-ocean interface prevent water from boiling, so heat transfer from the cryobot into the ocean is dominated by convection / advection and likely results in a large bubble of heated water forming around / above /

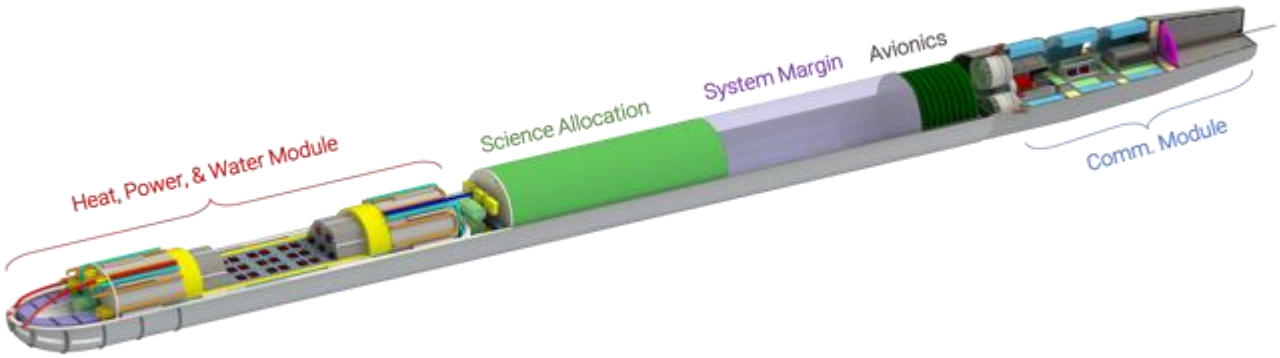

Fig. 1.2: PRIME Cryobot Concept Cut-Away, showing various subsystems within the ~3.5 m long, ~25 cm diameter robot. SWIM would be installed / deployed from the "Science Allocation" section of the robot. Used with author permission from [30].

downstream of the cryobot, potentially eroding or altering the regions of interest.

Given these limitations, we view SWIM's micro-swimmers as a critical enabling technology to dramatically expand the capabilities of SESAME-class ocean-access robotic missions:

- SWIM increases the accessible / explorable volume around a cryobot at the ice-ocean interface
- SWIM enables active sampling of ocean water beyond the reach of the cryobot, increasing the chances of detecting biomarkers (successful mission / unparalleled scientific result)
- SWIM enables temporally- and spatially-distributed measurement of desired ocean properties, habitability metrics, and potential biomarkers (infeasible with a single robot)

Existing underwater vehicles (see Section 2.1 and 2.2) do not meet the requirements imposed on a SESAME-class mission. SWIM micro-robots, however, can meet Size / Weight / Performance / Cost (SWaP-C) limitations of a SESAME-class mission while offering mission risk reduction through sensor and robot redundancy. Micro-swimmers can be designed with simple, untethered, solid-state hardware (to better survive cruise / drill phases) and monolithic construction (to ensure planetary protection). SWIM's redundancy also enables individual swimmers to be used as disposable probes if unexpectedly highvelocity currents are encountered. In these roles, SWIM can dramatically improve the PRIME mission feasibility – and decrease risks to critical mission hardware – by reducing cryobot mobility as a constraint on successful ocean exploration.

1.2.1 SWIM Use in Other Ocean-Access Missions

SWIM is widely applicable to any ocean-access mission, including crawling down existing plume vents (Exo-bot Extant Life Surveyor (EELS) [11], [31], [32] and Enceladus Vent Explorer (EVE) [33]). In each case, SWIM can provide distributed sensing in an expanded volume around the mothercraft, while harnessing existing communication systems and meeting mission size / weight / geometry constraints.

1.3 Phase I Key Findings

Our Phase I work advanced the SWIM concept in 3 key ways: developing a Science Traceability Matrix to identify scientific priorities for SWIM robots, performing a System Trade Study to identify preferred robot designs, and developing a Swimming Robot Swarm Simulation to explore design trade-offs.

Science Traceability Matrix (STM) – We have developed 3 science objectives (SO): (1) search for and characterize life, (2) characterize chemical environments / processes, and (3) characterize physical environments / processes at Europa's ice-ocean interface. These goals are divided into 13 science investigations (SI), informed by the science priorities of NASA programmatic bodies, including OPAG [34] and NOW [35]. While a cryobot mission provides access to the ice-ocean interface, fulfillment of the SIs – which require simple observations on long temporal and/or spatial baselines – is uniquely enabled or enhanced by mobile, swimming micro-robots. Swimmers can explore pristine ice / ocean inaccessible by the cryobot, collect water column profiles, and track signal gradients to their source. Our SIs are further categorized into investigations that small (~1-10 cm^3), medium (~100 cm^3), and large (~1000 cm^3) robots can achieve, based on relevant instrument sizes.

Our science team also defined environmental, integration, deployment, operational, and science requirements for SWIM, which are detailed in later sections. Critically, we also developed a thermal model to understand the impact of a cryobot (assuming ~8kW thermal from MMRTGs) on the surrounding environment, and found that a minimum exploration range of >1-10 meters (depending on ocean velocity) is needed to achieve sampling beyond the cryobot's thermal bubble.

System Trade Study – We conducted a comprehensive trade study and design workshop to explore multiple concepts for deployable SWIM robots. Our preferred Phase I design is the "Delta-Wing" robot concept illustrated in Fig. 1.1, and key findings for each sub-system trade are below:

Structure – Delta-wing and cylindrical forms are viable, but cryobot packing / deployment and internal component layout favors delta-wing. All components can be pressure-rated.

Sensing – Ocean composition suite is baselined, multispectral camera is viable with Mbps comms. Future work will explore MEMS sensors tuned to unique biomarker / chemical signals.

Communication – Ultrasound is baselined for ~10 kbps data rates / >100s meter range / <1 W power, but optical (wireless) and tether are viable at similar range and ~Mbps data rates.

Propulsion – Flooded, brushless motor is preferred; other actuators generate insufficient thrust.

Power – Primary battery (e.g. Li-CFx) is preferred, but rechargeable battery or tether is viable.

Simulation – We also developed a 3D swimming robot swarm simulation (Fig. 5.1) to investigate design trade-offs (e.g. number of deployed robots, exploration time, measurement uncertainty) and compare implementations of different swarm algorithms for underwater exploration.

2 BACKGROUND

The next set of steps of space exploration will focus on characterizing Ocean Worlds to assess each environment for habitability and search for signs of life. In order to explore the ocean beyond a cryobot while being highly limited in volume / size / weight, we propose using miniature swimming robots with integrated sensors.

The subsequent sections survey the current state-of-the-art capabilities in commercial / oceanographic underwater robots (Sec. 2.1), research-grade robots (Sec. 2.2), and sensors / instruments that measure ocean properties of scientific interest (Sec. 2.3). We also attempt to include most forms of underwater mobility systems for robots, ranging from traditional electric thrusters (motors / propellers) to more novel techniques like fins actuated by piezoelectric composites. A selection of these robots are illustrated in Fig. 2.1.

2.1 Oceanographic Robots

Commercial oceanographic robots have 3 primary designs – torpedoes, gliders, hoverers – that enable them optimally meet different mission categories:

Torpedoes – Long, streamlined bodies with circular cross-sections. Thrust is provided by a tail-mounted propeller (possibly with a pair of counter-rotating blades), and steering is provided by multiple (small) fins.

- This form-factor provides a good compromise between size, usable volume, drag / hydrodynamic efficiency, and ease of handling.
- Some vehicles use modular compartments to swap out sensor payloads.

Gliders – Long, streamlined bodies with circular cross-sections. Thrust is provided by the combination of an internal variable buoyancy engine (causing the glider to cyclically rise / fall in the water column) with hydrofoils that generate lift / thrust.

- This form-factor provides excellent endurance / power efficiency and low drag, at the cost of ease of handling.
- Vehicles can operate for weeks to months and cover thousands of km range.

Hoverers – Tall, wide, or boxy vehicles with typically rectangular cross-sections and limited streamlining. Thrust and steering is provided by a series of thrusters mounted in different directions across the vehicle body, allowing for vertical / horizontal translating motion and turning in place.

- This form-factor enables improved station-keeping, roll / pitch stability, and vertical motion (ideal for inspection / sampling tasks) at the cost of reduced hydrodynamic efficiency.
- Some robots exchange a rectangular body for two torpedo-shaped hulls aligned horizontally in the water and stacked vertically on top of each other for greater streamlining while maintaining roll / pitch stability.

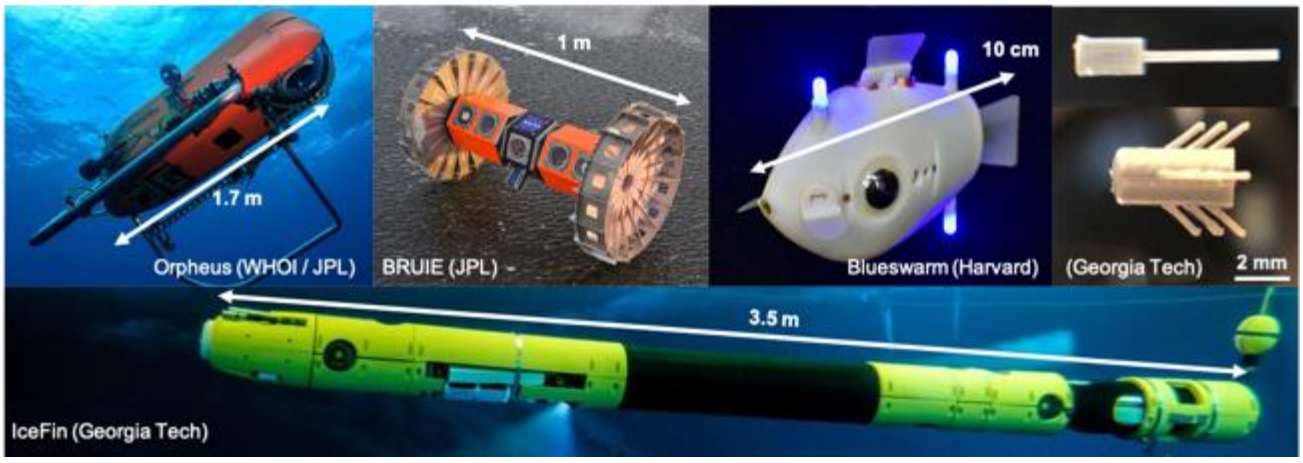

Fig. 2.1: Commercial- and Research-Grade AUVs, including Orpheus [36], BRUIE [11], [37], Blueswarm [38], [39], and IceFin [40].

For simplicity these three roles can be analogized to three types of aircraft – torpedoes have airplane-like behavior, gliders have glider-like behavior, and hoverers have helicopter-like behavior.

These underwater robots are also typically classified into **autonomous underwater vehicles (AUVs)** that are untethered and fully-autonomous**, remotely operated vehicles (ROVs)** that are tethered and operated by a human operator on a nearby ship, and **hybrid AUV/ROVs** that can operate in both modes (and may use a small optical fiber tether to relay video back to a science team during operation). A comparison of numerous commercial / oceanographic robots is provided in Table 2.1.

Woods Hole Oceanographic Institute – often in collaboration with institutions like NASA JPL and Northeastern University – designs, builds, and operates a wide variety of autonomous underwater vehicles (AUVs) and remotely operated vehicles (ROVs),

Table 2.1: Comparison of Oceanographic Robots.

Name (Operator)	**Design**	**Dimensions** (m)	**Mass** (kg)	**Speed** (m/s)	**Depth** (km) **Range** (km)	**Tether**
Slocum Glider [41], [42] (WHOI)	Glider	1.5 x ⊘ 0.22 m	60 kg	0.35 m/s	1 km 16.5k km	N
Spray Glider [43] (WHOI)	Glider	2 x ⊘ 0.2 m	52 kg	0.25 m/s	1 km 3.3k km	N
Liberdale Gliders [44] (ONR)	Glider	6.1 m	635 kg	1.5 m/s	0.3 km 1.5k km	N
Remus 100 [45], [46] (WHOI)	Torpedo	1.6 x ⊘ 0.19 m	37 kg	2.6 m/s	0.1 km 120 km	N
Bluefin-9 [47] (General Dynamics)	Torpedo	2.4 x ⊘ 0.24 m	70 kg	3.1 m/s	0.2 km 12 km	N
SwarmDiver [48] (Aquabotix)	Torpedo	0.75 x ⊘ 0.06 m	1.7 kg	2.2 m/s	0.05 km 7 km	N
IceFin [40] (GeorgiaTech)	Torpedo / Hovering	3.5 x ⊘ 0.23 m	130 kg	–	1 km 3.5 km	Y / N
SeaBED Jaguar [49] (WHOI / Northeastern U.)	Torpedo / Hovering	2 x 1.5 m	250	0.35 m/s	6 km 30 km	Y
Sentry [50] (WHOI)	Hovering	2.9 x 2.2 x 1.8 m	1,250 kg	1 m/s	6 km 70 km	N
Mesobot [51] (WHOI)	Hovering	1.5 x 1.5 x 1 m	250 kg	–	1 km	N
Mesobot [51] (WHOI)	Hovering	1.5 x 1.5 x 1 m	250 kg	–	1 km	N
Nereid Under Ice [52] (WHOI)	Hovering	–	2200 kg	1 m/s	5 km 10-40 km	Y / N
Orpheus [36] (WHOI / JPL)	Hovering	1.7 x 1.0 x 1.3 m	250 kg	–	11 km	N
Bluefin HAUV [53] (General Dynamics)	Hovering	1.33 x 0.9 x 0.4 m	72.6 kg	0.75 m/s	0.06 km	Y
BRUIE [11], [37] (JPL)	Wheeled	1 x ⊘ 0.5 m	–	–	–	Y

including: torpedo-type Remus 100 / 600 / 3000 / 6000 [45], [46], [54]–[56], hovering-type Orpheus (in collaboration with JPL) [36], [57], hovering-type Sentry [50], Mesobot [51], hybrid torpedo-/hovering-type SeaBED Puma & Jaguar [49], Slocum & Spray gliders [41]–[43], and a hovering-type Nereid Under Ice [52].

Orpheus [36], [57] is an untethered, hovering-type autonomous underwater vehicle designed for ultra-deep ocean exploration and has recently had successful field tests.

The Slocum / Spray gliders [41]–[43], are untethered, winged, low-power autonomous underwater vehicles ideal for longduration ocean sampling missions that have had successful missions all around the world. The Liberdale class gliders (XRay and ZRay, developed by the Office of Naval Research, ONR) [44] consist of a delta-wing bodies with a 6 m wingspan (and 635 kg mass) that is able to achieve ultra-high lift-to-drag ratios of 20-35:1 for long-term (6 month), long range (1500 km) missions.

Commercial oceanographic AUVs include the torpedo-type Bluefin-9 / 12 / 21 [47] and hovering-type Bluefin HAUV [53] by General Dynamics, and the comparatively miniature torpedo-type SwarmDiver [48] by Aquabotix, which are designed for high-agility swarm behaviors.

Research oceanographic AUVs are also manufactured at universities, including the IceFin by GeorgiaTech [40]. IceFin is a tethered, streamlined, torpedo-type autonomous underwater vehicle that contains additional thrusters for hovering behaviors and payload pods for numerous oceanographic science instruments. It has had successful science missions in Antarctica.

NASA JPL also developed BRUIE [11], [37], a 1 meter wide, 2-wheeled, positively buoyant, tethered robot designed to drive along the underside of ocean ice. BRUIE has had successful field tests exploring / characterizing the ocean-ice interfaces in the Arctic / Antarctic ocean.

A comparison of these robots is provided in Table 2.1. In general, all commercial oceanographic AUVs / ROVs are at least 1 order of magnitude too larger to fit within the SWIM mission concept – or within the payload volume of any SESAMEclass cryobot. On Earth, these robots are typically deployed from large research vessels and thus do not have the same size constraints as experienced in an ocean-access mission on an Ocean World. Their design and performance is instead optimized for endurance, ease / cost of manufacturing, and use of COTS components.

We must therefore examine research-grade robots that explore novel technologies for robot actuation / mobility, including those that leverage bio-inspiration and miniaturization, to identify concepts that are more viable for SWIM.

2.2 Research Robots

We have chosen to categorize the research-grade robots into four general groups, based on physical robot volume: true microrobots (<1s cm^3), small robots (~10s cm^3), medium robots (~100s cm^3), and large robots (~1000s+ cm^3). Research-grade robots often take advantage of novel / unique actuators or exhibit bio-inspired mobility techniques based on small, swimming animals, which may be of use for the SWIM micro-swimmers.

2.2.1 Micro- / Small-Scale Robots

Micro-scale swimming robots are typically monolithic (solid-state) bodies able to be manufactured with 3D printing or micro-machining techniques. These robots typically do not contain an internal power source, and are instead actuated externally through the use of magnetic and / or acoustic fields, which can be transmitted through the liquid medium. One such method is to generate a dynamic magnetic field (using electromagnets) to induce a rotational motion on a magnetized micro-swimmer. Another method is to generate acoustic vibrations in the liquid (using piezoelectric transducers), to induce resonant oscillations the micro-swimmer's fins or internal cavity. A research group developed a 3D-steerable micro-swimmer approximately 7.5 μm long (Fig. 2.2) for single particle manipulation, using a combination of both methods [58]. The fabricated microbot resembles half of an open pill, composed of polymer and Ni layers between two Au layers. Inside the pill cavity is an air bubble that reacts to the induced acoustic field and generates a propulsion force.

A compliant jellyfish robots [59] was also demonstrated at the mm-scale, and uses external magnetic actuation to induce a pulsating water-jet for of locomotion.

At these scales, the swimmers can only travel at low absolute velocities and short distances from the external actuation sources, and can only interact with microscopic particles.

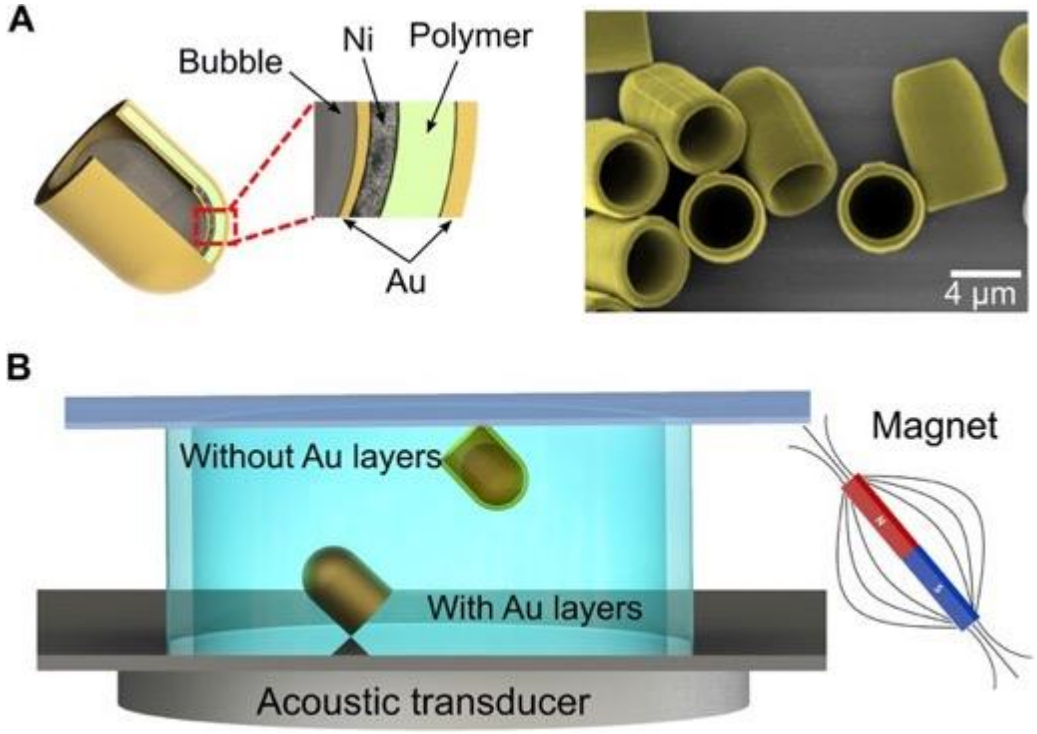

Fig. 2.2: Magnetic/non-magnetic layers that make up the micro bubble swimmer, and how its movements are controlled by both acoustic and magnetic forces [58].

When the robot size increases to the mm- to cm-scale, the individual robots still do not operate on internal power supplies (and remain reliant on external sources of energy for electricity / actuation), but they can harvest sufficient power from these external acoustic or electromagnetic sources to operate sensors and perform 2-way communication. At UC Berkeley, there is research on an implantable, ultrasound-powered nerve stimulator called StimDust [60]. This wireless system uses an external ultrasound source to excite vibrations in a small piezo-electric crystal (vibrating the crystal creates internal mechanical stress that generates an electric potential across the piezoelectric material), which provides power and communications to the implanted device. The StimDust is small enough to wrap around a sciatic nerve, but big enough to contain integrated circuits (IC) that:
(1) apply a stimulating electrical shock to the nerve, (2) contain voltage / capacitive sensing to measure the nerve response, and (3) a circuit to modulate the resonant frequency of the piezo-crystal as a method to report sensor reading back to the external ultrasound controller using ultrasound backscattering. A small, untethered swimming robot could potentially be powered and communicate using this same technique.

2.2.2 Medium- / Large-Scale Robots

Medium-scale robots, at the ~100 cm^3 volume scale, begin to focus more on bio-inspired robots and to implement novel forms of actuation. Large-scale robots, at the ~1000 cm^3 / 1+ L volume scale, continue to explore (larger) bio-inspired robots – often with more sophisticated control strategies – and implement additional forms of actuation. Actuator technologies that span these two size scales include pneumatic actuators [59], [61]–[63], magnet-in-coil (MIC) / solenoid actuators [38], [39], piezoelectric actuators [64], dielectric-elastomer actuators (DEA) [65], [66], and electric motors / servomotors driving fins, tails, and propellers [15], [67].

In one bio-inspired fish robot (Fig. 2.3), the tail fin is made from a macro-fiber composite (MFC) piezoelectric actuator that bends when a voltage is applied [64]. As described above (with the StimDust), piezoelectric materials accumulate electric charge in response to externally-applied mechanical stress, and also generate mechanical motion if an external voltage is applied. Thus, by applying an alternating positive / negative voltage, the MFC tail fin bends back and forth to generate a propulsion force.

The benefits of using a piezoelectric actuator, like an MFC fin, is that it is solid state (no sliding / rotating components to wear

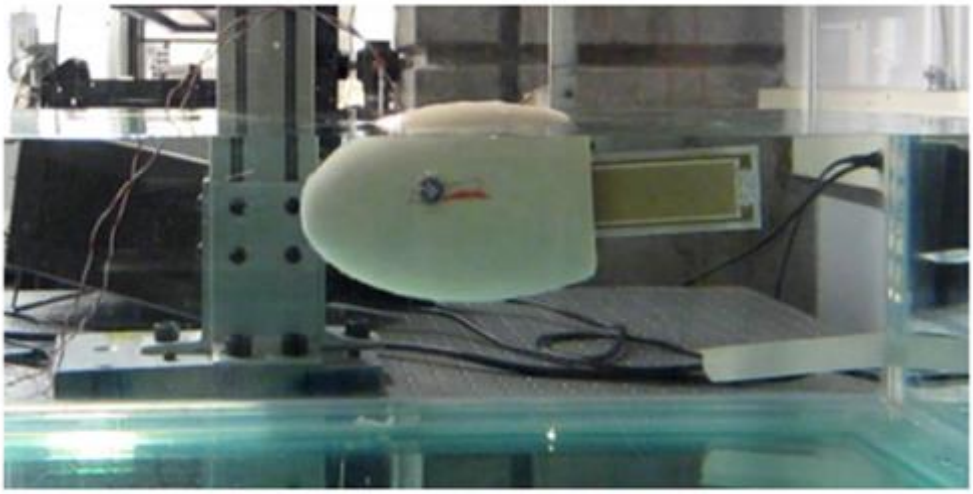

Fig. 2.3: Example of a 3D printed fish robot that utilizes a MFC piezoelectric fin for propulsion [64].

out), can generate high forces in small form-factors, can operate at high frequencies, and can operate more quietly than motors with propellers. The downsides of piezoelectric actuators is that they require extremely high voltage levels to function (often 100-1500 V, which poses a shorting risk), and typically have small stroke-lengths. These voltage constraints have necessitated that many piezo-actuated swimming robots be tethered for testing, but this challenge can be overcome by integrating high voltage amplifier into the robot.

Magnet-In-Coil (MIC) and solenoid actuators are an alternative actuator technology for medium-scale robots, and both consist of a permanent magnet placed within an electromagnetic wire coil. For MIC actuators (see Fig. 2.4), the magnet dipole is initially aligned perpendicular to the direction of the electric field generated by the coil (i.e. the axis of the coil), and when the coil is energized, the magnet will rotate to align with the electric field. By attaching the magnet to a hinged, spring-loaded fin and powering an oscillating current through the coil (to generate an alternating electric field), the magnet can be used to drive / generate a flapping fin motion [38], [39]. Solenoid actuators employ a similar electro-mechanical behavior, but align the magnet dipole axis along the axis of the wire coil so that the magnet translates up / down the length of the coil under an alternating current (and can also be used to drive a fin / flap).

This form of fin actuation was used in the BlueBots robotic research platform for controlling swarms of fish robots 2.4. The MIC actuators were selected to drive both tail (thrust) and fin (steering) actuators on the BlueBots for three main reasons: (1) the MIC actuators are exceptionally simple, robust actuators, (2) they can be easily miniaturized and have easily customizeable geometries, which permits easy integration into the BlueBots, (3) they are exceptionally easy to waterproof (the coil remains inside the sealed body, while the magnet and fin is attached outside in the water). Additionally, the MIC fins can be scaled up or down based on the size and strength of the magnet used and its appropriate coil, which could be used to design small and simple swimming robots with integrated actuation.

Dielectric elastomer actuators (DEA) offer a more compliant actuator alternative to piezoelectric actuators. Dielectric elastomers are a type of electroactive polymers (EAP) and transform electric energy to large strains / mechanical motion, and EAPs exhibit a significantly larger deformations compared to that of piezoelectric materials. Since DEAs tend to be lightweight and have a high elastic energy density, they are often employed as muscle-analogs in bio-inspired robots.

For example, a small-scale eel larva robot is made of entirely of DEAs [65]. The body is separated into three sections that alternate switching on and off, which gives it an Anguilliform motion. Another team used DEAs to actuate fins on a Snailfish robot (see Fig. 2.5) [66]: the bending motion of the DEAs generate a flapping motion for the two wing fins of the Snailfish robot.

Common DEA designs place a sheet of insulating elastomer between two compliant electrode films – although the specific actuator materials are an area of significant research. The elastomers require low stiffness, high dielectric constant, and high

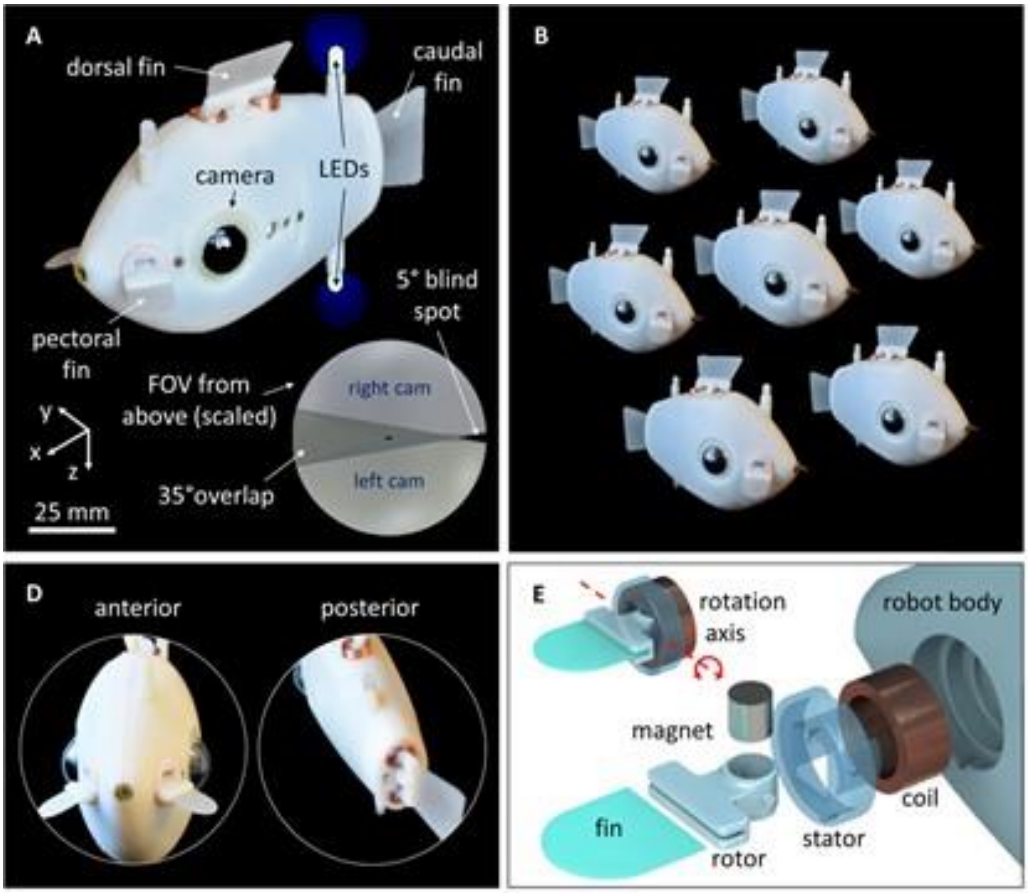

Fig. 2.4: BlueBots use a simple, robust form of actuation, Magnet-in-Coil fins, which enable packaging of electronics within the robot body for waterproofing while leaving the moving components outside the robot body in water [39].

electrical breakdown strength, while the electrodes can employ metal films, liquid metals, and conductive hydrogels. Some DEAs can even use surrounding ocean water as one of the electrodes, to simplify actuator design.

Pneumatic actuators offer an alternative soft-actuator technology to DEAs, and operate by adding and removing a fluid (air, water, etc.) from chambers within a compliant body to generate bending, extension, contraction and compound motions. One research team used a bending-type pneumatic actuator to mimic the swimming motions of a manta's wing fins (Fig. 2.6) [61]. Another research group used a pneumatic pump to actuate a piston and spring to mimic the pulsating motion of a squid [62]: the spring is connected to the ribs of a silicone web, and when the spring cyclically stretches / retracts, the silicone webbing opens to draw in water / closes to expel the water in a pulse (e.g. a water jet), which propels the squid robot in the opposite direction. This locomotion technique is also seen in an octopus [63], where an octopus intakes a large volume of water and releases it to propel itself at a speed of approximately five body lengths per second, and in jellyfish robots [59] (although these jellfish robots are actuated magnetically, as mentioned above).

The most widely used form of actuation in underwater robots is electric motors (including servomotors), used to drive propellers, fins, and more. Motors can be manufactured in a variety of sizes and form-factors, generate high torque, and generate efficient thrust at reasonable voltages. Motors do, however, have moving components susceptible to wear / fouling, and present greater waterproofing challenges if operated at depth.

To make an omni-directional, motor-powered underwater robots more compact, one researcher developed a variable-pitch propeller system for their robot (Fig. 2.7) [67]. Each propeller consists of a motor that drives it and a servo to control the pitch of the propeller. By using the combination of the various pitch angles of three propellers on the robot, the robot can make controlled movements in any direction.

Other researchers have explored using motors and servos to mimic efficient locomotion techniques of various underwater

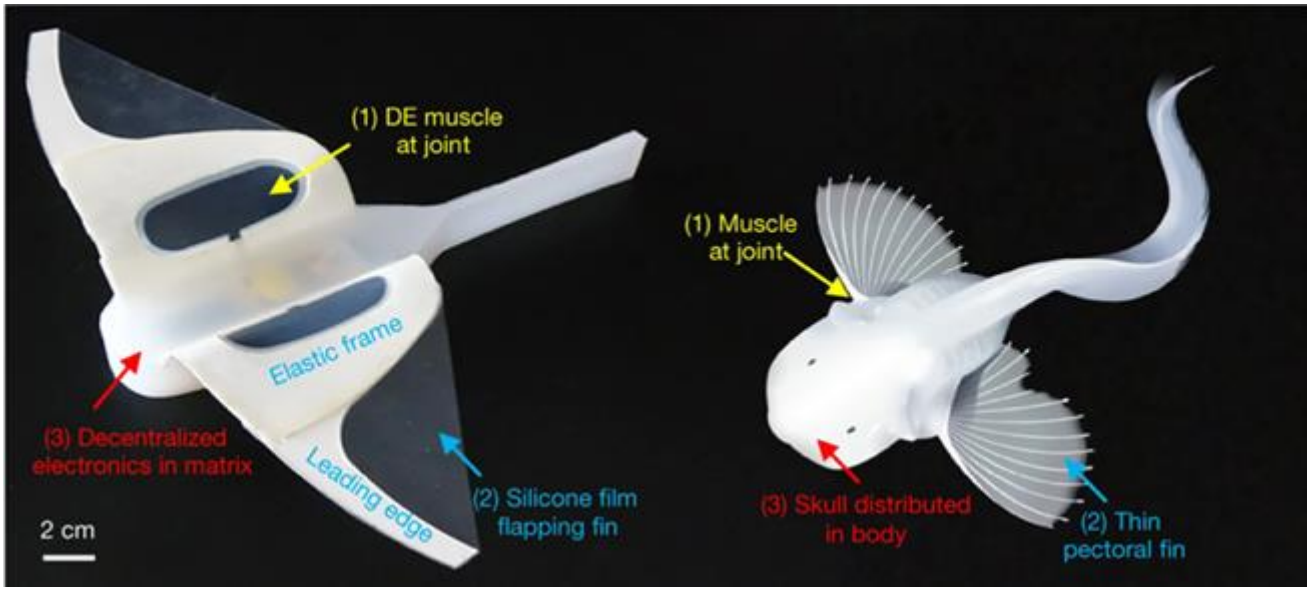

Fig. 2.5: The Snailfish robot utilizes dielectric elastomer actuators for mobility in conductive bodies of water [66].

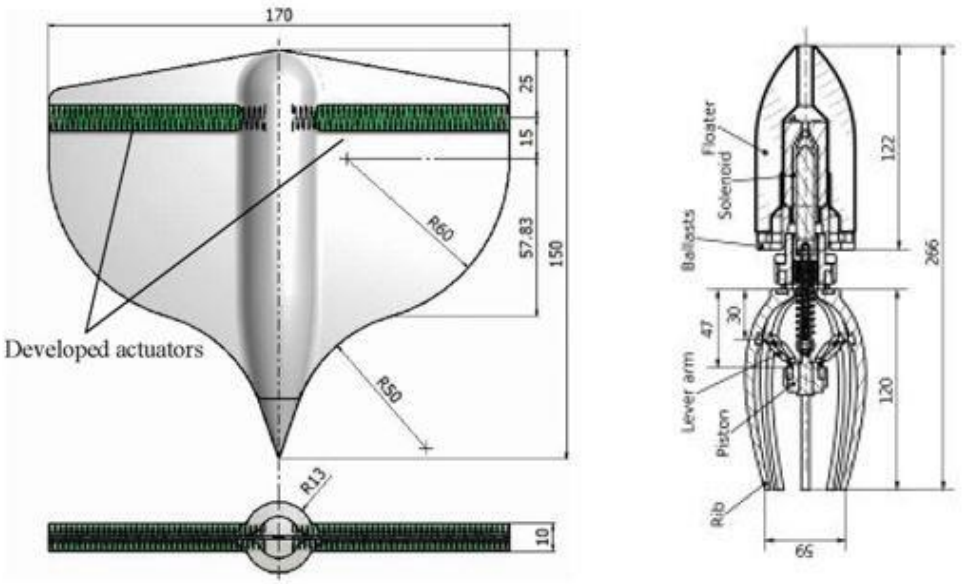

Fig. 2.6: Manta robot (left) with pneumatic-powered flapping fins [61], and squid robot (right) with pneumatic-powered piston / pump for resonant swimming motion [62].

animals. For example, Tunabot [15], a bio-inspired fish robot with a flexible 3D-printed body, uses an electric motor and kinematic linkage to flex a soft / flexible tail and demonstrated tethered, fin-based swimming in a tank with a maximum speed of ~1 m/s (4 body lengths per second) and cost of transport of 4-9 J/m (depending on speed). Almost the entirety of this robot is devoted to the actuation and transmission, leaving limited space for other subsystems (e.g. power, sensing, communication), but it does demonstrate fast swimming with fins.

Additionally, a robotic eel consisting of multiple servos and elastic joints can mimic anguilliform swimming, which allows it to travel through narrow spaces [68]. Anguilliform swimming also permits acceleration / deceleration comparable to what can be achieved with propellers. Other mimicry tends to be of fish-type or squid- / octopus- / jellyfish-type locomotion. The fish type of locomotion tends to have a faster swimming speeds and higher efficiency. The squid- / octopus-type of swimming is likely used to perform quick bursts of motion and slow but efficient swimming. One researcher implemented both forms of movement in the

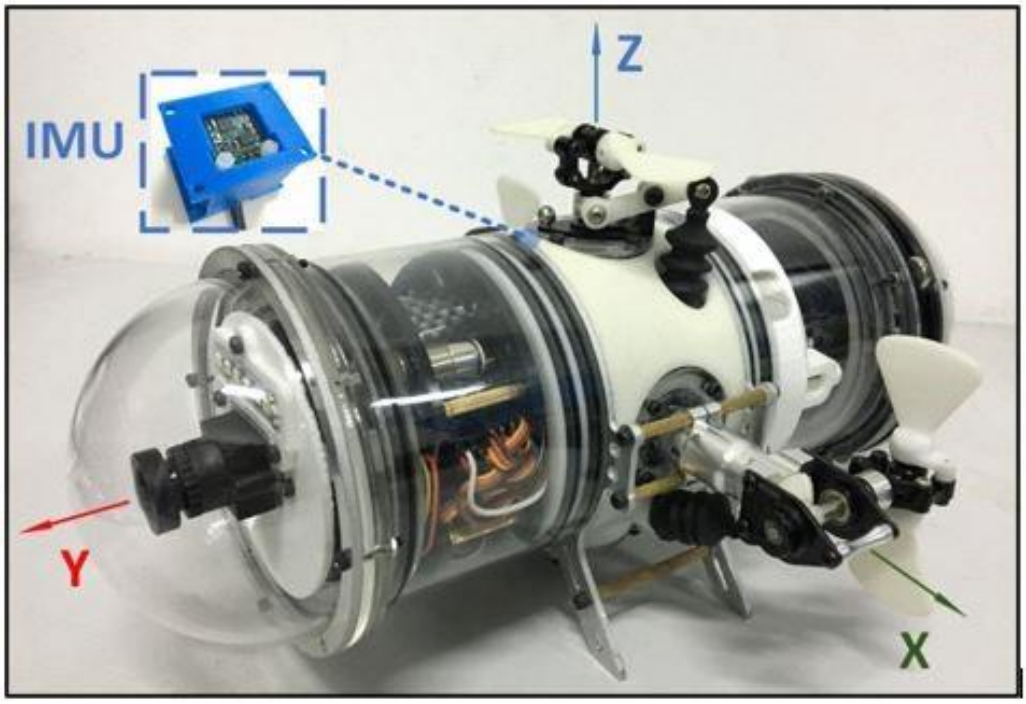

Fig. 2.7: By using an adjustable angled propellers and a complex gear box, this robot can move in any direction, while reducing the overall size of the robot [67].

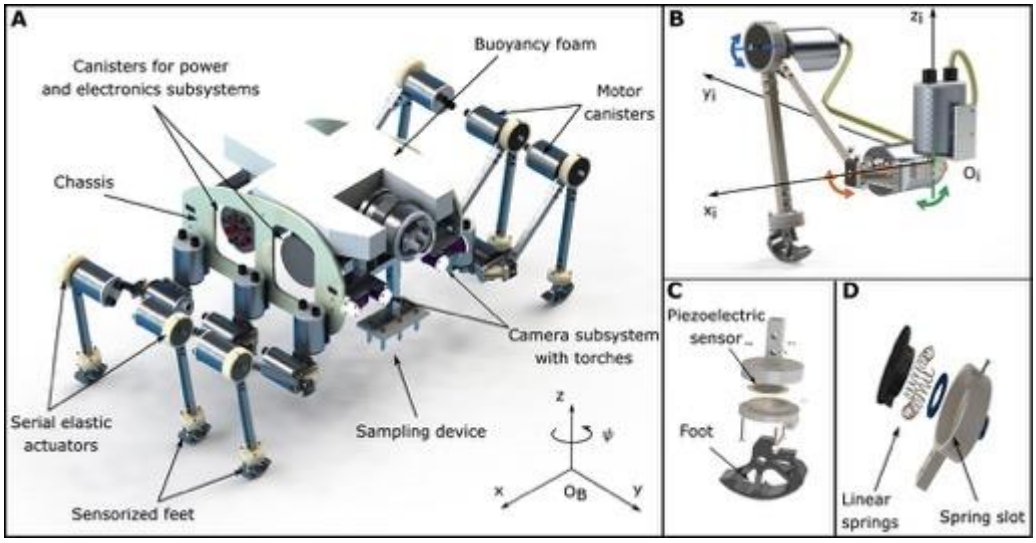

Fig. 2.8: A more complex legged robot designed to explore the sea-floor in regions with shallow water [70].

"Adaptive Fish" robot, which can switch between these two forms of swimming through the use of servos [69].

Finally, another team designed a crab-like robot with motorized legs (Fig 2.8), for shallow water exploration via walking and hopping [70].

2.2.3 Key Takeaways

Biologists have observed that in nature, fish length is a dominant, positive factor affecting the absolute or critical swimming speed of fish (in meters per second) – i.e. larger fish swim faster – while fish exhibit the opposite relationship for relative swimming speed (in body-lengths per second) – i.e. smaller fish have faster relative speed than larger fish [71]–[73]. Additionally, other factors correlated with fish length, such as hydrodynamic drag and fin size, have also been shown to impact absolute swimming speed. Tail beat frequency (i.e. frequency of tail oscillations) also correlates positively with swimming speed, however each fish

Table 2.2: Comparison of Research Robots, ordered from small to large.

Robot (Size-Scale)	**Dimensions** (cm) **Volume** (cm^3 / L)	**Mass** (kg)	**Actuation Technology**	**Power Source**	**Thrust**	**Speed**
Single-Particle Manipulators (Micro)	7.5 x 5 x 5 μm 188 μm^3	–	Magnetic / Acoustic Vibrations	External	–	2.6 mm/s (347 BL/s)
DEA Eel (Medium)	22 x 5 x 1.5 cm 165 cm^3	–	DEA Segments	Thether (20 mW)	42 $\pm$ 7 μN	1.9 mm/s (0.008 BL/s)
Pneumatic Manta (Medium)	17 x 15 x 1 cm 255 cm^3	–	Pneumatic Wings	Thether	–	10 cm/s (0.66 BL/s)
BlueBot (Medium)	13 x 6 x 4 cm 312 cm^3	0.20 kg	Magnet-in-Coil Fins	Battery (7 Whr, 7.4 V)	–	15 cm/s (1.15 BL/s) 7.5 cm/s (1.3 BH/s) (Diving) 0.3 rad/s (Turning)
Snailfish Robot (Large)	28 x 22 x 1 cm 616 cm^3	–	DEA Fins	Battery	–	<38.9 mm/s (<0.18 BL/s)
Tuna Robot (Large)	25.5 x 4.9 x 6.8 cm 850 cm^3	0.31 kg	Motor-Driven Kinematic Fin	Battery (10 Whr)	–	1 m/s (4.0 BL/s)
Resonant Squid (Large)	26.6 x 6 x 6 cm 958 cm^3	0.38 kg	Pneumatic / Solenoid Piston	Thether	–	26 cm/s (0.98 BL/s)
Piezoelectric Fish (Large)	25 cm –	0.54 kg	Piezoelectric Fin	Battery (9 V)	2.5-14 mN (200-800 V)	7.5 cm/s (0.3 BL/s)
Variable Pitch Robot (Large)	24 x 12 x 12 cm 3.5 L	0.9 kg	Propellers	Battery	–	0.29 m/s (1.2 BL/s) (Horizontal) 0.22 m/s (1.83 BH/s) (Vertical) 1.41 rad/s (Turning)
Adaptive Fish (Large)	60 x 50 cm >6 L	2.1 kg	Soft Silicon / Servos	–	–	10 cm/s (0.16 BL/s)
Servo Eel (Large)	87 x 12 x 12 cm 12.5 L	–	Servos	6x AA Batteries	–	0.36 m/s (0.41 BL/s)
Pneumatic Fish (Large)	47 x 23 x 18 cm 19.5 L	1.6 kg	Pneumatic Tail	Li-Po Battery (35 WHr)	–	21.7 cm/s (0.46 BL/s) 14 cm/s (0.61 BH/s) (Dive)
Legged SeaBed Explorer (Large)	70 x 60 x 35 cm 147 L	22.0 kg	Servomotor Legs	Li-Po Battery (300 Whr, 12 V)	–	<12 cm/s (Hopping) <5.8 cm/s (Walking)
LBV150 (Commercial)	53 x 25 x 25 cm 33.0 L	10.4 kg	4 Brushless DC Thrusters	Tether	69 N (Fwd.) 29 N (Vertical) 29 N (Lateral)	1.54 m/s (2.9 BL/s)

or robot has an optimally efficient swimming speed and corresponding tail beat frequency; swimming above this speed results in decreased efficiency and increased cost of transport (i.e. energy consumed per meter travelled) [73].

We (and [73]) observe that similar relationships exist in bio-inspired / swimming robots, and this thus presents a challenge for SWIM to balance the competing goals of robot miniaturization, efficient underwater locomotion, and ability to locomote (with margin) above the predicted ocean current velocities of ~ 1 m/s on Europa. Our efforts to balance these needs will be discussed further in Sec. 4.2.

2.3 Sensors for Oceanographic / State Measurements

We identified a series of sensors that are essential in studying the ocean composition, including temperature / salinity / conductivity / pressure / pH gradients, and micro-swimmer position / motion, summarized in Table 2.3 and informed by the goals of the Science Traceability Matrix in Sec. 3.1. In addition, a number of additional research-grade MEMS sensors, summarized in Table 2.4, are likely to mature in the coming years.

One of the more useful potential technologies for SWIM is to use Quartz Crystal Microbalances (QCMs) or other MEMS resonators (e.g. disk resonators) as a gravimetric sensor [74]–[77], for detection of biomarkers of interest (such as chlorophyll, and big organic molecules), which could be indicative of life in the water (see Fig. 2.9). Mass spectrometers are currently the gold standard to analyze the mass of molecules and provide unprecedented accuracy in chemical detection / identification. However, mass spectrometers (e.g. Orbitrap MS) are large, bulky, costly, require vacuum, cannot easily be integrated on robotic platforms, and require extensive sample preparation by ionizing chemical species and sorting the ions into a spectrum based on their mass-to-charge ratio [78]. In recent years, many efforts have focused on developing a miniaturized, low-cost, chip-scale solution to mass spectrometers, that can be formed into arrays of sensors and simultaneously detect multiple target molecules in a parallel fashion [74], [76].

These MEMS gravimetric sensors are fabricated by coated a MEMS resonator with a chemically-functionalized layer that will preferentially absorb a target molecule of interest. As these unique molecules adhere on to the QCMs / resonators, the QCMs experience frequency and quality factor shift proportional to the mass / quantity of the particular target absorbed on the surface. MEMS resonant-based gravimetric sensors that operate with the same principle as QCMs have been used to detect masses down to levels of a single molecule in vacuum (zeptogram scale mass resolution) and nanogram resolution while operating in a fluid environment [74], [77], [79].

Importantly, target molecules are only absorbed to specific substrates based on the affinity binding of the molecule to the functionalization layer. Therefore, arrays of MEMS gravimetric sensors with different functionalization layers are envisioned to be used on a single sensor chip, to parallelize the chemical sensing process and detect multiple biomarkers simultaneously.

2.3.1 Miniaturized Multi-Sensor MEMS Chips

While a selection of COTS sensors are available for the majority of our sensing needs, we envision that any ocean composition sensor payload designed for SWIM would instead have all the sensors co-fabricated on the same wafer / chip in a compact array using standard MEMS fabrication processes. Such a chip would likely consist of co-fabricated MEMS gravimetric sensors (for biological / chemical detection), as well as MEMS temperature (resistive or bandgap), pressure (capacitive or piezoresistive), salinity (conductance), and pH sensors. An existing example of such a co-packaged multi-sensor chip is shown in Fig. 2.9 [80]. Manufacturing this type of multi-sensor MEMS chip provides two key advantages:

- Enables us to dramatically scale down the volume and (to a lesser extent) power requirements of the sensor payload, by eliminating separate packaging and analog-to-digital converters (ADCs) found on many COTS sensor.
- Simplifies sensor data fusion (i.e. localizing multiple types of sensor data to their positions in 3D space), by flowing / sampling the same small volume of fluid across all sensors.

The IMU and velocity / flow sensors can also be co-packaged on this chip, or separately, depending on the optimal placement within the robot. For example, the IMU does not need to sample the water flow like the other sensors, and thus can be placed

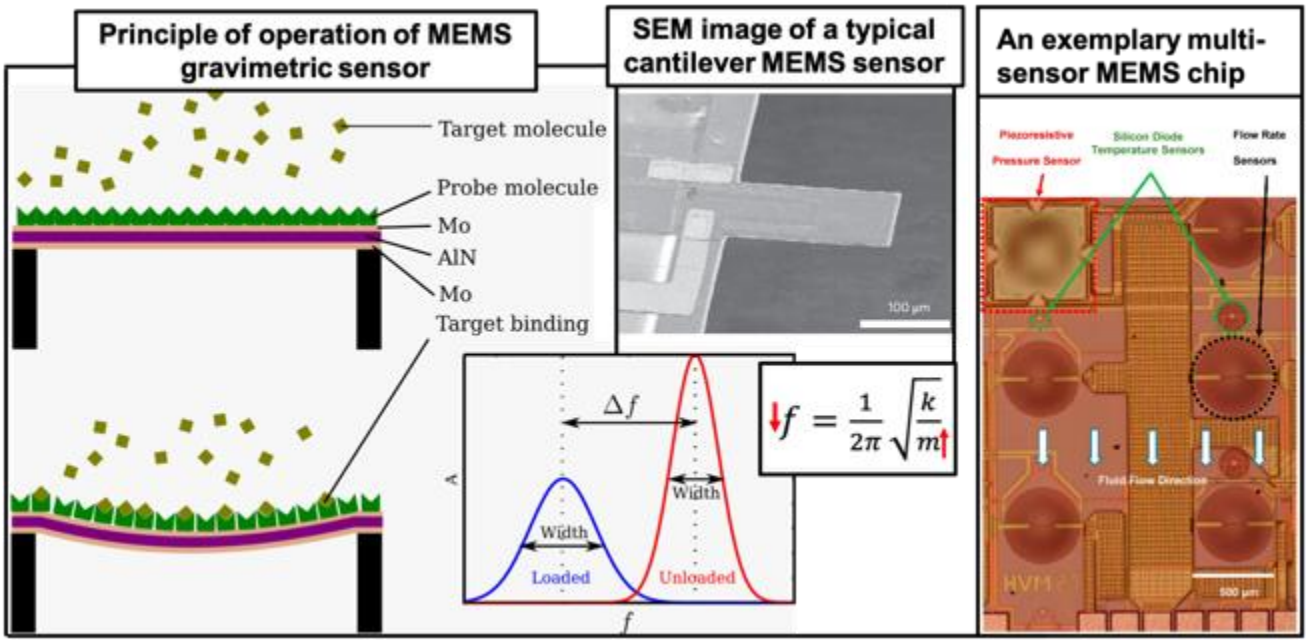

Fig. 2.9: (Left) Principle of operation of a MEMS resonant gravimetric sensor, where an absorbed target molecule causes a frequency shift. (Center) Scanning Electron Microscope image of a MEMS cantilever sensor. (Right) An example multi-sensor MEMS chip [80], containing a piezoresistive pressure sensor, a silicon bandgap temperature sensor, and multiple flow rate sensors.

adjacent to the micro-controller with additional waterproofing. Conversely, the flow velocity sensors can be arrayed across the surface of the SWIM robot to measure fluid flow at key locations.

2.4 Prior NIAC Work on Europan Ocean Exploration

Additionally, one prior NIAC 2012 Phase I study – Exploration of Under-Ice Regions with Ocean Profiling Agents (EUROPA) [81] – has performed a comprehensive mission trade study of a Lander / Cryobot / Hydrobot concept to explore the full sub-surface water column on Europa. Results from this study have found their way into SESAME-class cryobot designs, however the inclusion of 3-4 autonomous glider hydrobots has not. Our NIAC study differentiates from this earlier study in several key ways. We focus exclusively on the design of micro-swimmer hydrobots that conform to NASA's current SESAME mission architecture, developed over the decade since the EUROPA study. Additionally, gliders are not designed for high-speed sampling / exploration and instead focus on long-range measurements of weekly / monthly changes ocean properties. SWIM pursues a different mission concept of operations (ConOps) using smaller robots that have greater agility, evaluates actual performance of these subsystems, and generates operational system prototypes for testing.

Table 2.3: Commercially Available Sensors. Data on sensors is retrieved from commercial sites (e.g. Digikey) for the temperature sensors [82]–[84], IMUs [85], [86], and cameras [87], plus other specialized stores for sensors for pH [88], [89], salinity [90], pressure [91], and DVLs [92], [93].

Type	Sensor	Technology	Size (mm)	Weight (g)	Power (mW)	Range		Output	Sensitivity
						Min	Max		
Temperature	TMP35FT9	Silicon based	17 x 5 x 4	-	0.3	10° C	125° C	Analog	10 mV/c
	TMP12FP	Silicon based	11 x 8 x 7	–	2	-40° C	150° C	Digital SPI	5 mV/C
	AD590KRZ-RL	Silicon based	6 x 5 x 2	–	1.2	-55° C	150° C	Current	1 uA/K
pH	ZPS CIO-000-00064	–	24 x 7 x 1	0.4	0	2 pH	10 pH	Analog	60 mV/pH
	pH1400	Glass electrode	150 x 12 x 12	–	0	0 pH	14 pH	Analog	-
Salinity	PS-2195	Conductive	–	–	–	1 ppt	55 ppt	Conductance	2.5 uS/ppt
Pressure	89-05KA-0U	–	⌀ 9.0 x 13.2	–	7.5	0 MPa	35 MPa	Analog	15-28 mV/V
9-DOF IMU	BNO055	Acclerometer	3.8 x 5.2 x 1.1	3	40.6	±2g/4g/8g/16g		Digital SPI	14 bits
		Gyroscope				±125 dps to ±2000 dps			16 bits
		Magnetometer				±1300 uT(x,y-axis), ±2500 uT (z-axis)			13/13/15 bits for x/y/z
	LSM9DS1	Acclerometer	3.5 x 3 x 1	3	16.5	±2g/4g/8g/16g		Digital SPI	.061/.122/.244/.732 mg/LSB
		Gyroscope				±245/±500/ ±2000 dps			8.75/17.5/70 mdps/LSB
		Magnetometer				±4/8/12/16 gauss			.14/.29/.43/.58 mgauss/LSB
DVL	DVL-75	Accoustic	430mL	0.665g	8W			Ethernet/TTL	
	DVL A50	Accoustic	66 x 66 x 25	170g	3W	0 m/s	3.75 m/s	UART/ Ethernet	0.1 mm/s
	DVL A125		125 x 125 x 30	986g	3W	0 m/s	9 m/s	UART/ Ethernet	0.1 mm/s
Camera	OV5647	5MP	36 x 36		3V	2592x1944, 1080p, 30fps			
	IMX219PQ	8MP	36 x 36		3V	3280x2464, 1080p, 30fps			

Table 2.4: Research Grade Sensors (note that sensors are developed by the corresponding research group in each row)

Type	Technology	Research Group	Size (mm)	Power (mW)	Range		Output	Sensitivity
					Min	Max		
Temperature	Resonator	Stanford University [84]	-	-	-40° C	120° C	Frequency	25 Hz/C
Temperature	Resistive	Shanghai Institute of Microsystem and Information Technology [94]	0.2x0.6	60	25° C	200° C	Resistance	1 ohm/C
pH	Capacitive	Monash University [89]	0.02x0.04x0.06	-	1 pH	4 pH	Frequency	10 MHz/pH
					10 pH	12 pH		2 MHz/pH
pH	Conductive	Ulsan National Institute of Science and Technology [95]	-	-	2 pH	12 pH	Conductance	5.7 nS/pH
Salinity	Conductive	University of Washington [90]	3x3	-	0 ppt	67 ppt	Voltage	11 mV/ppt

3 SCIENCE TRACEABILITY

This section discusses our effort to build a Science Traceability Matrix (STM), focused on science goals at the ocean-ice interface. We define and rank ocean-access mission science objectives and investigations (focused on ocean characteristics / habitability), as well as identify relevant scientific instruments and estimate the ocean volume to explore / mission duration to collect sufficient data for these investigations.

The SWIM Science Traceability Matrix (Table 3.1) complements STMs for other ocean-access missions, but highlight specific objectives that benefit from micro-swimmer mobility / redundancy, and sets minimum sensing capabilities for these vehicles.

3.1 Science Traceability

One of the most important insights in planetary science in the last few decades is the discovery that many worlds throughout our outer solar system may hide vast global oceans of liquid water [96]. As the first discovered likely ocean world beyond Earth, Jupiter's moon Europa has captivated the science community and general public. The Voyager missions first revealed a disrupted surface at Europa renewed through recent or active geologic activity, and Galileo mission magnetometry indicated the presence of a global saltwater ocean beneath the icy shell [97]. Recent observations also suggest the presence of plumes that may spew internal water into space [98], indicating the potential for shallow liquid water reservoirs beneath Europa's icy surface.

Intense radiation from Jupiter at Europa's surface likely forms water and impurities into oxidants. Moreover, active geologic cycling of seawater through rocky material on the Europan seafloor is expected to be chemically reducing [99]. If mixing

Goal	Science Objectives	Investigations	Observations	Vehicle Scale	Notes
Explore an alien ocean	SO1. Search for and characterize life in the ocean of Europa	1A. Detect and characterize any extant micro- or macroorganisms	Microscopy, biomarkers, flouresence, spectrometry, spectroscopy	Large	Size reduction via MEMS mass spec.? Size reduction via sample return to probe?
		1Ba. Detect and characterize any organic indicators of past or present life	Microscopy, biomarkers, flouresence, spectrometry, spectroscopy Composition (x,y,z,t)	Large	Size reduction opportunities for instruments? Size reduction via sample return to probe?
		1Bb. Detect and characterize specific identified biomarker	Lab on a chip?	Medium	e.g. chlorophyl is cheap on Earth Depends on comms. reqs.
		1C. Identify and characterize structural indicators of life	Microscopy, biomarkers, flouresence, spectrometry, spectroscopy	Medium	
		1D. Detect and characterize any inorganic indicators of past or present life	Microscopy, spectrometry, spectroscopy Composition (x,y,z,t)	Medium	Medium / Large for high-fidelity sensors Small / Medium for lab-on-a-chip
		1E. Determine the provenance of sampled material	Microscopy, spectrometry, spectroscopy Composition (x,y,z,t) Temperature, salinity, etc. of water column	Small	Composition sensors are Small / Medium Temp, Salinity sensors are Small
	SO2. Interrogate Europa's ice-ocean interface and ocean to characterize the chemical environments and processes	2A. Characterize the reduction-oxidation (redox) state	REDOX potential measurements Lab-on-a-chip	Small	Small COTS meters exist, can miniaturize
		2B. Determine the nature and distribution of of chemical constituents	Composition (x,y,z,t) Spectrometry, spectroscopy	Small	Could be small, if each swimmer is tuned for a different, limited number of chemical constiuents
		2C. Characterize the chemical exchange processes at the ice-ocean interface	Composition (x,y,z,t), including in ice	Large	Requires a stand-off optical instrument
		2D. Identify spatial and temporal variations in boundary and ocean composition and state	Any chemical measurement that fits (lab-on-a-chip)	Small	Could be small, if each swimmer is tuned for
	SO3. Interrogate Europa's ice-ocean interface and ocean to characterize physical environments and processes	3A. Identify and characterize the deformation response of the ice-ocean interface shell to geologic forcing, including diurnal tides (e.g. does the ocean feel the tides?)	Changes in depth of the interface as a function of time (pressure) Changes in visible structure with time Search for bubbles (camera)	Medium	Maybe best done on probe (e.g. pressure) Maybe better on swimmers
		3B. Characterize the structure and topography of the ice-ocean interface, and variability of this structure with time	Ice topography and morphology (shape, texture, size of features and their relief) Visible images, temp., sonar/radar backscatter over short distances for texture/clutter, acoustics might also be sensitive to changing melt volume in ice	Small	Need to be very close to or touching ice
		3C. Characterize material and heat transport with space and time at the ice-ocean interace, including vertical transport within the water column and horizontal transport within the ice and ocean	Temperature(x,y,z,t) Composition(x,y,z,t) Velocity(x,y,z,t)	Small	S, M, or L depending on fidelity

Table 3.1: SWIM Science Traceability Matrix, focusing on Ocean World science objectives and investigations that can be uniquely performed at the ice-ocean interface. Investigations are categorized by the size-scales (volume, power) of instruments and the associated micro-swimmers that could operate these instruments: Large (~1000 cm^3-scale robots), Medium (~100 cm^3-scale robots), and Small (< 10 cm^3-scale robots).

between the surface oxidants and the reduced ocean water occurs [100], [101], there is an opportunity in Europa's ocean or ice shell to produce a reduction-oxidation (redox) potential. All known life relies on such redox potentials for heat energy and entropy, enabling cellular maintenance, metabolism and reproduction.

Thus, the key components for life are present: water, chemical building blocks in disequilibrium, energy, and time. Embodied in the search for life is a focus on the planetary and local conditions that enable (or restrict) the emergence and persistence of life. This includes exploring the range of habitable environments present in the outer Solar System and expanding the techniques for accessing potential habitats and identifying signs of past or present life. Hence, the search for life among Ocean Worlds can fulfill a major role in both Planetary Science and Astrobiology if it simultaneously addresses key questions related to planetary system and body processes, focusing on the physical and chemical processes that shape these environments.

To explore these environments, NASA and the scientific community are pursuing cryobot technologies. In 2017, NASA commissioned a Keck Institute for Space Studies (KISS) investigation into subsurface access on Ocean Worlds. This study surveyed more than half-a-century of research into deep-ice access technologies in the context of our current understanding of the icy environments of the outer Solar System. One technology concept emerged to be robust against the potential hazards and challenges of planetary exploration: the ice penetrating robot, or "cryobot," that can effectively penetrate ice shells tens of kilometers thick, starting initially in vacuum at cryogenic temperatures and descending under control through the ice column, into and through an ocean water column. The 2017 KISS study concluded that for the first time, the science and technology of ocean access have reached a level of maturity to credibly enable flight implementation within the next two decades. NASA's Science Mission Directorate then took the next step towards ocean access by establishing the Scientific Exploration Subsurface Access Mechanism for Europa (SESAME) program. Cryobot technologies to enable planetary ocean access missions are now in the engineering development phase.

SESAME-class cryobot studies have now begun to explore the science and instrument requirements and science concepts of operations for through-ice access and ocean exploration. Here, we leverage the Probe Using Radioisotopes for Icy Moons Exploration (PRIME) cryobot architecture and design [102], [103], in addition to the science traceability matrix and science concept of operations [104], [105]. The PRIME architecture considers the overarching Science Goal, "Explore and alien ocean," comprising three Science objectives related to Life, Chemical Context, and Physical Context. Within the PRIME STM, we drew on Investigations that could be reproduced, enhanced, or enabled by a SWIM payload 3.1.

In this study, we assume that the PRIME vehicle has a capable, notional payload, and investigate the added science return from deployable sensors. We found natural break points in the science return per asset per volume that allowed the mapping of science investigations to Small, Medium, and Large deployable. Rather than define any specific payload at this stage, we instead place requirements on these size classes to bound the required payload capabilities. Thus, we remain flexible in our ability to respond to future innovations, programmatic changes, and discoveries.

Sensor precision and accuracy requirements for SWIM are not defined at this time, and instead the STM serves as a guide for the types of instruments that would be most useful for SWIM 3.1. We consider Small-class SWIM robots capable of hosting integrated MEMS (micro-electromechanical system) sensors for measurements such as conductivity, temperature, pressure, and the presence of select molecules. We consider Medium-class robots capable of basic wet chemistry and/or optical devices such as cameras, microscopes, and spectrometers. Finally, we consider Large-class robots capable of conveying instrumentation similar to that in the cryobot's primary science bay, including large in situ instrumentation

3.2 Design Requirements

SWIM has identified 3 key sets of requirements, that inform the trade study and ultimate selection of a preferred robot design:

1) Environmental requirements (Sec. 3.2.1)
2) System Integration / Deployment requirements (Sec. 3.2.2)
3) Science / Operational requirements (Sec. 3.2.3)

A detailed summary of ocean world environmental properties and key scales that drive these requirements are provided in Table 3.2.

3.2.1 Environmental Requirements

The Europan ice-ocean interface characteristics are truly unknown at this time, but it is predicted to share commonalities with sub-glacial and sub-ice-shelf environments on Earth. The ice sheet may contain flat, scalloped, or fissured features, and stalactites / brinicles may also be present [106]. The ocean at the interface may exist as a slushy, water-ice slurry (e.g. if there is low current velocity in this location), have low clarity (e.g. if the water is turbid), or be relatively clear (e.g. if a strong ocean current dominates).

The estimated maximum ocean current velocity is predicted to be <1 m/s, and it is also expected that ocean currents vary periodically with time across the diurnal cycle (85.2 hours diurnal, with a tidal timescale (high-tide to high-tide) of 42.6 hours on Europa).

Ocean pressure at the ice-ocean interface is significant at 25-50 MPa, depending on actual thickness of the ice crust (currently predicted at 20-40 km thick). This pressure is significant enough to reduce likelihood of cavitation (due to motion of propellers).

Ocean temperature is expected to remain at ~273 K (~0°C), or the melting point of water. However, the PRIME cryobot continuously generates ~8 kW thermal energy from its Radioisotope Power System (RPS) that is dumped directly into the ocean, and the significant water pressure under the ice prevents water from boiling. As a result, heat transfer from the cryobot into the

		Europa	Enceladus	Earth
Environment	Ice-Ocean Interface Depth	20 - 40 km	10 km (to base of ice) 50 km (to ocean floor)	<1 km
	Interface Temperature	~273 K		~273 K
	Gravity	0.134 g	0.0113 g	1.0 g
	Pressure	25 - 50 MPa (interface) 170 MPa (seafloor)	1.0 MPa (interface) 5.0 MPa (seafloor)	<9.0 MPa (interface) <110 MPa (seafloor)
Key Scales	Diurnal Timescale	85.2 hours	32.9 hours	24.0 hours
	Tidal Timescale (high-tide to high-tide)	42.6 hours	16.5 hours	12.4 hours
	Est. Maximum Ocean Current Velocity	≲1 m/s	No known estimate (potentially extreme beneath south pole)	~0.5 m/s (Tidal Currents) ~1.5 m/s (Gulf Stream) ≲6.5 m/s (Colorado River)
	Cryobot Data Rate to Surface	1 kbps baseline / 0.1 kbps threshold		1 kbps – 10 Mbps
	Cryobot Deployment Duration	~750 hour campaign		1 – 200 hours
	Cryobot Payload Volume Allocation	Trade Ongoing (~40L, margined to 23L, with 7L definitely pre-allocated)		~1s L (BRUIE) ~30 L (Orpheus)
	SWIM Volume	5 - 16 L (Trade Ongoing)		~50 L (BRUIE) ~3,000 L (Orpheus)

Table 3.2: Ocean World environmental properties and key scales that that impose mission requirements and engineering constraints on SWIM designs, building on JPL's PRIME cryobot concept of operations. Relevant requirements for a SWIM mission to Europa are highlighted in red, and information on equivalent conditions on Enceladus and Earth are provided for comparison.

ocean is dominated by thermal diffusion / convection (if no current is present), or thermal advection (if a current is present), and likely results in a large bubble of heated water forming around / above / downstream of the cryobot, potentially eroding or altering the regions of interest.

This thermal bubble sets a minimum exploration range for the SWIM robots of 1-10 meters (depending on ocean current velocity), which is necessary to swim beyond the thermally-affected region and sample pristine ocean / ice. It also provides motivation for the swimming robots to have sufficient mobility to maneuver up-stream (in an ocean current) to reliably explore outside of any down-stream thermal plume.

3.2.2 System Integration / Deployment Requirements

SWIM robots must be designed to integrate within the PRIME cryobot, and have a controllable and reliable means of deployment from the cyrobot once at the ice-ocean interface. An example of one such method of integration / deployment is shown in Fig. 3.1.

System Integration – The overall PRIME cryobot concept vehicle is ~23-25 cm diameter and ~3.5 meters long, with a full internal payload volume allocation of ~40 L that is margined to ~23 L and has ~7 L pre-allocated to known instruments. Individual payload slots (i.e. for specific instruments) are nominally allocated for science instruments in ~5-6 L increments, with up to 16 L of payload volume remaining available for use in the mid-section (along the fore-to-aft axis) of the cryobot.

Thus, for the purpose of this study, we are baselining the use of a single instrument payload slot with a volume of ~5 L (roughly equivalent to 25 cm diameter x 10 cm height volume within PRIME).

No pressure vessel provided, so the payload volume / SWIM robots are at equilibrium with environment at all stages of the mission, unless we intentionally allocate a portion of that 5 L volume for a pressure vessel.

The PRIME cryobot generates significant electric (800-1200 W) and thermal (~8 kW) power, and a surplus of both forms of power are available once the cryobot is anchored at the ice-ocean interface and no longer using its drilling / jetting mechanisms

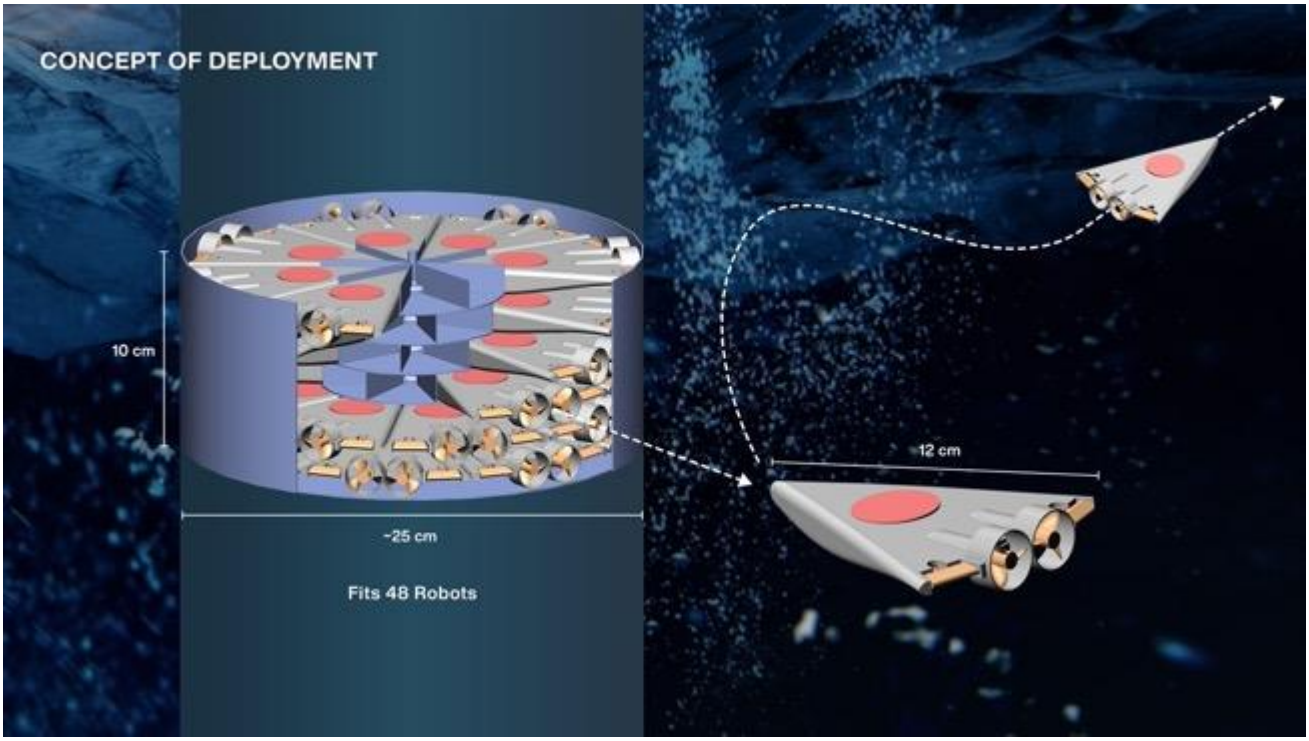

Fig. 3.1: Integration / Deployment requirements within a SESAME-class cryobot like the PRIME cryobot. The overall PRIME cryobot concept vehicle is ~23-25 cm diameter and ~3.5 meters long, with a full internal payload volume allocation of ~40 L, margined to ~23 L, with ~7 L pre-allocated to known instruments. Individual payload slots are nominally 5-6 L, with up to 16 L of payload volume remaining available for use in the mid-section of the cryobot. SWIM robots stored within the PRIME cryobot must have a method for deploying out of the cryobot and maneuvering away.

for tunneling through the ice. A percentage of this electrical / thermal power is also assumed to be available for use at other phases of the mission – including cruise (in-space) and descent (in-ice) – to maintain SWIM subsystems at survival temperatures.

The SWIM payload volume must also maintain 1+ structural paths across payload volume, to ensure structural integrity of the overall cryobot and allow feed-through channels for the thermal, electrical, and communication systems from the fore to aft sections of the cryobot. In Phase I, however, no specific demands are currently placed on the specific distribution / allocation of these feed-through channels and structural elements - just that they need to exist (i.e. the SWIM deployment mechanism cannot rely on the PRIME cyrobot splitting in half).

Deployment – SWIM robots stored within the PRIME cryobot must have 1+ methods for **controllably deploying** out of the cryobot and maneuvering away. This can include a combination of mechanical restraints on the cryobot (e.g. launchlocks, frangibolts, cable-cutters), passive deployment mechanisms (e.g. compressed springs, gas-generators), and active mobility systems (e.g. thrusters on individual SWIM robots). Post-ejection from the cyrobot, the SWIM robots can maneuver away using either active (e.g. thrusters / fins) or passive (e.g. ocean currents) means.

3.2.3 Science / Operational Requirements

Science / Operational requirements are derived from the science objectives and investigations outlined in the Science Traceability Matrix (Sec. 3.1), and used to define minimum capabilities of the SWIM robots necessary to perform these investigations.

Exploration Range – The SWIM robots have a **minimum range** requirement of maneuvering >1-10 meters (depending on the current velocity) away from the cryobot, defined by the need to sample pristine ocean water outside of cryobot's thermally-affected bubble.

Our team scientist expects variation in environmental features of interest (e.g. physical / chemical properties) on the order of 1s-10s meters and 1s-10s km, but not on scales of 100s meters to a few kms. In other words, the ice sheet / ocean likely has short-range feature variation at the meter scale (e.g. sites a few meters apart may look quite different) and long-range feature variation at multi-kilometer scale (e.g. sites multiple km apart may look quite different), but limited novel feature variation at intermediate scales of 100s meters to 1 km (e.g. exploring sites 250 m vs. 500 m vs. <1 km apart may not reveal new information).

SWIM robots are therefore baselined at exploring an ocean volume with a ~100 meter radius **maximum range** requirement, and can (but are not required) to explore beyond this distance. Since the next break-point for feature variation is expected at several kilometers, and exploration range is a significant driver for increasing per-robot energy / volume requirements – by increasing robot operational time, increasing communication power required at long ranges, and increasing energy storage volume allocation relative to other subsystems – this strikes an optimal balance between exploration range and robot capabilities on an initial ocean-access mission.

Mission concepts that do choose to explore multi-km ranges on Europa may need to rely on alternate robot designs, such as meter-scale gliders [81].

On Europa, the ocean is predicted to be <100 km deep (to sea floor). The SWIM baseline plan is to stay relatively near the ice-ocean interface, however the **maximum depth** of SWIM exploration remains an open trade, because scientists don't understand the bulk / local structure of the ocean, and can benefit from collecting vertical profiles of the water column.

Exploration Goals / Mobility Capabilities – In addition to explicit exploration range requirements, the SWIM robots must also be capable of controlled vertical mobility (to understand signal gradients from the ice interface into the water column), and controlled horizontal mobility is ideal (to explore a variety of locations). The SWIM robots should also be able to localize their position in 3D space (in order to map sensor instrument signals to physical positions in the environment), and to understand and react to environmental measurements (e.g. identify signal gradients and track them to their source, potentially with higher-level autonomy supervision / path planning provided by the cryobot).

SWIM robots will be required to collect data at ice-ocean interface – where there are expected to be the most significant gradients in physical / chemical properties, and correspondingly the greatest likelihood of finding life – and can explore the open ocean as a significant, but lower, priority. See the Science Traceability Matrix (Sec. 3.1) for additional details.

Mission Duration – The SWIM robots need to explore at 2+ times (ideally 4+ times) during a 85 hr diurnal cycle on Europa. The robots do not need continuous sampling across 85 hr diurnal, but have the option to do so if sufficient power is available.

It remains an open trade as to whether SWIM should maximize the total explored ocean volume (better coverage in search for signs of extant life), maximize the duration over which data is collected (better visibility into slow signal variation), or maximize the explored ocean volume per unit time (better visibility into transient signals).

3.3 Value of Multi-Robot Exploration

The conventional design trades for a cryobot-deployable robot with limited payload allocation (e.g. 5-15 L) typically push engineers to maximize per-robot capabilities in 1 (or maybe 2) robot deployables. This allows each robot to have larger (and more sophisticated) mobility, power, and instrument subsystems, and potentially greater redundancy or robustness within each system.

However, when exploring an alien Ocean World, some of the most important science-motivated questions involve acquiring measurements in parallel across long temporal and / or large spatial baselines, which are exactly the types of questions that motivate multi-agent / multi-robot exploration. Key enabling advantages of multi-robot exploration in Ocean Worlds include:

- Mission redundancy across multiple robots – critical on a 9-15 year mission that passes through high radiation environments
- Expedited exploration of the ocean through coordinated, distributed robot agents
- Enhanced sensor data reliability through multiple measurements of similar ocean volumes by independent robots (reducing sources of per-unit sensor error)
- Ability to map ocean properties / gradients in 3D – for example, thermal gradients in the meter beneath the ice can tells scientists the rate of basal melting / freezing and current vectors in 3D
- Ability to explore high-risk locations of potentially high scientific value without risking the entire mission
- What other new questions we can ask with the new capabilities we might demonstrate in SWIM?

This work is also not limited to an icy moon – the ultimate test of SWIM on Earth would be deploy at a sub-sea vent to perform active, distributed chemical / temperature mapping in 3D. This would have a different set of driving science questions (understanding thermal vent environment vs. the underside of a ice sheet), but could achieve similarly novel results.

With SWIM, our goal is to design robots that can best suited to inform these science questions through simultaneous, distributed measurements over at least one diurnal cycle, and we believe that multi-robot deployables can be key to this goal. We thus pursue the simplest, smallest possible robots that achieve our science goals, providing for the greatest redundancy across robots.

4 TRADE STUDY OF MINIATURIZED ROBOTIC SUBSYSTEMS

The following subsections discuss the **seven robotic subsystem** trade spaces explored in this study, including: Sensing (Sec. 4.1), Actuation (Sec. 4.2), Communication (Sec. 4.3), Compute (Sec. 4.4), Power (Sec. 4.5), optional Tethers (Sec. 4.6), and Structure (Sec. 4.7).

Micro-swimmer concepts are presented in Sec. 6, which make specific selections among these trade space options to generate complete SWIM robot concepts.

4.1 Sensing Subsystem

We have identified representative sensors (see Table 2.3 and 2.4) that are fall within classes of sensors / instruments viable for studying ocean composition (temperature / pressure / salinity / pH gradients) and micro-swimmer position / motion, and that have form-factors compatible with swimming micro-robots (or a reasonable miniaturization path through MEMS fabrication). Together, these sensors enable SWIM to perform scientifically-valuable measurements that inform the science objectives / investigations outlined in our STM.

4.1.1 Scientific Instruments

The sensors identified in Sec. 2.3 and Table 2.3 reflect current capabilities of relevant, miniature scientific instrument payloads, including MEMS sensors (redox potential, temp., salinity, pressure, pH), cameras / microscopes, and spectrometers. Due to the > 10 year timeline for a SWIM mission, we have considered both research and commercial devices, we document key performance characteristics (e.g. sensitivity, operating range, power) and system integration constraints (e.g. form-factors, sensor signal output type), and briefly highlight further predicted technology miniaturization / advances in the next decade.

The sensors identified cover the standard oceanographic suite of Conductivity, Temperature, Depth (CTD) sensing, which is "the primary tool for determining essential physical properties of sea water. It gives scientists a precise and comprehensive charting of the distribution and variation of water temperature, salinity, and density that helps to understand how the oceans affect life" [107].

A MEMS-fabricated "ocean composition" sensor payload containing temperature, pressure, salinity / conductivity, pH, and possibly RedOx potential sensors co-manufactured / co-packaged on a single micro-fluidics chip can feasibly fit within a 1 cm^3 volume and consume < 100 mW of power. The addition of arrays of MEMS resonant-based gravimetric sensors, each functionalized to target specific organic molecules of interest (currently an area of active research), would further expand the biomarker detection capabilities of this sensor payload with minimal additional volume or power usage.

4.1.2 Localization

Robot localization can be implemented via dead-reckoning (using an onboard 9-DoF IMU), possibly supplemented with a flow sensor or sonar beacon for ranging (e.g. distance from cryobot) to increase accuracy and reduce sensor drift over longer duration operation.

Cameras (e.g. optical, optical flow, or event cameras) or LIDAR are commonly used for simultaneous localization and mapping (SLAM) on Earth, and could be leveraged for position tracking on SWIM. However, they require greater onboard computation and power, and there may be limited features to observe / track at the ice-ocean interface.

Doppler velocity logs (DVL) are ideal for improving state estimation and measuring flow velocity underwater, but current DVLs are 100-250 cm^3, which is one order of magnitude too large for SWIM [108].

Forward- and upward-pointing sonar can also be used for hazard avoidance / collision detection.

4.2 Actuation Subsystem

We initially surveyed a variety of research- and commercial-grade underwater robots – see Sec. 2.1 (Table 2.1) and Sec. 2.2 (Table 2.2) that employ a wide array of actuators and techniques (fins, tails, bodies, and propellers / thrusters) for underwater mobility. Where information is available, we also classified capabilities of these vehicles, including size, power, actuator technology, thrust, and top speed.

The key take-away from current state-of-the-art UAV performance is as follows:

Research UAVs employ a variety of novel actuators, but all surveyed robots have max speeds << 1 m/s, especially as robot size shrinks to dm-scale.

Commercial UAVs use motors with propellers to achieve speeds > 1 m/s, but at meter-scale are roughly 1-2 orders of magnitude too large to fit inside of the PRIME cryobot.

More generally, **Research UAVs** employ a variety of novel actuators (solenoids, piezoelectric actuators, dielectric elastomer actuators, pneumatics, etc.) for thrust and steering, but all surveyed robots have max speeds ≤ 1 m/s, which leaves no margin to the predicted current velocity on Europa. Specific robots do achieve high normalized speeds (in body-length-per-second, BL/s) or highly-efficient swimming (due to fish-inspired geometry / locomotion), but all robots that can feasibly fit inside the required payload volume and SWIM mission context are limited to absolute speeds <0.36 m/s. Therefore, our review of novel actuation technologies did not identify any viable candidates for generating requisite thrust in a micro-swimmer, but several options – especially **solenoid actuators** and **piezoelectric actuators** – are viable options for controlling steering fins / flaps.

In contrast, **Commercial / Oceanographic UAVs** use conventional **electric motor / propeller thrusters** to almost uniformly achieve the > 1m/s speeds needed for the Europan ocean, and often have 100-200% margin over this speed. However these robots are 1-2 orders of magnitude too large to fit within the cryobot payload volume, since Earth-based exploration prioritizes robot endurance, payload volume, range, and cost / manufacturability over miniaturization. Therefore, it is incumbent on us to confirm that such electric motor thrusters can maintain performance as they are scaled down to the requisite size for a SWIM micro-swimmer.

4.2.1 Propeller Thrust Estimation

We proceeded to calculate the thrust generated and power consumed by a miniature motor-driven propeller, to determine if a self-propelled micro-robot at the ~100 cm^3 size-scale can viably achieve the >1 m/s velocities necessary for exploring the Europan ocean while using existing electric motors / propellers . Calculations are implemented according to [109] and summarized from this source below for clarity. Throughout this section, variables are defined according to Table 4.1. Drag parameters are identified in [110].

First, we solve for the force balance of a self-propelled vehicle between fluid resistance (R_{sp}) on the robot body and thrust (T_{sp}), under steady-state conditions:

$$T_{sp} = R_{sp} \tag{4.1}$$

A propeller typically increases the resistance of a vehicle relative to its towed resistance (R_t), by creating a low-pressure region near the propeller intake / hull. A thrust deduction ($t \sim 0.2$) is used to compensate for this:

$$R_{sp} = R_t/(1-t), \text{ with} \tag{4.2}$$

$$R_t = \frac{1}{2}\rho c_d A_w U^2 \tag{4.3}$$

where c_r is the resistance coefficient, A_w is the wetted area, and U is the relative flow velocity.

Propeller performance in open water (denoted by subscript 'o') is described by a thrust coefficient (K_T) and torque coefficient (K_Q), that are both functions of the propeller advance ratio (J) and can be approximated as linear functions of J as follows:

$$J = \frac{U_p}{n_p D} \tag{4.4}$$

$$K_T(J) = \frac{T_o}{\rho n_p^2 D^4} \Leftrightarrow T_o = \rho n_p^2 D^4 K_T(J), \text{ and } K_T(J) \approx \beta_1 - \beta_2 J \tag{4.5}$$

$$K_Q(J) = \frac{Q_{p_o}}{\rho n_p^2 D^5} \Leftrightarrow Q_{p_o} = \rho n_p^2 D^5 K_Q(J), \text{ and } K_Q(J) \approx \gamma_1 - \gamma_2 J \tag{4.6}$$

The open-water propeller efficiency (the ratio of useful thrust power to shaft power) is calculated as:

$$\eta_o = \frac{T_o U}{2\pi n_p Q_{p_o}} = \frac{J(U) K_T}{2\pi K_Q} \tag{4.7}$$

The wake fraction ($w \sim 0.1$) is used to compensate for differing water speeds flowing across the vessel (U) and at the

Table 4.1: Nomenclature for propeller thrust calculations, reproduced from [109]. Model values are provided where appropriate, and left empty if derived from other values or swept. Motor performance values are derived from [111].

Term	Model Value	Units	Description
U		m/s	Speed of vessel
U_p		m/s	Speed of water at the propeller
R_{sp}		N	Resistance / drag of vessel under self-propulsion
R_t		N	Resistance / drag of vessel when towed (no propeller)
T_{sp}		N	Thrust of self-propelled propeller
Q_m	< 5.18	mNm	Torque of motor
Q_p		mNm	Torque of propeller
P_m		W	Power of motor
P_p		W	Power of propeller shaft
D		m	Diameter of propeller
n_m	< 590	Hz	Rotation speed of motor
n_p	< 59	Hz	Rotation speed of propeller
c_s	102.7	Hz/V	Speed constant for motor
c_{sqg}	118.9	Hz/mNm	Speed-torque gradient constant for motor
λ	10	–	Gear ratio of gearbox
η_g	0.6	–	Efficiency of gearbox
η_R	1	–	Rotative Efficiency
t	0.1	–	Thrust deduction
w	0.2	–	Wake fraction

propeller (U_p) due to operating in the vehicle wake:

$$U_p = U(1 - w) \tag{4.8}$$

the rotative efficiency (η_R) is used to map self-propelled torque (Q_{psp}) to open water torque (Q_{po}):

$$Q_{p_o} = \eta_R Q_{p_{sp}} \tag{4.9}$$

and the self-propelled torque (T_{sp}) equates to open water torque (T_o) when the flow velocity is the velocity observed at the propeller, or:

$$T_o(U_p) = T_{sp} \tag{4.10}$$

Motor and propeller performance maps with the gearbox design / efficiency, as follows:

$$n_p = n_m/\lambda \tag{4.11}$$

$$Q_p = \eta_g \lambda Q_m \tag{4.12}$$

$$P_p = \eta_g P_m \tag{4.13}$$

For steady-state conditions, Eqs. 4.2- 4.7 can be combined to solve the initial force balance in Eq. 4.1 (directly derived from [109]):

$$T_{sp} = R_{sp} \tag{4.14}$$

$$T_o = R_t/(1-t) \tag{4.15}$$

$$K_T\left(J(U_p)\right)\rho n_p^2 D^4(1-t) = \frac{1}{2}\rho c_d A_w U^2 \tag{4.16}$$

$$\left(\beta_1 - \beta_2 J(U_p)\right)\rho n_p^2 D^4(1-t) = \frac{1}{2}\rho c_d A_w U_p^2/(1-w)^2 \tag{4.17}$$

$$\beta_1 - \beta_2 J(U_p) = \frac{c_d A_w}{2D^2(1-t)(1-w)^2} J(U_p)^2 \tag{4.18}$$

$$\beta_1 - \beta_2 J(U_p) = \delta J(U_p)^2 \tag{4.19}$$

$$J(U_p) = \frac{-\beta_2 + \sqrt{\beta_2^2 + 4\beta_1\delta}}{2\delta}, \text{ with } \delta = \frac{c_d A_w}{2D^2(1-t)(1-w)^2} \tag{4.20}$$

We first solve for δ in Eq. 4.20, using t = 0.2, w = 0.1 (as discussed above), and body drag terms (c_d, A_w) based on the modeled robot body shape. For the results shown in Fig. 4.1, we assume a submerged wedge with base length (L_b) = 4.0, 8.0 cm, height = 12.0 cm, thickness = 2.0 cm, and $c_d \sim 0.195$ from [110]. The modeled propeller diameters (D) = 1.0, 5.0 cm.

We then solve for $J(U_p)$, based on Eq. 4.20 and the calculated δ. The linear models for $K_T(J)$ and $K_Q(J)$ as a function of $J(U)$ (Eq. 4.5) are based on a empirical propeller model that assumes a 3-bladed propeller with 1-degree pitch. Solving for $J(U_p)$ also allows us to compute K_Q.

We then solve the motor / propeller torque balance to obtain the rotation rate of the motor, using the $J(U_p)$ value derived in our force balance and based on the motor torque-speed curves. Condensing the motor performance equations above, we can solve for the propeller rotation speed (n_p) necessary for the thrust balance:

$$B = \frac{\eta_g \eta_R \lambda}{\alpha c_{sqg}}, \text{ where } \alpha = K_Q \rho D^5 \tag{4.21}$$

$$C = -V_m c_s \frac{\eta_g \eta_R \lambda}{\alpha c_{sqg}} \tag{4.22}$$

$$n_p = -B/2 + \sqrt{((B/2)^2 - C)} \tag{4.23}$$

Which finally allows us to calculate the vessel's steady-state forward velocity (U):

$$U = J n_p D/(1-w) \tag{4.24}$$

the motor torque (Q_m), as a function of motor voltage (V_m), which we sweep across a range of values – effectively as a stand-in for using PWM-based control of the motor torque / speed up to the maximum rated motor voltage ($V_{m,\max}$):

$$Q_m = \frac{V_m c_s - n_p}{c_{sqg}} \tag{4.25}$$

the motor power (P_m):

$$P_m = 2\pi n_p Q_m \tag{4.26}$$

and the propeller thrust (T_{sp}):

$$T_{sp} = \rho n_p^2 D^4 K_T\left(J(U_{sp})\right) \tag{4.27}$$

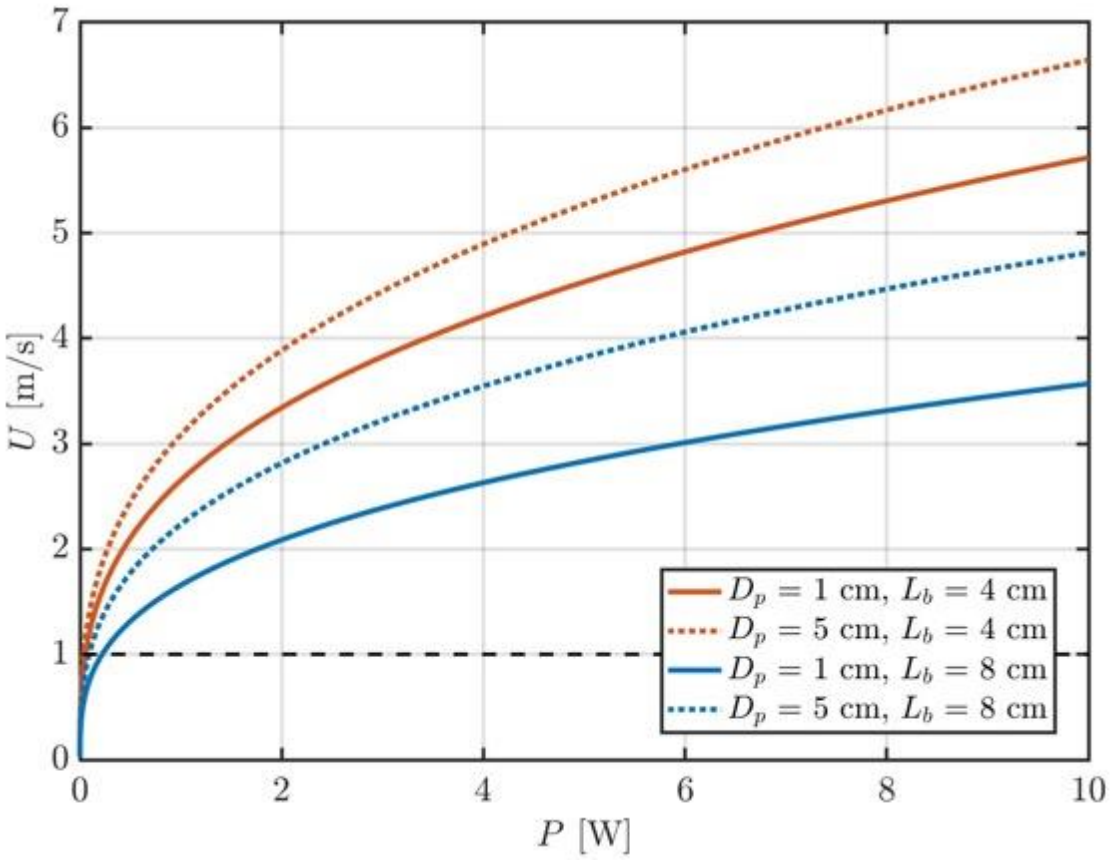

Fig. 4.1: Thruster power vs. robot terminal velocity, as generated by a pair of motors, using two configurations of propeller diameters (D_p) and two configurations of robot beam length (L_b, or width). Dotted line is the predicted maximum Europan ocean velocity (1 m/s).

Under all four bounding cases explored in Fig. 4.1, a pair of miniature motor + propeller thrusters is sufficient to generate steady-state velocities of > 2 m/s, while consuming < 2 W power. This implies that a micro-swimming robot can maneuver with a minimum of 100% margin to the the expected maximum ocean velocities on Europa while consuming a reasonable quantity of power. The mapping of power consumption to micro-swimmer operational life will be explored further in the Power Subsystem discussion (in Sec. 4.5) and in the micro-swimmer point-designs (in Sec. 6).

In conclusion, existing motors / propellers do generate sufficient thrust to exceed predicted Europan ocean velocities (1 m/s), as shown in Fig. 4.1.

4.2.2 Robot Control & Stability

Conventional UAVs on Earth that are designed for passive stability may not as efficient in the reduced 0.134 g gravity on Europa (and definitely not in the 0.0113 g gravity on Enceladus). Under Europan conditions, robots experience the same levels of fluid drag forces (F_d):

$$F_d = \frac{1}{2}\rho v^2 c_d A \tag{4.28}$$

which are only proportional to fluid density (ρ), fluid velocity (v), body drag coefficient (c_d), and body area (A). However, robots experience dramatically-reduced buoyancy / restoring forces (F_b):

$$F_b = -\rho g V \tag{4.29}$$

due to the reduced gravity (g). On Earth, this buoyancy force translates into a buoyancy-driven pitch and roll restoring moment, that provides passive stability as the center of volume / buoyancy attempts to settle above the center of gravity. This restores a

torpedo that pitches up / down back to horizontal (tall underwater vehicles take advantage of this phenomenon for stability).

SWIM robots will thus likely need to accept poor roll / pitch stability on Europa unless they are moving and using active control via fins / propellers. If robot orientation is important when stationary, that will be hard to achieve passively with either a torpedo or delta wing body configuration.

4.3 Communication Subsystem

Multiple hardware options for underwater communications exist (summarized in Table 4.2) as well as communication protocols (Table 4.3).

Wireless acoustic (ultrasound) communications are generally the preferred communication technique for SWIM, due to broad commercial usage on Earth, uncertainty over Europan ocean turbidity, relatively low data volumes for all non-imaging sensors, and desire to operate / transmit data at >100 m distances from the cryobot without imposing an operational requirement to return to the cryobot for data downlinking (or requiring a tether).

Table 4.2: Comparison of communication techniques for aquatic use, drawn from [25].

Comm.	**Use Case**	**Data Rate** (bps)	**Range** (m)	**Power** (W)	**Transmitter Size** (m)
Acoustic	Long range, low data rates	1s-10s kbps	0.1-10 km	1s-10s W	< 0.1 m
RF	Short range, high data rates	Mbps	$<<$ 10 m	0.1-100s W	< 0.5 m
Optical	Medium range, high data rates	Gbps	10-100 m	1s W	< 0.1 m
Tether	Similar to Optical / RF; range limited by tether length and signal attenuation (optical) or resistive losses (electrical), and fiber diameters of 25 μm (optical) to 3-5 mm (hybrid optical + electrical)				

Table 4.3: Comparison of communication protocols for aquatic use.

Design	**Advantages**	**Disadvantages**
Frequency Shift Keying (FSK)	Simple, robust and reliable modulation scheme that can be used in harsh conditions. Appropriate for communication channels that exhibit rapid phase variation (e.g. caused by Doppler effects in the underwater medium).	Slow data bit rates compared to other modulation schemes. Creates large propagation delays between transactions, resulting in comparatively low throughput and high energy consumption. In addition, a low throughput leads to difficulty in transferring images and videos of scientific data, decreasing usefulness of acoustic communication.
Phase Shift Keying (FSK)	Coherent modulation scheme and provides higher data transfer rates, approximately one order of magnitude higher than FSK.	Not suitable for dynamic channel environment and may lead to high Doppler spread.
Orthogonal Frequency Division Multiplexing (OFDM)	Multi-carrier modulation schemes, and has been adopted as a standard for many of the wireless RF systems as it can maximize data throughput.	Acoustic OFDM has shown limited success due to the fact that it is very sensitive to Doppler shift. Recently, benefiting from advanced machine learning techniques and data processing algorithms, OFDM is being considered for higher data rate acoustic communication modulation schemes.

4.3.1 Acoustic Transceiver Design for SWIM Robots

For communication between SWIM robots or between mothercraft and SWIM robots in Europa ocean, various transducer designs have been considered to achieve reliable, real-time, communications. Several underwater acoustic transducer design types, such as piston type, ring type, flexural disks and flextensional type transducers, have been used on Earth's oceans and each design has its own advantages and disadvantages in terms of either size and performance. Each design is schematically shown in Fig. 4.2. Piston type transducer offers high directional and high source level, compared to other transducer designs; however, the frequency related to size (i.e., half wavelength) is limited, so it is not suitable for compact form factor. Flextensional type transducers with a metallic flexure can generate very low frequency (<1 kHz) waves; however, they are not suitable for high hydrostatic pressure conditions. The ring type, free flooded transducer, is considered to have the best configuration because of the capability to generate low frequencies (20-30 kHz) in compact form factor. Most importantly, free-flooded rings have high hydrostatic pressure tolerance so that it can be used at depths that other transducer types cannot withstand and this is critical for Europa underwater environments. Therefore, based on such advantages of ring type transducers, we down-selected ring shaped free-flooded transducers for the transceiver design for SWIM robots.

4.3.2 Operating Frequency / Power Estimation

The selection of operating frequency is one of key parameters for the design of acoustic communication, which determines the size of the transducer as well as the max communication range for a given input power. We are considering two main communication technologies, active, mesh network communication and passive backscatter communication. Schematic diagram of communication methods is depicted in Fig. 4.3.

To select appropriate operating frequency of SWIM robot communication, we studied the relationship between size and frequency as well as power vs communication range using available attenuation of sound in seawater and sonar equations. The results are summarized in Fig. 4.4. Note that the acoustic output is the transmitted power from the transducer. The input electrical power depends on the efficiency of electroacoustic coupling efficiency, (i.e., electro-mechanical (EM) efficiency + mechano-acoustic (MA) efficiency). For a given power budget (less than 1 watt of input electrical power) with required communication range (>100 m), we selected 20 kHz∼40 kHz as operating frequencies, as these frequencies allow for the communication range over 100 m with milliwatt electrical power.

For passive, backscatter communication, micro-swim robots do not require active power to transmit signals as the commu-

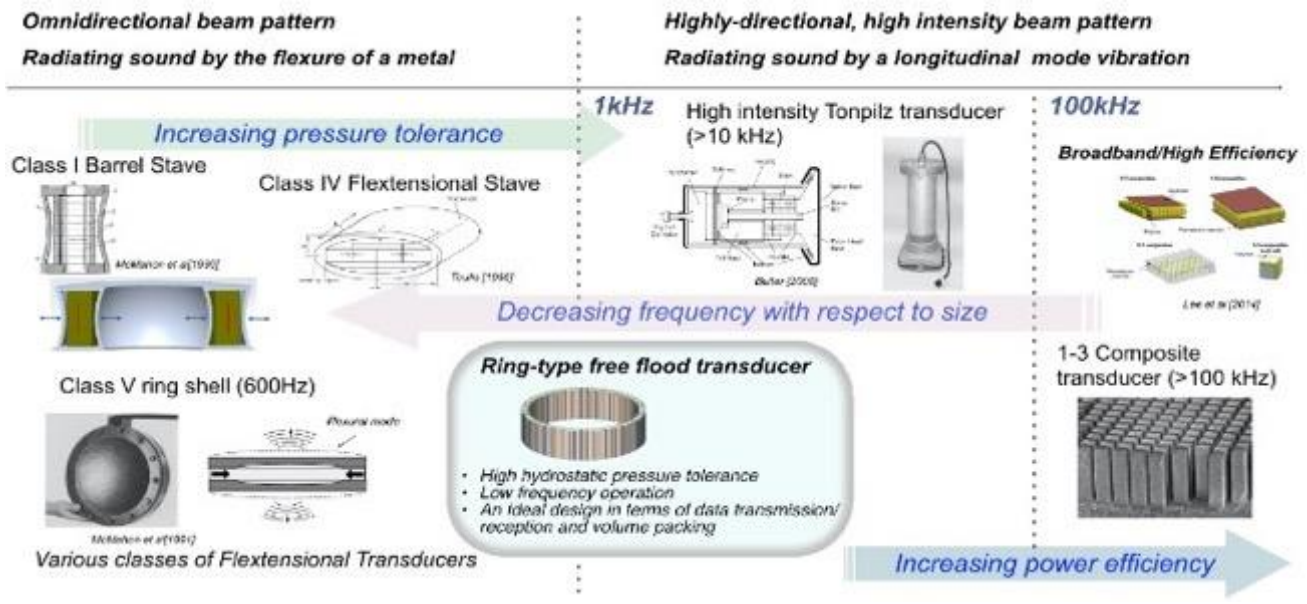

Fig. 4.2: Characteristics of various acoustic transducer configurations that have been used for underwater acoustic communication. Ring-type free flood transducer is found to be best suited for deep ice acoustic communication due to high hydrostatic pressure tolerance and low frequency operation.

Table 4.4: Comparison of Ultrasound Transducer Designs, including operating frequency range, advantages, and disadvantages.

Type	Transducer Design	Operating Frequency	Advantages	Disadvantages
Ring	Free flooded transducer (d31 or d33 mode)	Low–medium freq. (1-10 kHz)	Low frequency operation, virtually unchanged performance regardless of hydrostatic pressure, wide band, can be stacked for high power output	Radiation pattern is not convenient for forming arrays, Omni-directional
Piston	Tonpliz transducer (d33 mode)	Mid freq. (10∼40 kHz)	High power, high efficiency, directional beams	Difficult to design low frequency operation
Flextensional	Moonie, Cymbal, Barrel Stave	Very low freq. (< 1 kHz)	Low frequency operation with small volume, high acoustic power	Design cannot withstand high hydrostatic pressure
Composites	1-3 composites	High freq. (> 100 kHz)	Very broadband operation	Difficult to design low frequency operation.

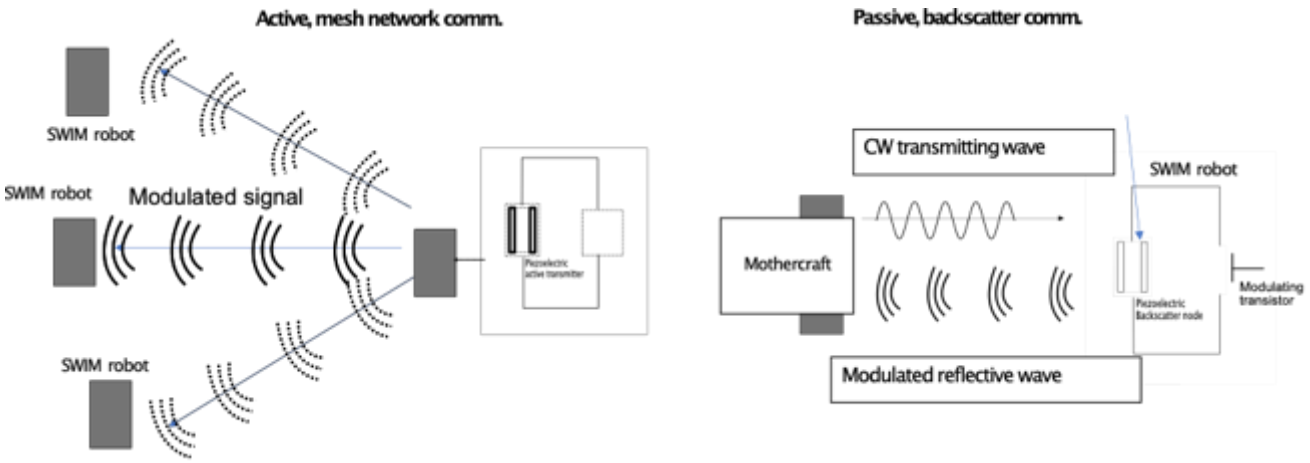

Fig. 4.3: Schematics of active, mesh network communication (left) and passive, backscatter communication (right) among the SWIM robots and with PRIME cryobot. The advantage of active communication lies in long communication range with battery power, while those of passive, backscatter communication is ultra-low power, enabling battery-free underwater robots.

nication from micro-swim robots is based on modulating its reflection by changing the state of short/open of piezoelectric transducer when the signal is coming from mothercraft.

The communication range from mothercraft to micro-swim robots for backscatter communication is calculated as a function of acoustic power. The result of max communication range is plotted as a function of output power and is shown in Fig. 4.5. For this calculation, it is assumed the noise level (>10 kHz) is ∼80 dB, and the reflection coefficient, R, between water and backscatter node is 0.93 based on acoustic impedances of swim robot and communication medium (water). Due to the round trip and reflection losses, the communication range is shorter for a given power, compared to one-way, active communication, requiring watt range powers for >100 m communications.

4.3.3 Communication Protocol / Data Rate

Advanced digital modulation methods have been used for RF communication systems to support high data transmission. However, unlike RF, a limited available bandwidth of the acoustic channels and unknown propagation characteristics of

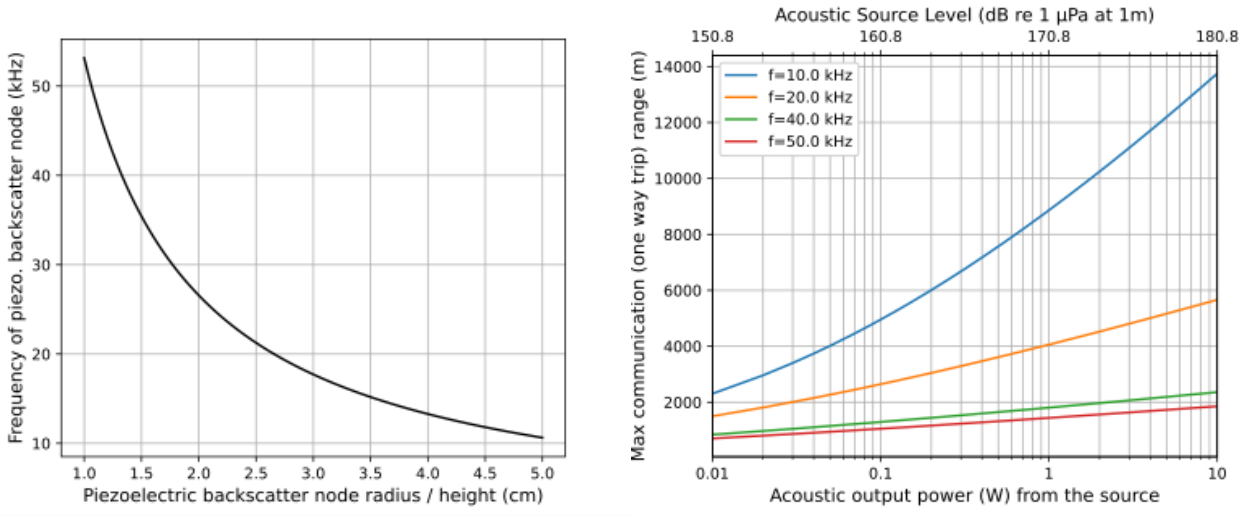

Fig. 4.4: Size of acoustic communication transducer as a function of frequency (left), and max communication range as a function of acoustic output power and frequency, with active acoustic communication transducer (right). Note that these calculations are for one-way, powered communication.

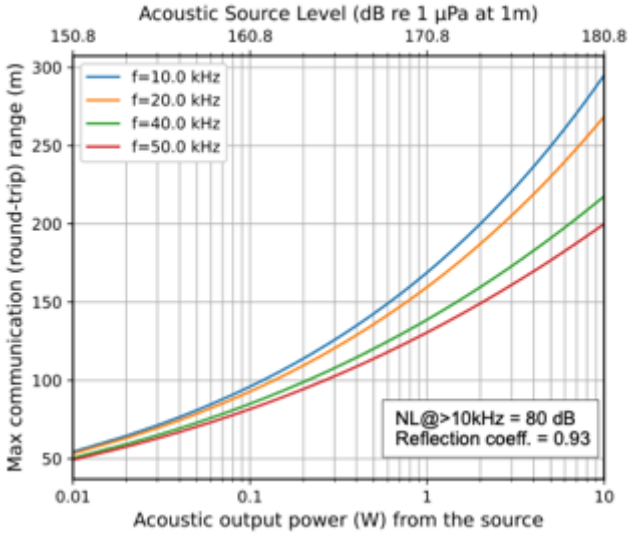

Fig. 4.5: Max round-trip communication range from mothercraft to micro-swim robot as a function of acoustic output power. Note that the communication range is the round-trip traveling range from the transmitting source to receiving source and back to the transmitter, so the actual distance between transmitting source and micro-swim robot is half of the max communication range.

the acoustic waves in Europa ocean create a challenging environment for reliable communication. Thus, using the same data rate/communication protocol for acoustic communication is almost impractical. In an effort to develop suitable acoustic communication protocols, several different modulation schemes were investigated (Table 4.3). Frequency Shift Keying (FSK) is a simple, robust and reliable modulation scheme that can be used in harsh conditions, and it is considered to be appropriate for communication channels that exhibit rapid phase variation. However, the major issue with FSK is its slow data bit rates compared to other modulation schemes, which creates large propagation delays between transactions, resulting in low throughput and high energy consumption. In addition, a low throughput leads to a difficulty to transfer image and video of scientific data. Phase Shift Keying (PSK) is a coherent modulation scheme and provides higher data transfer rates, approximately one order of magnitude

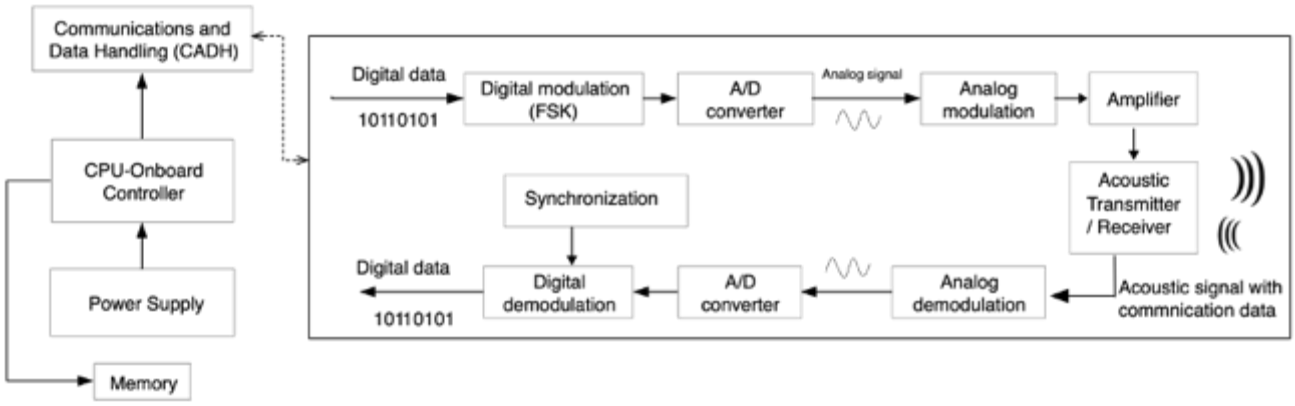

Fig. 4.6: Block Diagram of the Acoustic Communication Link

higher than FSK. The drawback is that it is not suitable for the dynamic channel environment and may lead to high Doppler spread. Orthogonal Frequency Division Multiplexing (OFDM) is multi-carrier modulation schemes, and has been adopted as a standard for many of the wireless RF systems as it can maximize data throughput. Acoustic OFDM, however, has shown limited success due to the fact that OFDM is very sensitive to Doppler shift. Recently, benefiting from advanced machine learning techniques and data processing algorithms, OFDM is being considered for higher data rate acoustic communication modulation schemes. For the application in micro-SWIM robots, we selected FSK despite of low throughput as it is likely that there would be relative motions (e.g., ocean waves, currents and tides) between a transmitter and a receiver, (i.e., Doppler distortion), and FSK is suitable to be implement in the presence of rapid phase variations caused by Doppler effects.

The general block diagram for acoustic communication in a SWIM robot is shown in Fig. 4.6. The principle of operation of acoustic communication is as follows: In **transmit mode** – the message data is converted to ASCII 8-bit integers, and a known header is added to the beginning of the set of integers to track the state of communication between two acoustic data links. Then, the onboard CPU converts the logical information (0 and 1) into an analog signal, amplifying and modulating it and sending it to the transmitter. Then, the modulated analog signal is converted into an acoustic pressure wave, and the wave propagates through the acoustic channel. In **receive mode** – the received wave is converted back to the modulated analog signal, and processed onboard in real-time, converting it back into the original digital information through signal processing. **Multiple active SWIM robots** can simultaneously communicate with the cryobot by either: 1) transmitting at distinct frequencies, or2) transmitting at one frequency, but synchronizing clocks and allocating distinct time windows for each robot to transmit.

Based on the communication protocol (FSK) and carrier frequency (20∼30 kHz), it is expected that we can transmit and receive the 1 bit per ∼100 µs, so we can send/receive the data bit as fast as 9600 bps. In future work, we will determine best possible data rate by studying the tradeoffs between transceiver power, error rate, data rate, and communication range.

4.4 Compute / Intelligence Subsystem

SWIM's onboard flight computer / intelligence subsystem must be selected to balance the competing demands of SWIM sensing capability, power usage, per-robot autonomy, and per-robot operating time. Radiation protection may also be necessary during the cruise / orbit phases of the mission. As a result, there is a sliding scale of onboard processor performance:

Analog-only Circuitry – directly coupling sensors / actuators to comms., enabling the mothercraft to fully remote-control the micro-swimmers.

Radiation-Tolerant Micro-Controllers – able to perform simple path planning based on data collected by onboard sensors or execute more sophisticated pathing based on instructions / maps generated by the mothercraft [27].

Radiation-Hardened CPUs / FPGAs – able to perform detailed environmental measurements, map construction / SLAM, and path planning onboard [112], [113].

Commercial-grade micro-processors have been successfully demonstrated on flight missions (e.g. Qualcomm Snapdragon 801 on Ingenuity helicopter) [29]. Research-grade single-chip micro-motes (e.g. SCµM, 2 x 3 mm) [114] demonstrate sufficient

capabilities for processing / control / communication in miniature form-factors with extremely low power draw. Radiation-hardened CPUs (e.g. RAD750 on Perseverance) [112] and FPGAs (e.g. Xilinx Virtex-5 on Perseverance) [113] also have a long heritage on flight projects and can feasibly operate on a PRIME cryobot, but are likely too large for SWIM robots.

As alluded to above, the degree of per-robot autonomy is also highly impacted by the SWIM robot processing, sensing, and communication capabilities. Autonomy in SWIM can range from full remote control (by the cryobot), to high-level swarm guidance (on cryobot) with local navigation and control (on SWIM), to complete local autonomy (on SWIM) with pre-programmed behaviors like sensor gradient tracking or water-column profiling. Swarm exploration techniques and a brief discussion of their associated sensing / processing requirements are further discussed in Sec. 5, but in general, greater autonomy requires greater onboard processing capabilities (and correspondingly greater power consumption).

A number of the more detailed questions regarding the degree of robot autonomy will be addressed in future work, after an initial SWIM robot concept it identified.

4.5 Power Subsystem

Multiple competing technologies also exist for energy storage elements (i.e. batteries, capacitors, fuel cells, and radioisotope power supplies), so here we survey technologies that can be packaged within a micro-swimmer, survive the Europan ocean conditions, and supply sufficient energy and power (to meet the requirements of the various subsystems), all while maximizing the operating time for each micro-swimmer.

We also briefly consider various energy harvesting or recharging strategies (e.g. ultrasound or electromagnetic energy harvesting system on the micro-swimmers for wireless recharging) and tethered options, to extend individual robot operating life beyond the limitations of a finite battery capacity.

The high-level questions to consider, when designing the power system are as follows:

How much power do robots require? Order-of-magnitude estimates of < 3.5-15 W are reasonable, based on per-subsystem power requirements aggregated in the prior subsections and listed below:

- Sensing: <<1 W
- Processing: 0.4 - 5 W (survey of cellphone processors)
- Communication: <1-4 W (at current range / frequency specs)
- Propulsion: <2-5 W (at >1 m/s currents with worst-case drag)

How long will robots operate? 10 mins to 100+ hrs, depending on the design point

How will we power the robots? Options include:

- Onboard Batteries (or capacitors, but lower power density), Wireless Energy Harvesting, and Tethers

Will you recharge the robots? Can be achieved via a dock, via wireless power transfer (ultrasound or electromagnetic), or by using propellers as generators (but need to anchor)

Considerable background research has been conducted on state-of-the-art energy storage technologies for NASA planetary science missions [115], with the main takeaways summarized below:

Primary (Single-Use) Batteries – have higher energy density than rechargeable batteries, and are viable if no recharging is necessary (e.g. if the concept of operations does not include returning to cryobot).

Secondary (Rechargeable) Batteries – enable extended ocean exploration mission duration, where robot operation is power limited and recharging is feasible (e.g. if the concept of operations includes periodically returning to cryobot).

Capacitors (including Double-Layer and Super-Capacitors) – are useful if high-power discharge is required in short pulses, but have low specific energy relative to batteries. Capacitors not expected to be a viable option for SWIM.

Fuel Cells – can offer extended discharge times and take advantage of energy-dense fuels, but require additional packaging for fuel storage / piping and produce byproducts.

For SWIM, We care about (sub) surface, non-nuclear options; and the radiation tolerance of batteries around Jupiter is something to consider. Capacitors don't provide sufficient energy for multi-hour operations, and fuel cells introduce additional challenges of fuel packaging and long-term storage. This means that batteries are the most viable option for small swimming micro-robots, unless a tether is used.

4.5.1 Battery Chemistry Options

A number of viable Primary (Single-Use) vs. Secondary (Rechargeable) battery chemistries exist, and several are flight qualified / have flow on prior NASA missions. Additional chemistries are in active development and on a path to flight qualification. A summary of specific batteries is provided in Table 4.5.

Key advantages of in-development primary batteries like Lithium CF_x (Li-CF_x) are the significantly higher energy density / specific energy and the fact that they lose ~0.5% energy / year, which works out to 97.5% charge at 5 years, 95.1% at 10 yrs, and 92.8% at 15 years. The high energy density is of particular interest to SWIM, due to the fact that that these robots are significantly volume-constrained (more-so than mass-constrained) due to packaging requirements within PRIME. Li-CFx batteries are already being considered as an option for Ocean Worlds missions (per [115]), where strict planetary protection considerations restrict the ease of using a Radioisotope Power System.

Table 4.5: Comparison of battery chemistries, including operating frequency range, advantages, and disadvantages, taken sfaasdf from [115]. Capacitor options are also provided for comparison, but are not competitive for SWIM applications.

Chemistry (Type)	**Energy Density** (Wh/L)	**Specific Energy** (Wh/kg)	**Shelf Life** (Years)	**Operating Temp.** (°C)	**Flight Qualified**
Li-SO_2 (Primary)	~250	135-150	> 10	-20 to +60	Yes
Li-$SOCl_2$ (Primary)	~400	250	> 10	-20 to +40	Yes
Li-CF_x (Primary)	600-800	400-500	> 10	-30 to +60	No
Li-CF_x/MnO (Primary)	550-600	350-450	> 10	-40 to +60	No
Li-O_2 (Primary)	700-800	500-600	5	-20 to + 60	No
Li-Ion (Secondary)	150	90-110	14+	-20 to +30	Yes
Adv. Li-Ion (Secondary)	200-300	> 150	> 20	-10 to +25	No
Adv. Solid State (Secondary)	400-500	250-350	> 20	+10 to +80	No
Adv. Li-S (Secondary)	300-350	250-300	< 5	-30 to +30	No
Supercap. (Capacitor)	–	6	> 10	-40 to +60	Yes
Li-Ion Cap. (Capacitor)	19-25	14	> 10	-20 to +60	–

Also, while most conventional batteries use a liquid electrolyte, ongoing work is pursuing solid electrolyte (solid state) batteries, which can achieve significantly higher energy densities, eliminate combustible electrolytes, and reduce / eliminate risks of thermal runaway (i.e. battery fires). Liquid electrolyte batteries use very little electrolyte, but require a stable separator in their cathode / separator / anode stack. The stack is assembled dry, then sealed in a pouch or canister and filled with electrolyte; any electrolyte not in the separator is excess. Over time gas can generate within the liquid electrolyte, and cause the battery pack / pouch to swell. For this reason, and to enable proper operation in general, batteries require 0.1-1 MPa (for liquid electrolyte) of external pressure to function. Solid state batteries swap out the liquid electrolyte and separator material for a solid electrolyte. They also typically operate under higher pressures of ~ 5+ MPa (for solid-state electrolyte).

A main concern with liquid electrolyte batteries (in particular) is that over-compression of the stack can cause shorting between cathode and anode layers are forced together under high pressure. However, prior research shows that Li-Ion pouch cells can operate nominally while being mechanically squeezed between plates up to 93 MPa (limit of machine) without failure [116], which is well above pressures at ocean-ice interface (25-50 MPa).

4.5.2 Battery Packaging Options

Batteries are typically packaged in two ways, as explained below:

Hard-Case Cells – battery stacks are pre-packaged in standardized form-factors, including cylindrical and prismatic cells. Standardization enables large-quantity manufacturing, but makes it difficult / expensive to design hard-case cells in custom form-factors for low-quantity applications.

Pouch Cell – battery stacks are die-cut into desired form factor during manufacturing, and vacuum-sealed inside a polymer pouch. Pouch cells are fairly incompressible (vacuum sealed), but require externally-applied pressure to prevent ballooning from gas. They are not currently flight-qualified by the US (but have been successfully flown by Japan)

For SWIM, it's likely most advantageous to use pouch cells, to better conform to and maximize usage of the internal volume within a streamlined micro-swimmer body.

4.5.3 Recharging

As noted above, recharging individual micro-swimmers can be achieved via a dock, via wireless power transfer (ultrasound or electromagnetic / RF), or by using propellers as generators (but need to anchor).

Each option has limitations, and imposes additional capability requirements on the micro-swimmers, including:

- Needing to return to the cryobot and navigation to a precise location (the dock or charging region) to enable power transfer, under unknown and potentially significant ocean current conditions
- Needing to maintain close proximity to these sites for charging, as RF and ultrasound waves have fairly rapid attenuation in water
- As discussed in the structure section (Sec. 4.7) below, most micro-swimmer designs will likely be negatively buoyant, and thus require active thrusters to maintain constant depth for charging (unless the micro-swimmers are able to latch onto a charging dock)

Given these constraints, we are not recommending recharging as a baseline strategy for extending micro-swimmer life.

4.6 Tethers

Tethers are commonly used in oceanographic robots, especially remotely-operated vehicles (ROVs). Depending on the tether composition, the tether can provide a **communication** (e.g. optical comms. over fiber-optic cable at 1 Gbit/sec over 10s km, or electrical comms. over copper wire (similar to DSL) at 10 Mbit/sec over 1 km), **power** (e.g. electricity over copper wire), and/or a **mechanical link** (e.g. steel wire, vectran / kevlar fiber) between two robots. Tethers typically require 2+ separate fibers for 2-way communication (optical) and power + ground (electrical). **Hybrid tethers** braid multiple wires of different types together to provide a combination of capabilities, at the cost of a thicker, heavier tether. Details on various tether compositions are provided in Table 4.6.

Tethers are typically pre-wound in spools, and can either **passively deploy** using tension in the cable to unwind the spool, or use an **actively-controlled tether management mechanism** (i.e. motor) that maintains fixed tension on the tether and can

Table 4.6: Comparison of tether designs for aquatic use, including optical, electrical, and structural tethers. Tether size asdfa information sourced from [117].

Design	Min Diameter	Notes
Bare Fiber-Optic Tether	25+ μm	Ultra-light weight, but limited mechanical strength. Enables 100s m long tethers in a few cm^3 volume.
Polymer-Clad Fiber-Optic Tether	125+ μm	Polymer-clad tethers can have pre-defined buoyancy, allowing them to float, sink, or remain neutrally-buoyant.
All-Copper Tether	2+ mm	Lower resistive power losses, at the cost of thicker, stiffer wires and larger overall diameter.
Braided Hybrid Tether	3+ mm	Braided copper round wire and optical fiber. Efficient power transmission via electricity in copper wire and communication via optical signals in optical fiber. Typically requires 2+ separate fibers for 2-way communication (optical) and power + ground (electrical).
Copper-Clad Fiber-Optic Tether	–	Power transmission via electricity / communication via optical signals.
Copper-Clad Vectran Tether	–	Structural tether, with power / communication capability using electrical signals.

Table 4.7: Comparison of tether deployment techniques for aquatic use.

Design	Advantages	Disadvantages
Passive Deployment	Cable tension unwinds the pre-wound tether spool. Simple deployment, with no mechanisms required. Pre-wound tether spools remain stationary while unraveling from inside-out, which eliminates the need for slip-rings.	Doesn't allow for tether management or retraction. In high currents, the tether can actually be deployed just due to water drag.
Active Deployment	Motorized spool with load sensing maintains fixed tension on the tether and can both deploy / retract the tether.	Additional rotating mechanism is required, and slip-rings are necessary to transfer data across the rotating spool.
Deploy from Robot	Robot has minimal tether drag when deploying, and can continue moving if a portion of the tether gets stuck on an environmental feature	Robot has to allocate space for the full tether volume
Deploy from Cryobot	Robot has minimal onboard volume devoted to tether interface	Robot has to expend extra energy to pull / deploy tether, and has higher risk of

both deploy / retract the tether. Tether spools can also either deploy from the mobile robot or from the stationary mothercraft. Details on the advantages of different tether deployment techniques are provided in Table 4.7.

4.6.1 Other Considerations

Tethers require electronic hardware on both ends of the tether, and have optical / electrical losses that can limit maximum tether length.

Optical transceivers are roughly the size of quarters, and used to convert electrical signals on the robots to / from optical signals in the fiber. Optical fibers experience optical losses of 0.25-4 dB/km, as well as recommended operating load ratings of 15-20% the fiber's ultimate tensile strength (as low as ~680 Pa, or 45 N on a 0.28 mm diameter optical fiber) and a recommended

maximum bending radius of 20 x cable diameter [117]. Fiber reinforcement with coatings or Kevlar wraps can increase the tether tensile strength, at the cost of increased diameter.

Electrical power transmission often operates at high voltages to minimize Ohmic power loss (small-diameter wires have high resistance over long distances), which requires electrical step-up / step-down converters at each end of the tether. The power delivered by the tether (P_T) and lost due to resistance ($P_{\text{Ohmic Loss}}$) are calculated below:

$$P_T = V \cdot I \rightarrow I = P_T/V \tag{4.30}$$

$$P_{\text{Ohmic Loss}} = I^2 \cdot R_T = P_T^2 \cdot R_T/V^2 \tag{4.31}$$

with copper wire resistance (R_T) of 870 Ω/km (for 0.16 mm ⌀ (34 AWG) wire) to 20 Ω/km Ω/km (for 1.02 mm ⌀ (18 AWG) wire) [117]. V is the operating voltage of the tether.

Drag on the tether in the ocean current must also be considered, and is defined by:

$$F_d = \frac{1}{2}\rho v^2 c_d A_T cos(\theta) \tag{4.32}$$

with v = ocean current velocity, c_d = drag coefficient (~1 for a cylinder), $A_T cos(\theta)$ = apparent cross-sectional area of the tether orthogonal to the fluid flow (where θ defines the angle between tether and fluid flow direction). Note that $A_T = ⌀_T \cdot l_T$, or the tether diameter ($⌀_T$) times the tether length (l_T), which can become significant for long or thick tethers (and often exceed drag on the AUV itself).

4.6.2 Failure Modes

Tethers do introduce new failure modes that are not found on untethered underwater robots, including:

Cold-Creep / Cable-Memory – tethers can experience plastic deformation due to long term storage in wound form at cold temperatures (as would be experienced on the multi-year cruise and descent phases)

Tether Entanglement / Fouling – Multiple tethers increase the chances that they become entangled with one another, or get sucked into / foul a robot propeller. Tether location is predictable if held in tension (e.g. using active tether control), but the tether can follow an unknown path if allowed to go slack. Thus, tethers can be viable if a limited number of robots are used, if all robots swim as a group in similar directions, or if all robots swim in completely different directions, but risks increase if robots crisscross paths (as some swarm exploration strategies can allow), or if the robots follow a grid-based exploration path.

Tether Drag – long tethers can have significant surface area and a high drag coefficient ($c_d \sim 1$ in cross-flow), which introduces significant drag forces in cross-flowing currents that can exceed the drag on the robot body itself. For example, a tether 125 μm in diameter and 100 meters long in a 1 m/s cross-flowing current will experience 6.25 N of drag, whereas body drag on a cylindrical robot 10 cm long and 2.5 cm in diameter is only 1.25 N:

$$F_{d,Tether} = \frac{1}{2}\rho v^2 c_d A_{\text{Tether}} = \frac{1}{2}\left(1000\text{kg/m}^3\right)(1\text{m/s})^2(1)(125\mu\text{m})(100\text{m}) = 6.25N \tag{4.33}$$

$$F_{d,Robot} = \frac{1}{2}\rho v^2 c_d A_{\text{Robot}} = \frac{1}{2}\left(1000\text{kg/m}^3\right)(1\text{m/s})^2(1)(2.5\text{cm})(10\text{cm}) = 1.25N \tag{4.34}$$

4.7 Robot Structure

The SWIM robot structure has a number of design variables to select among, including body shape, buoyancy control, and water / pressure control. Details on each of these design choices are laid about below, and a wide array of possible design points are possible – informed by the desired mission concept of operations, science requirements, and other subsystem form-factors listed above.

4.7.1 Robot Structure Constraints

As discussed in Sec. 3.2.2, the PRIME cryobot imposes a number of physical constraints on potential SWIM robot structures, including:

Volume: < 5 L (notional payload volume for single instrument)

Max Dimensions: ∅ < 25 cm, H < 10 cm (PRIME cryobot is a cylinder, notionally 23-25 cm ∅ x 3.5 m long)

Pressure: 0 MPa (in Space), to 25–50 MPa (at Ice-Ocean Interface)

Temperature: ~0 degC (in Ocean) and warm (in Space)

Misc.: Corrosion / shorting risk from water on unprotected electronics

4.7.2 Robot Body Shape

Oceanographic robots with a variety designs have been fabricated, tested, and fielded on Earth at the meter-scale, as discussed in Sec. 2.1 and Table 2.1.

These robots typically use streamlined bodies with cylindrical (e.g. torpedo), ellipsoidal, or rectangular prism form-factors, however other form-factors are also possible, such as wedges, wings / hydrofoils, spheres. The shapes of oceanographic robots on Earth have fewer design constraints than are imposed by a mission to Europa, and form-factors are often selected that maximize robot stability and payload volume (i.e. for sample collection) or minimize robot drag vs. payload volume (for efficient exploration on long-duration missions). For example:

Orpheus (1.5 m) [57] – a untethered, autonomous, box-shaped underwater vehicle, is optimized for exploring ultra-deep ocean canyons.

IceFin (3.5 x 0.23 m, 130 kg) [40] – a tethered, streamlined, autonomous underwater vehicle with oceanographic science instruments, is optimized for both deployment through holes cut / drilled in an ice sheet (small diameter) and under-ice hovering (via multi-axis thrusters).

Slocum Glider (1.5 x 0.22 m, 60 kg, 0.35 m/s) & Spray Glider (2 x 0.2 m, 52 kg, 0.1 m/s) [41]–[43] – untethered, winged, low-power autonomous underwater vehicle, are optimized for long-duration / long-distance ocean sampling missions.

A summary of these robot form-factors, drag coefficients (c_d), and advantages / disadvantages are presented in Table 4.8.

4.7.3 Swarm Composition

SWIM's concept of operations can also be designed around either a **homogeneous** or **heterogeneous** swarm of robots.

A **homogeneous** set of robots, with uniform size / sensors / capabilities, is easier / cheaper to design, fabrication, validate, and operate. Homogeneous robots can deploy from the cryobot in groups (or individually) over time to collect distributed measurements of a consistent set of ocean properties.

Table 4.8: Comparison of underwater robot body shapes.

Design	Drag (c_d)	Advantages	Disadvantages
Cylinder / Ellipsoid	0.29-0.89 0.1-0.2	Torpedo form-factor is standard for many oceanographic robots, with reliably low drag, relatively easy integration of control fins and propulsion at rear.	Poor packing efficiency in a cylinder (<75%), even if aligned along the cylindrical cryobot's primary axis, and more challenging deployment out of the cryobot.
Wedge / Hydrofoil	0.19-1.4 0.045-0.1	Delta-Wing form-factor has good packing efficiency inside a cylinder (if wedges are arrayed radially about the cylinder's primary axis) and easy deployment out the cylinder's sides.	Potentially unstable lifting body requires sufficient control surfaces (e.g. elevation / yaw flaps)
Rectangular Prism / Cube	<0.8	Simplified control for hovering in place and easy mounting of thrusters, instruments, etc.	High drag (minimal streamlining), poor packing in a cylindrical tube

Alternately, a **heterogeneous** set of robots can be used, where robots of differing sizes / sensors / capabilities deploy in groups to collect complementary measurements, deploy strategically to explore high-value targets once they are identified (e.g. cheap, small scouts vs. sophisticated samplers), or deploy in waves (e.g. to build a global map with high-data-volume imaging / mapping drones, then use cheap, small ocean-composition profiliers to safely explore across the mapped region).

4.7.4 Buoyancy Control

There are two primary ways to control buoyancy, as described in Table 4.9. The specific Europan ocean depth and pressure not currently known, but this value will be refined by Europa Clipper and Fig. 4.7 shows minimal density variation of water (<2.5%) across the predicted pressure ranges (0-50 MPa). Given the challenges of incorporating active buoyancy control into extremely small form-factors, it is likely that passive buoyancy control will be used in SWIM. SWIM robots ideally have positive or neutral buoyancy, and use thrusters / fins to controllably ascend / descend in the water. Optionally, SWIM robots can be shaped such that the vehicle body itself is a lift-generating surface to create net positive (or negative) lift when moving to counter the robot's static buoyancy.

Water density is predicted to range from 1012.5-1025 kg/m^3 at 25-50 MPa [118], [119]. Many robot components have greater density than water, which can be (partially) offset by low-density syntactic foams [120]. Syntactic foams are composed of glass microspheres that can be custom-shaped, have densities of 460-550 kg/m^3 at corresponding operating pressures of 40-60 MPa, and are rated for hydrostatic crush pressures of >60-95 MPa.

4.7.5 Water + Pressure Control

There are multiple techniques that can be employed to control the pressure and water exposure of internal components in a submerged robot, as described in Table 4.10. For the purposes of SWIM, we will likely focus on the mechanically simple solutions of flooded and potted components, to avoid devoting limited volume (and mass) to the most robust techniques like

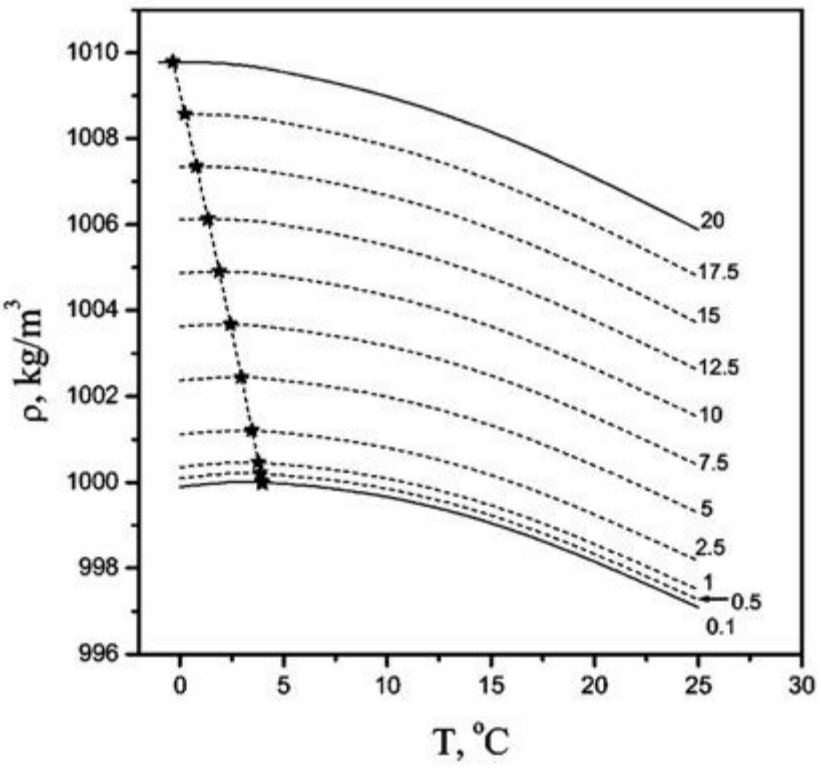

Fig. 4.7: Density of water versus temperature and pressure (in MPa), acquired from [118] and originally reported in [119]. Each curve represents the temperature-density relationship at a fixed pressure (in MPa), reported on the right side of the figure. The line crossing the curves for different pressures specifies the point maximum density. Water density is relatively constant, and increases by ~1% over 20 MPa.

Table 4.9: Active and passive techniques for controlling vehicle buoyancy.

Technique	Advantages	Disadvantages
Fixed Buoyancy	Known buoyancy achieved by balancing component density, water density, and low-density foams [120]. Robots with Positive or Neutral Buoyancy can passively float at the ice-ocean interface to conserve energy. Robots rely on lifting surfaces / flaps / thrusters to controllably generate net negative / positive lift when moving.	Robots with non-Neutral Buoyancy require constant thrust to maintain fixed depth. Robots with Negative Buoyancy require constant thrust to avoid sinking (will permanently sink after running out of power), and cannot passively rest at the ice-ocean interface to extend operating life (without an anchor). Specific ocean depth / pressure not currently known, but will be refined by Europa Clipper.
Active Buoyancy	Provides active depth control (without needing thrusters or elevation flaps), by adding or displacing water inside a pressure vessel. Ideal for performing vertical profiles of the water column, and performing close inspection of the ice crust.	Adds mechanical complexity (i.e. requires pressure vessel and piston), and consumes limited internal volume.

Table 4.10: Techniques for controlling water and pressure exposure on robotic subsystems, ordered according to mechanical complexity from simplest (top) to most complex (bottom).

Technique	Advantages	Disadvantages
Flooded	Expose components directly to the water. No additional structures required, and will automatically equilibriate to local pressure.	Can only use on components that can handle pressure and water. May require filters / gaskets to prevent particle infiltration / contamination of moving components
Solid / Potted	Fully-encase components in an epoxy or other material. Prevents implosion and keeps components dry.	Transmits some pressure to internals, and thermal conductivity of potting material must be considered to avoid overheating. A stiff epoxy will limit the pressure transmission (will deamplify the stress deeper in robot), while a flexible epoxy will transmit pressure (but sufficient if internals are pressure-rated)
Oil-Filled	Fully-submerge internal components in oil. Prevents implosion and keeps components water-free across external interfaces.	Transmits pressure to internal components, and requires a piston or bladder to adjust oil volume (adds complexity)
Pressure Vessel	Fully-encase internal components in a solid-walled vessel with sufficient strength to avoid implosion. Keeps components dry and minimizes pressure on sensitive parts.	Large mass / volume, need pressure-rated vias for external interfaces (e.g. sensors / wires)

oil-filled chambers or a pressure vessel. To do so, however, all robotic components must be capable of surviving exposure to high pressure and/or water.

A high-level summary of the per-subsystem performance is listed in Table 4.11. All components should be able to operate at the full Europan ice-ocean interface pressures (25-50 MPa) and all of components can be operated in a combination of flooded and potted states.

Table 4.11: Subsystem Performance in Water / Pressure, for standard COTS components.

Subsystem	**Pressure Rating**	**Water Rating**
Sensing	Operate at **full pressure**. MEMS sensors should be pressure-resilient, but certain packaging may need to be strengthened (i.e. IMU components operate in vacuum)	Operate **flooded / dry**, with MEMS sensors exposed to water and remainder potted / sealed
Actuation (Motors)	Operate at **full pressure**	Operate **flooded**, with wire windings coated / epoxied
Actuation (Steering)	Operate at **full pressure**	Operate **flooded**, with wire windings coated / epoxied
Communication (Transducer)	Operate at **full pressure** (transducers are rated for any depth)	Operate **flooded**, with wiring coated / epoxied
Power (Batteries)	Operate at **full pressure**, or seal inside shell (Li-ion pouch cells squeezed up to 94 MPa without shorting / failure) [116]. Outgassing possible in pouch cells if pressure drops.	Operate **dry**, with battery potted / sealed inside robot
Compute Electronics	Operate at **full pressure**	Operate **dry**, with boards potted / sealed inside robot

5 MICRO-SWIMMER SWARM SIMULATION

To facilitate the investigation of different trade-offs and future implementation of swarm algorithms in the swimming robot swarm for underwater exploration applications, we developed a 3D simulator which had already generated meaningful results that can inform the robot design process.

5.1 Simulation Overview & Implementation

The simulator is implemented in Java and uses the open-sourced graphical library named Processing (https://processing.org). The user interface of the simulator is shown in Fig. 5.1. The simulator uses forward Euler method [121] to double integrate each robot's force components (gravity, buoyancy, current force, water drag, and actuation force) to simulate robot motions (Fig. 5.2). The actuation force is governed by rules of the chosen swarm algorithm. Each robot is equipped with a sensor that sense local data of a programmable field of interest, such as the vertical linear gradient used in the following figures. The exploration ratio (explored volume over total volume) and mean square error (MSE) of the reconstructed map from sensor data compared with the ground truth are used to evaluate the efficiency and accuracy of the swarm, respectively, under various conditions – robot specs, swarm algorithms, sensor noises, and current changes of the domain. The simulator provides separate and overlay-able live visualizations (referred as views) of different variables of interest as shown in Fig. 5.3.

The simulator currently has two algorithms implemented (with more to come in future development) – flocking (Fig. 5.4a) and a custom repulsion-based coverage algorithm (Fig. 5.4b). Both algorithms use local interaction rules among neighbor robots. The flocking algorithm is a modified version based on Reynolds' rules [122], which originally includes three virtual forces – neighbor centering, velocity matching, and collision avoidance. A random virtual force is added to improve the exploration efficiency. As for the custom coverage algorithm, neighbor robots experience a repulsive force from each other thus changing their orientations. This provided a good mixing of paths which results in a high efficiency. As shown in Fig. 5.5a and Fig. 5.5b, the simulation results justify the use of multi-robot swarm to improve exploration efficiency and can be used to determine the optimal swarm size give desired mission duration and exploration ratio. Different algorithms also show different efficiency.

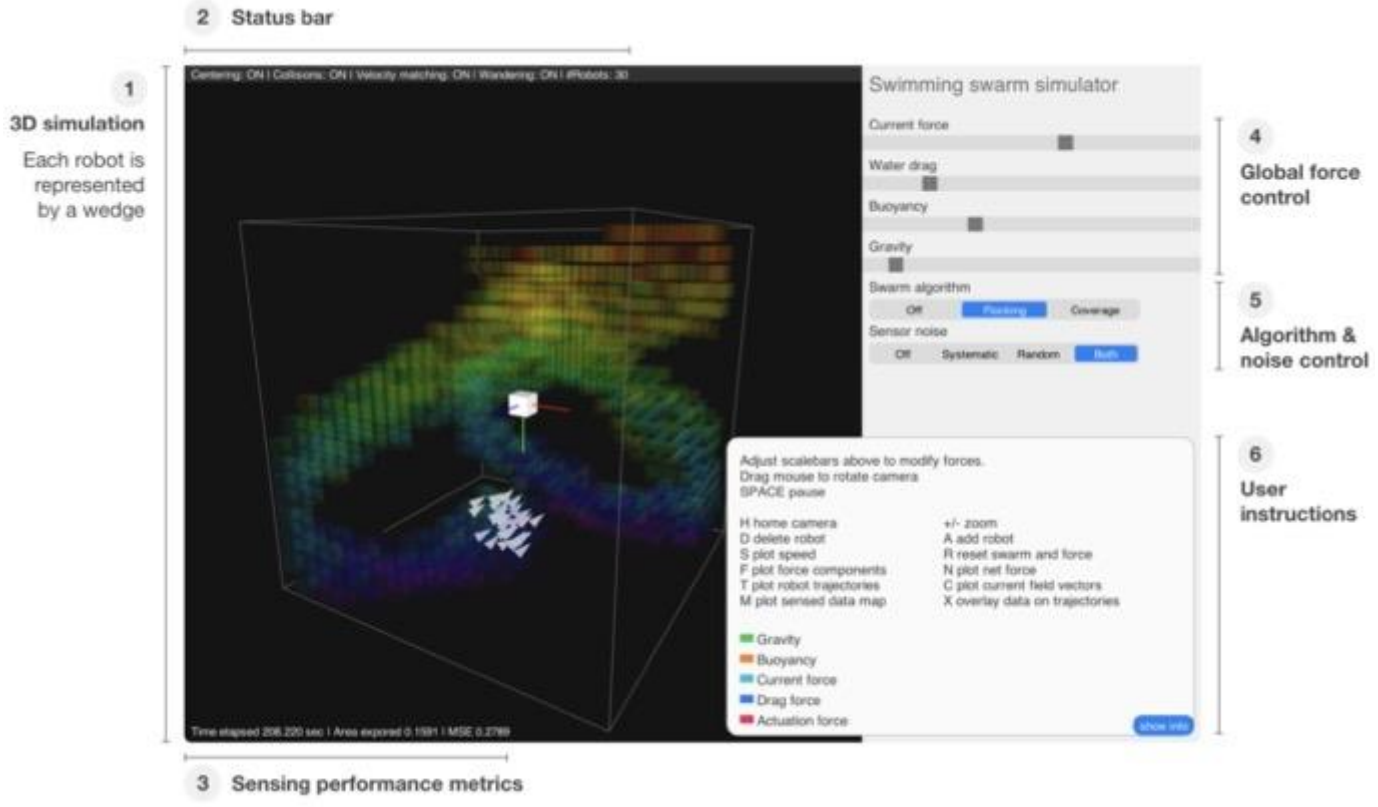

Fig. 5.1: Custom-built swarm simulator that simulates swarm behaviors under different algorithms and environmental conditions.

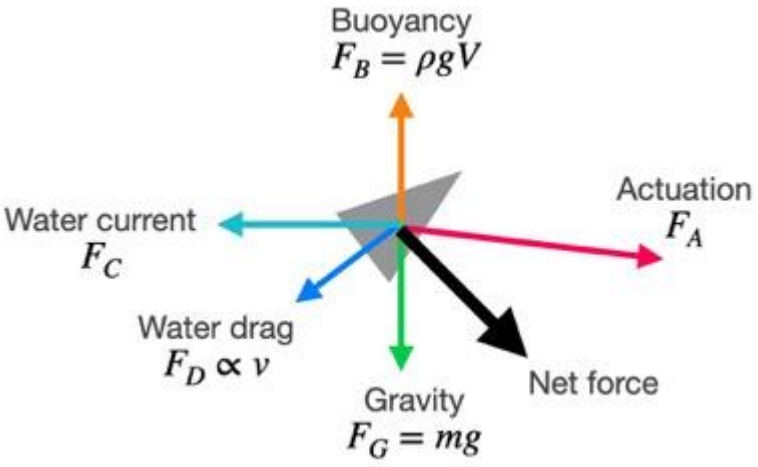

Fig. 5.2: Robot force components considered in the simulator.

Out of the two algorithms implemented thus far, the coverage algorithm is more efficient than the flocking algorithm due to less repeated search.

Besides exploration efficiency, another advantage of deploying a swarm of robots is improving data accuracy. Both systematic error due to calibration variation and random error cause by sensor noise are modeled in the simulator. Table 5.1 summarizes the two errors modeled. Larger swarm is more advantageous due to the redundancy of robots and sensors (Fig. 5.6). Fig. 5.7 is a simulation result of swarm of different sizes with the presence of systematic and random errors. As shown, a single robot has a persistent signal offset when compared to the ground-truth due to systematic error. The larger the swarm size, the closer the reconstructed signal map gets to the ground truth thanks to repeated search from multiple robots.

The basic infrastructure of the simulator has been completed, including object classes of robot and data map, a user interface to visualize data and adjust simulation parameters, back-end codes to export data, and multiple keyboard shortcuts for simulation controls such as adding/deleting robots and pause/continue simulation. This enables easy expansions of more swarm algorithms, visualizations, and sensing scenarios in future versions and can assist with defining robot specs, tuning swarm algorithm parameters, and validating experimental results.

In future developments, we will enhance and use the simulator to 1) iteratively test and optimize swarm control strategies in more realistic Europan conditions, 2) improve the robustness of the swarm control strategies to make SWIM network resilient to individual failures for reliable exploration, and 3) validate the model / and refine model fidelity (of the robots dynamics) based on measured real-world test results. Specifically, we plan to:

- Implement state-of-the-art control strategies for swarm exploration and signal gradient tracking through simulation, with a particular focus on algorithms that require minimal actuation, sensing, communication and computation capabilities.
- Perform reliability analysis and optimize control strategies to guarantee robustness of overall swarm exploration performance, in the presence of identified per-robot failure modes.

Table 5.1: Sensing data error sources and effects with small vs. large swarms.

	Systematic Error	**Random Error**
Source	Calibration error	Sensor noise
Small Swarm	Cannot be fixed	Can be fixed at the cost of efficiency with longer mission time and repeated search of the domain
Large Swarm	Can be fixed by averaging data from multiple robots	Can be fixed with high efficiency with more robots

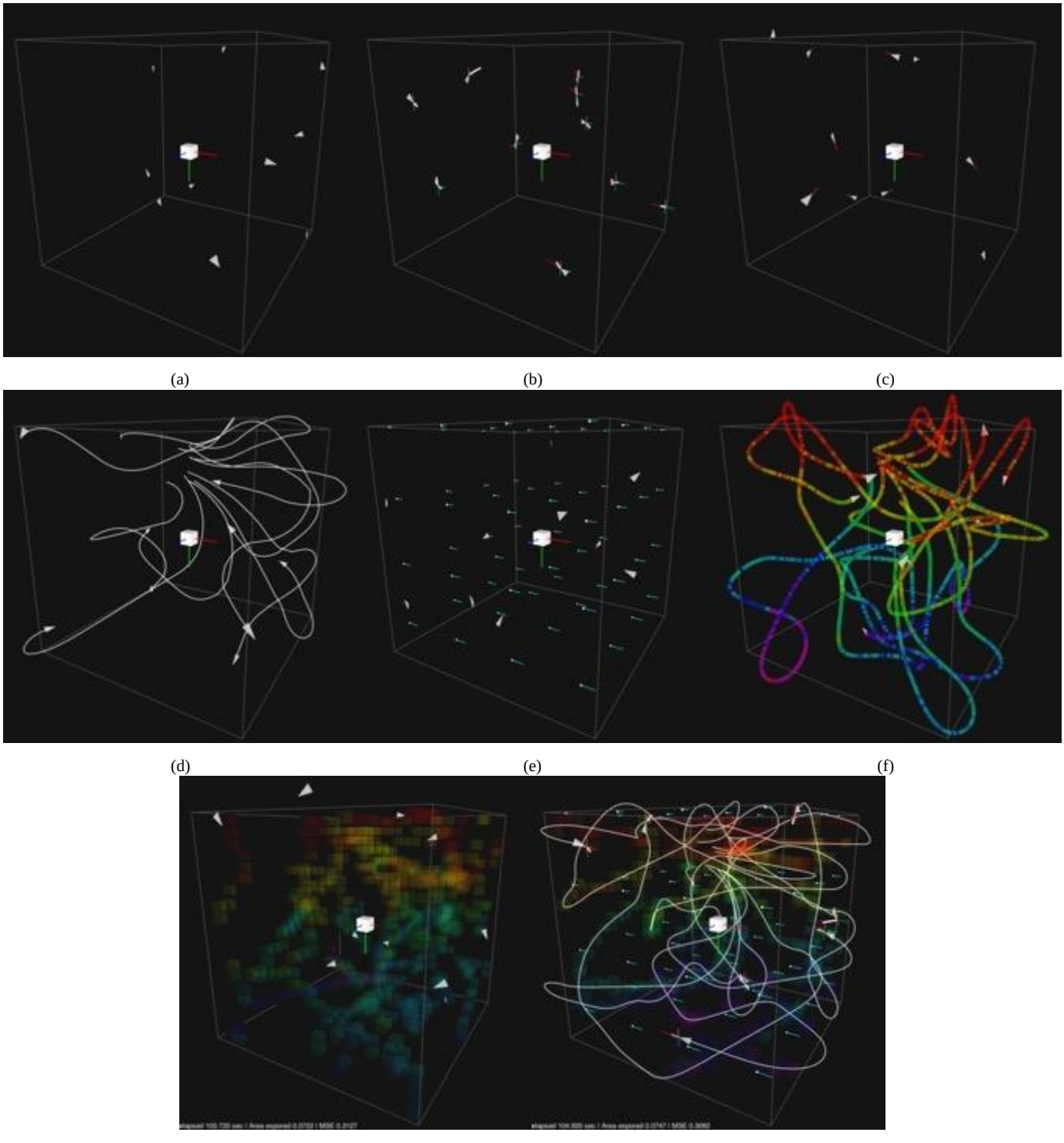

(a) (b) (c)

(d) (e) (f)

(g) (h)

Fig. 5.3: Simulator views: (a) robots-only, (b) force components, (c) speed vector, (d) trajectories, (e) water current field, (f) individual robot's data, (g) reconstructed data map from all robots' data, and (h) mixture of multiple views.

- Implement time- and spatially-varying environmental features, including ocean velocities (diurnal tidal variation expected on Europa), non-uniform temperature gradients (to differentiate between the thermal bubble around the cryobot and potential temperature anomalies at the ice-ocean interface), and irregular chemical signals (e.g. convecting / advecting / diffusing in the water from a point source), for high-fidelity simulations.

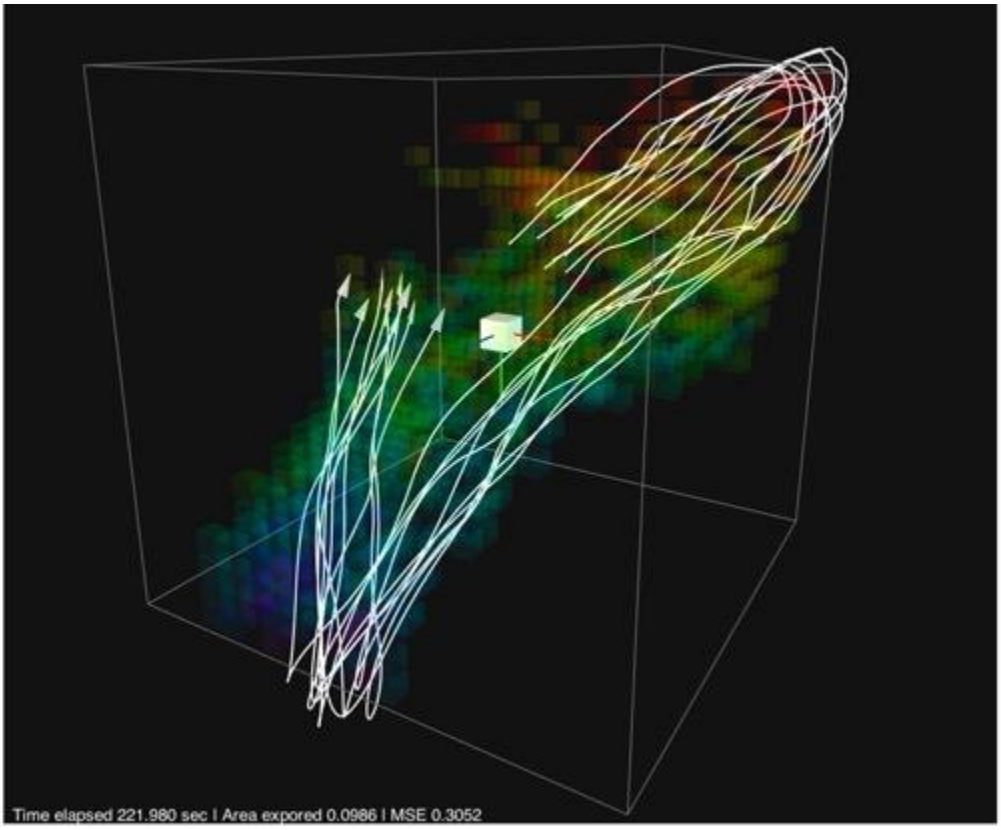

(a)

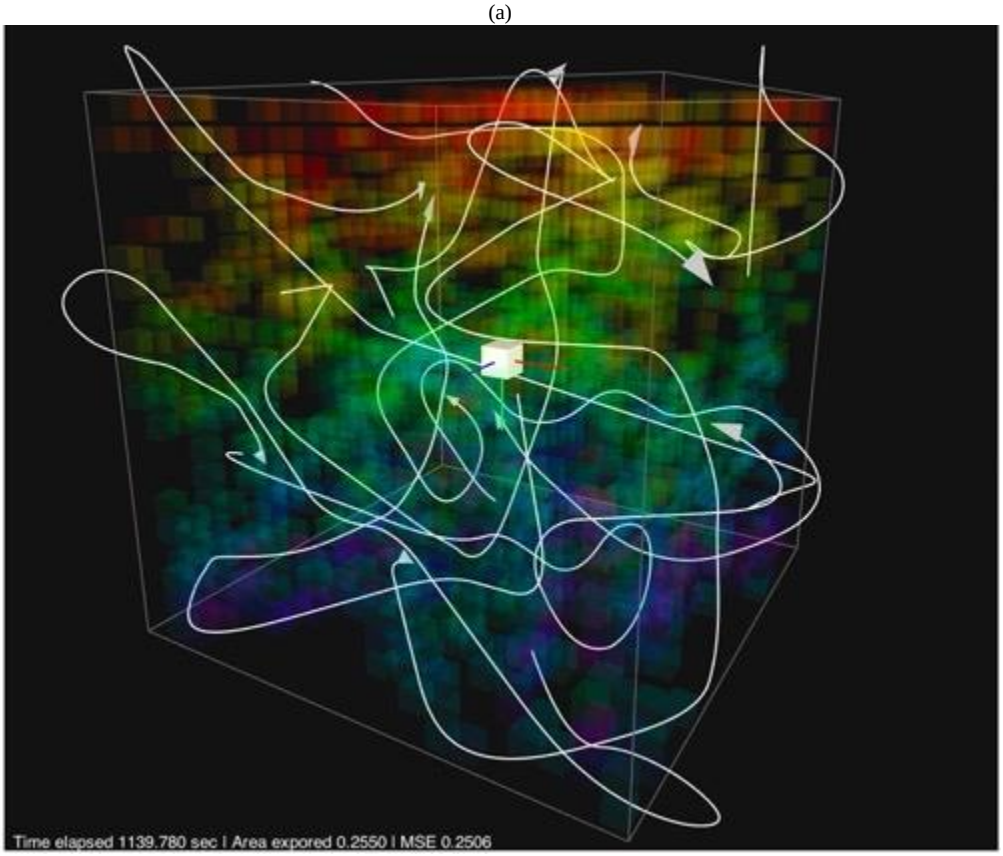

(b)

Fig. 5.4: Swarm algorithms implemented in the current version of the simulator: (a) flocking and (b) custom repulsion-based coverage algorithm. White lines plot the trajectories (partial) of individual robots.

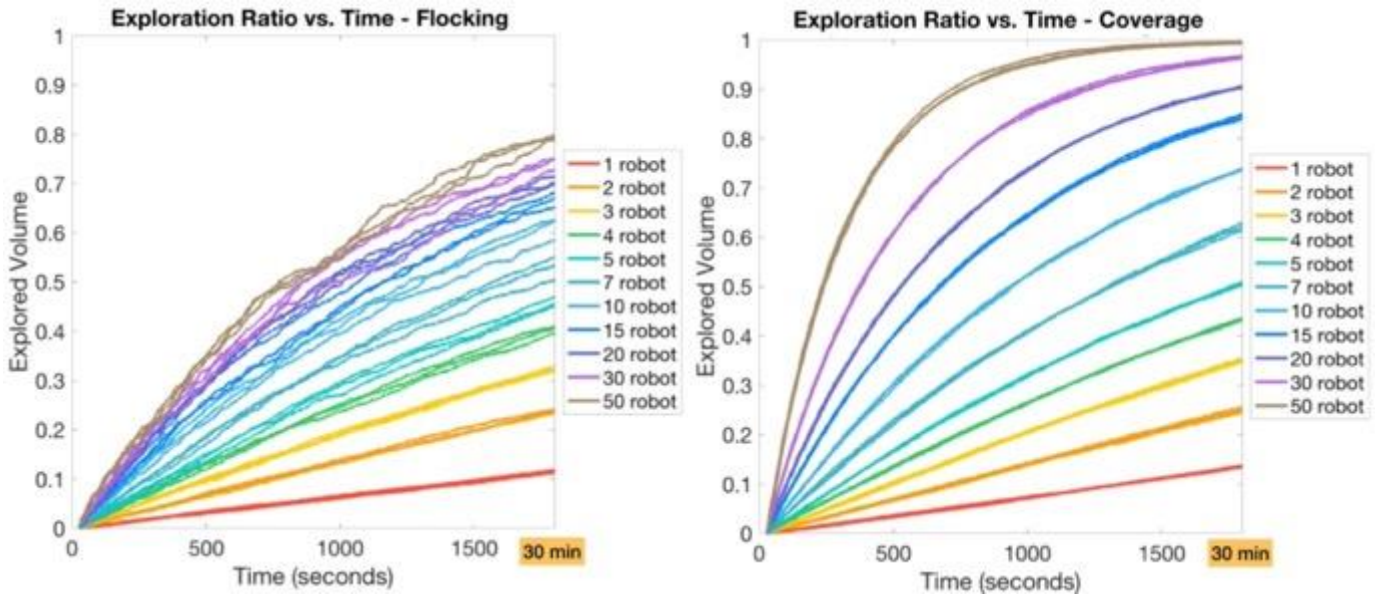

(a) (b)

Fig. 5.5: Simulation results (N = 3) of exploration ratio vs. time of a total 100×100×100 m^3 volume with various swarm sizes under flocking algorithm and custom coverage algorithm, respectively. More algorithms will be developed.

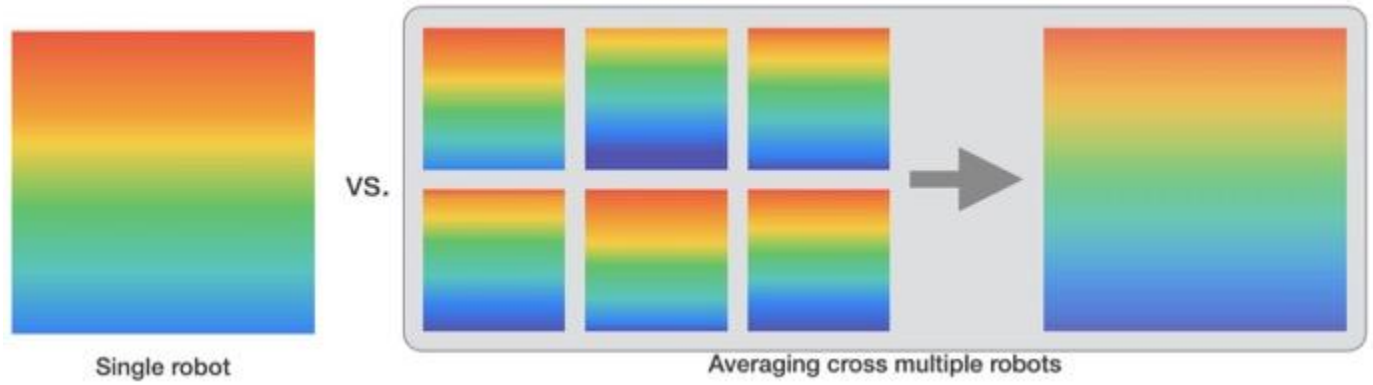

Fig. 5.6: Illustration of how large robot swarm can improve sensing accuracy with the presence of systematic errors.

- Implement physics-derived models for robot mobility, and then refine these models with experimental data from the physical robot testing.

We will use simulation results to inform the degree of communication, state awareness, and environmental awareness that each robot needs (of the world and all other robots), and use that to determine best strategies for estimating range between robots (e.g. measure sonar ping strength, or actively communicate positions among all robots, or communicate position to a central controller that then gives individual robots goals that avoid each other) and to the environment (e.g. use forward-/ upward-looking sonar, a camera, or just detect / recover from collisions after they occur). The most promising swarm strategies in simulation will eventually be implemented on SWIM robots.

5.2 Relevant Swarm Algorithms

Swarm algorithms coordinate robots either implicitly using local interactions (sensing and communication) among robots or explicitly by commanding robot motion to achieve functionalities including creating coverage, formation, and source seeking to achieve coverage or formation, which are the important building blocks for more complex environmental sensing missions [123]. We have surveyed swarm algorithms which are relevant to our application of underground exploration. The goals are to find

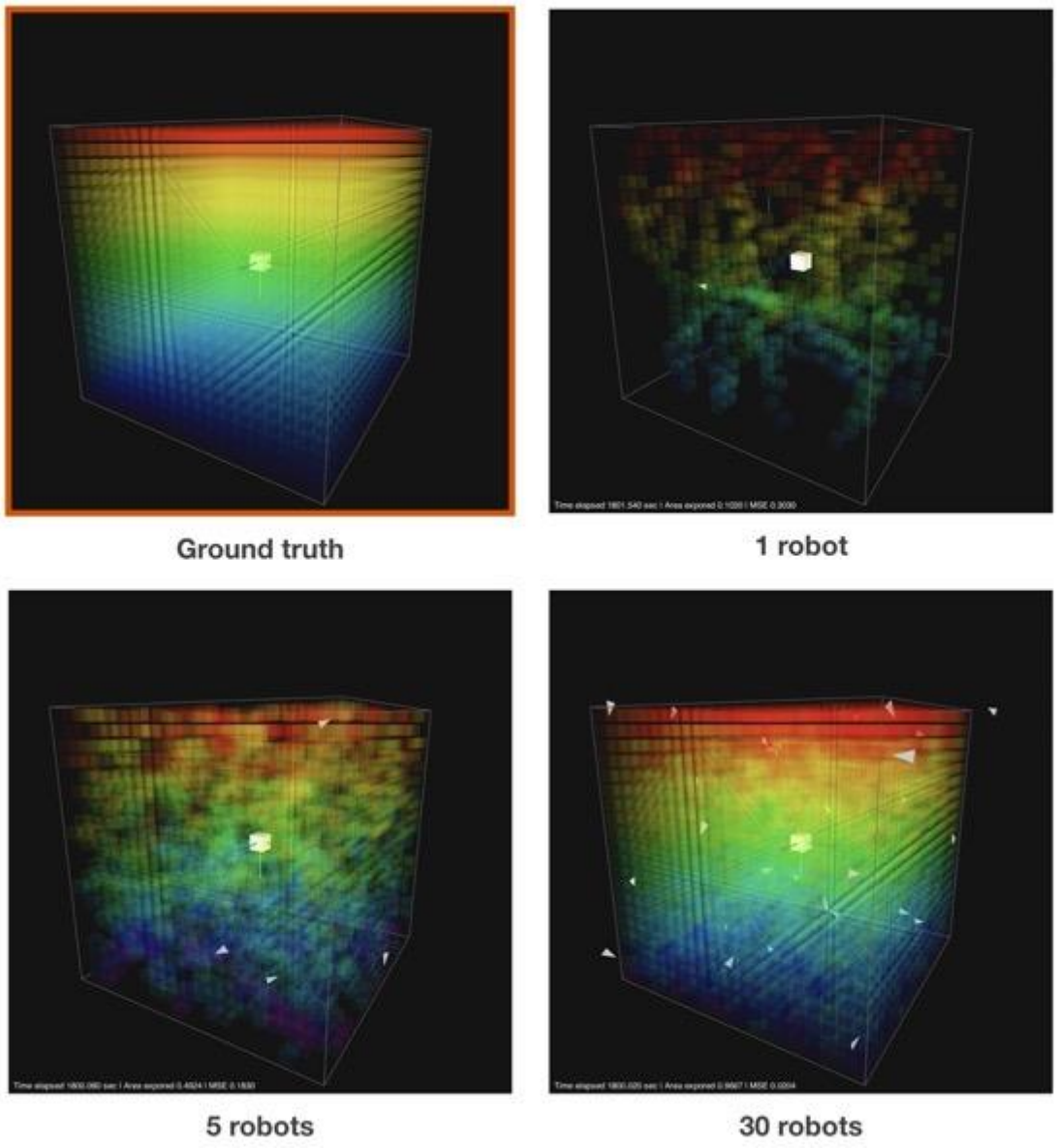

Fig. 5.7: Simulation results of swimming robot swarm with sensor noises. Averaging measurements across increased numbers of robots reduces the overall measurement error, relative to the ground truth.

promising swarm strategies that can enhance exploration efficiency and the accuracy of data collected by multiple robots, as well as to cope with different environments and exploration missions. Algorithms of interest include flocking, coverage control, random walk, and formation control.

Flocking behavior widely (wildly) exists in the nature – from fishes to land animals to birds. In 1987, Craig Reynolds proposed a way to model and simulate the flocking behavior using a set of local rules computed individually for each agent based on its perception [122]. The rules are collision avoidance, velocity matching, and flock centering (Fig. 5.8). When implemented in robotic swarms, such flocking algorithms ensure robots stay grouped while avoiding collision without explicitly regulate the path of each individual robot. These are useful for underwater applications as long-range communication and sensing maybe impaired and the swarm must rely on local rules and data. Since the first implementation of Reynolds' algorithm, more theoretical studies on flocking mechanisms emerged [124]–[127]. In a recent article, Reza Olfati-Saber consolidated the separation and cohesion terms and introduced two virtual agents – β-agent for obstacle avoidance and γ-agent as a virtual leader of the swarm. It was proven that the addition of the virtual leaders always ensures cohesion of the swarm, in contrast to the frequent fragmentation that happens under Reynolds' rules [124]. Virtual leaders can also guide the swarm to minimize repeated search / enhance efficiency.

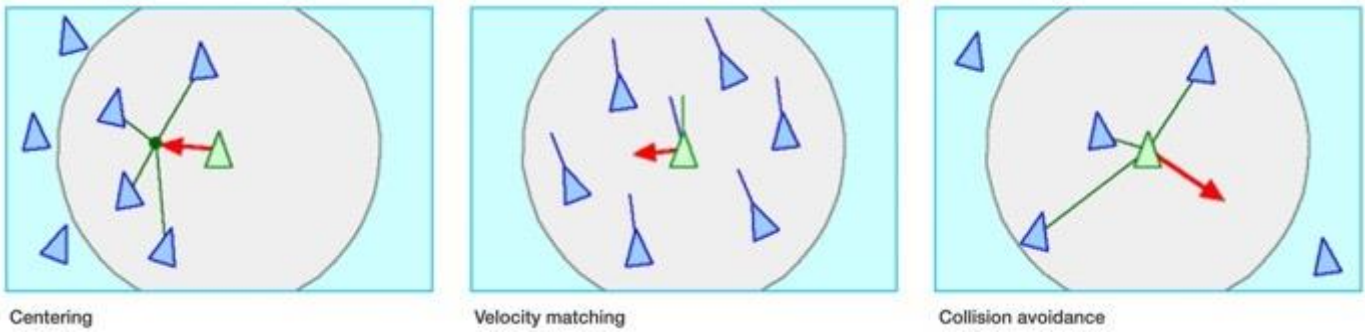

Fig. 5.8: Flocking algorithm (Reynolds' rules) [122].

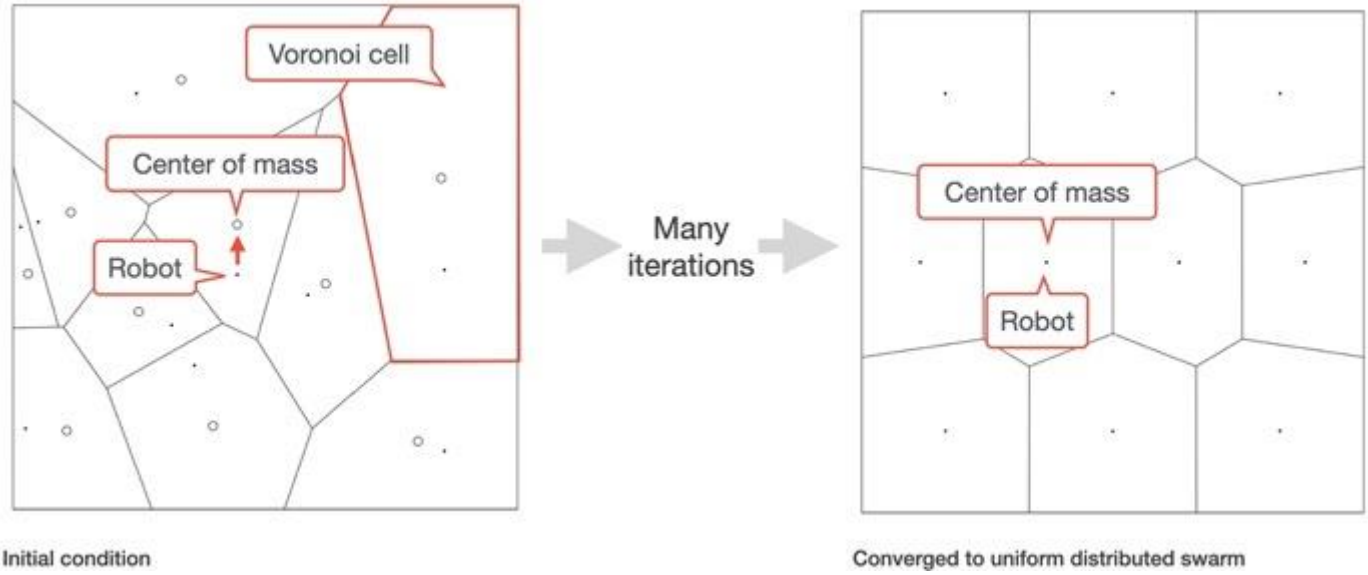

Fig. 5.9: Lloyd algorithm for coverage control [128].

Coverage control algorithms aim to optimize the distribution of robots inside the domain [129]. One of the commonly used algorithms for coverage control is Lloyd algorithm [130]. Lloyd algorithm starts by partitioning the domain based on proximity to agents, and then moves agents to the centroid of each partition (Fig. 5.9). By iterating the process, the partition converges to centroidal Voronoi tessellations [128]. It is possible to modify Lloyd algorithm to concentrate more robots near regions of interest by computing the center of mass of each partition (instead of centroid) as weighted by a density function corresponding to the importance of the region [129], [131]. This allows the swarm to collect more data in areas that are most relevant to the sensing objectives (for example, where the gradient is high). This can result in a more accurate reconstruction of the sensed data map. In addition, the swarm can redistribute when the environment changes, which is suitable for time-varying sensing applications [132].

Random walk is a commonly used exploration strategy, which has a minimal sensing and processing overhead [133]. The two common types of random walk are Brownian diffusion and Levy flight [134]. Brownian diffusion is the random motion of particle in a fluid due to collision with other particles [135], [136]. Levy flight has step sizes following a long-tailed Levy distribution, which allows individuals to move a long distance in a single step with a small probability [137]. Works had shown increased search efficiency of Levy flight compared to Brownian diffusion [138], [139]. The drawback of random walk revolves around its poor search efficiency due to repeated searches, which can be more problematic in robotic swarms as robots could also repeat search done by each other (Fig. 5.10). Works had shown that search efficiency can be improved by limiting step sizes in a pre-distributed swarm [133], creating artificial fields to repel robots [140], and sharing information about the searched area [141].

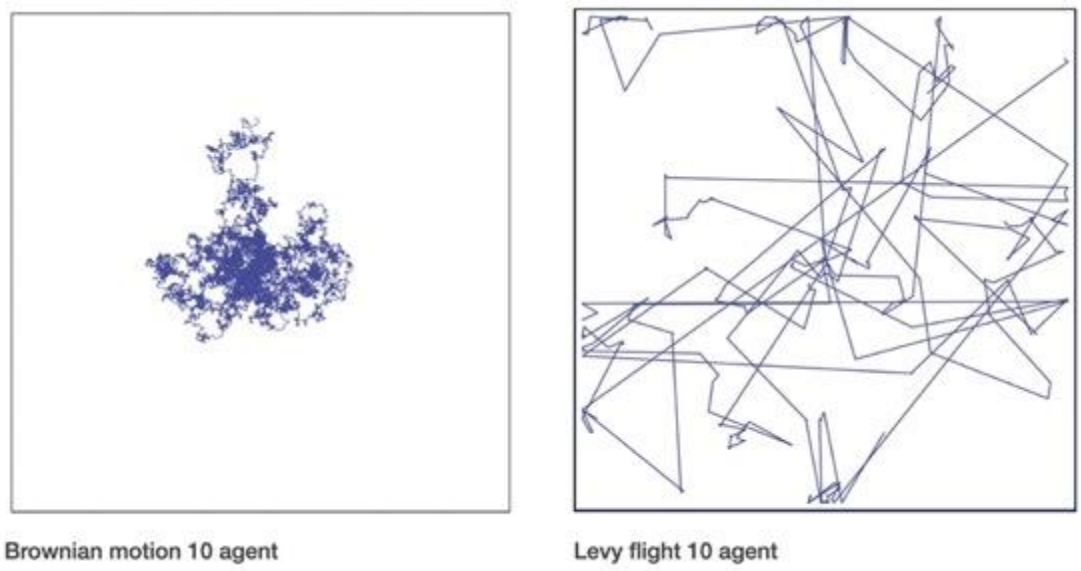

Fig. 5.10: Random walk methods with a swarm of 10 robots: (a) Brownian diffusion and (b) Levy flight. [133]

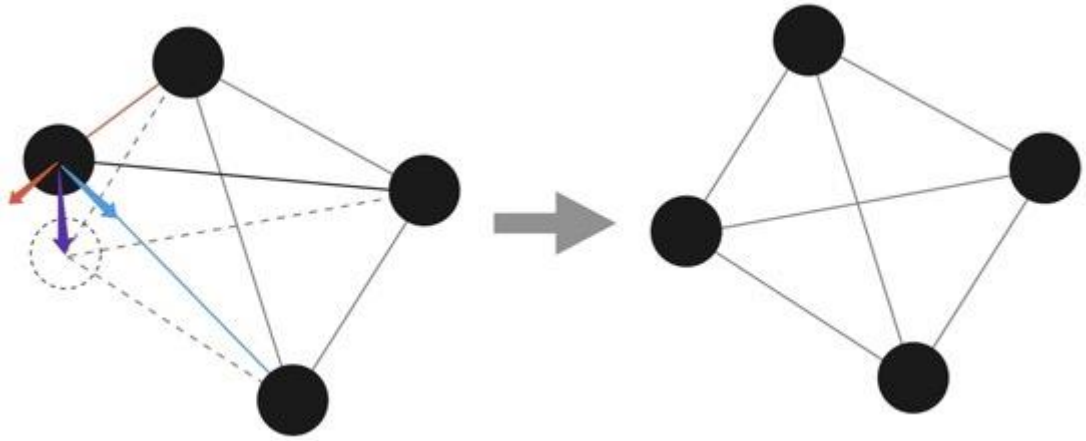

Fig. 5.11: Distance-based formation control.

Formation control aims to achieve specific formations in multi-robot systems [142]–[145]. This compliments the flocking algorithm above as it can define the exact formation that can be more useful in scenarios such as forming arrays of robots to collect equally distanced data points or create formation that optimize the fluid dynamics of the swarm under the presence of strong underwater currents. Formation control algorithms generally use a set of constraints, which can be categorized as: position-based, displacement-based, or distance-based with different sensing and network topology requirements [142]. For example, in distance-based formation control (Fig. 5.11) the robots move to correct the relative distance error (or cost) with neighbor robots and the swarm converges to the desired formation. However, this requires the graph formed by the swarm to be rigid, yet the formation is invariant to translation and rotation (i.e., the whole swarm can move together in the domain).

Table 5.2 compares these common swarm algorithms in terms of advantages, disadvantages, and sensing requirements. Optimal algorithms will be simulated and developed for the proposed swimming micro-robot swarm using these algorithms as building-blocks with their parameters optimized. Multiple algorithms will be combined / sequenced for more complex usage scenarios.

Table 5.2: Comparison of relevant swarm algorithms.

Algorithm	**Random Walk**	**Flocking**	**Lloyd's Relaxation**
Advantages	Easy computation; No sensing or communication	Mimic fish schooling; Maintain robot cluster; Collect multiple local data simultaneously	Distribute robots uniformly
Disadvantages	Low efficiency due to repeated search	Low efficiency due to repeated search	Computation of Voronoi cell and center of mass are expensive; End stage is static (still need other algorithms)
Sensing Reqs.	None	Neighbor robots' relative positions	All robots' global positions; Global boundaries
Implemented?	To be developed	Yes	Not planned

Algorithm	**Repulsion-Based Coverage Algo.**	**Distance-based Formation Control**
Advantages	Good efficiency; Simple computation; Collect multiple data across a wide area	Position robots in predefined patterns
Disadvantages	Repeated search	A rigid formation is computation heavy
Sensing Reqs.	Neighbor robots' relative positions	All robots' relative positions (rigid formation)
Implemented?	Yes	To be developed

6 MICRO-SWIMMER SYSTEM DESIGN

Over the course of this task, we developed 4 micro-swimmer concepts, whose capabilities are guided by the Science Traceability Matrix / mission requirements (Sec. 3) and based on the results of our subsystem trade studies (Sec. 4). The 4 concepts include a "Delta-Wing" concept (Sec. 6.1), a "Dragon Kite" concept (Sec. 6.2), a "Twister Pod" concept (Sec. 6.3), and an "Ultrasound Swimmer" concept (Sec. 6.4).

Our goal for each design was to develop a micro-swimmer system architecture based on the best candidates (including an initial CAD model and high-level component selection). As viable micro-swimmer designs exist at multiple size scales, we evaluated / scored / ranked the capabilities of the three best candidates to converge on a single preferred SWIM robot design, the "Delta-Wing" concept (Sec. 6.5).

6.1 Delta-Wing Concept

The "Delta-Wing" Concept (Fig. 6.1) consists of ~48 untethered, independent, powered, steerable robots that are each ~6075 cm^3 in volume. Details of the robot design can be seen in Fig. 6.2 and Table 6.1. Robots can be deployed from the PRIME cryobot individually or in a swarm, and each robot contains volume allocations for science payload (pressure, temperature, etc.), an ultrasound transducer (for 2-way wireless communication), a battery (~2 hours of power), a microprocessor, two thrusters for actuation, and three flaps for steering. This concept is inspired by and named after other delta-wing airplanes. It is the **preferred micro-swimmer concept for SWIM**, as it provides the best balance of redundancy, unconstrainted mobility, active exploration, and targeted sensing.

Reasonable structural modifications can be made to expand the internal volume of the micro-swimmer from 60^3 to 67.575 cm^3. Volume allocations for comms., compute, thrust, and steering are all relatively fixed, so additional volume can

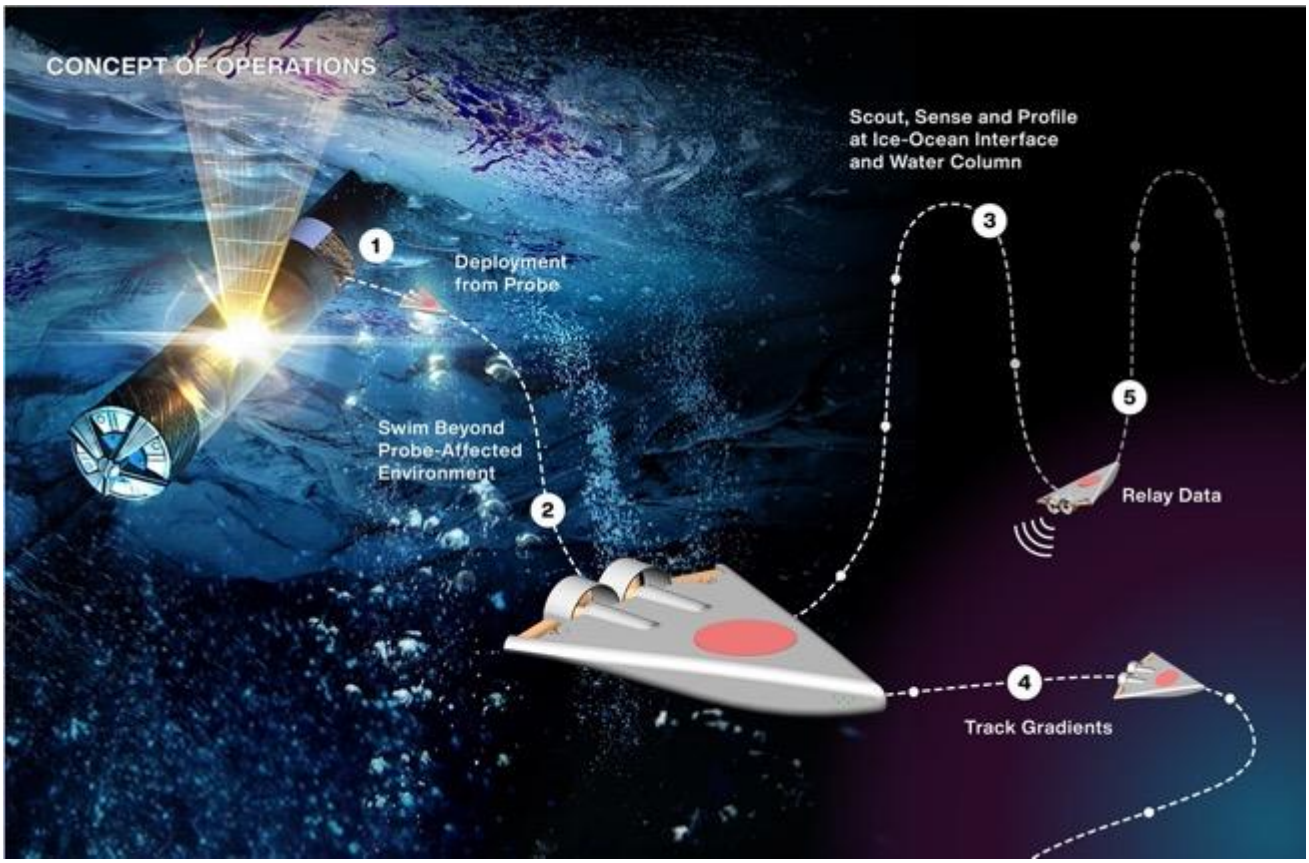

Fig. 6.1: Delta-Wing Robot Concept of Operations, where 48 robots are deployed in waves over the course of 1+ Europan diurnal cycles to perform swarm-based exploration, ocean profiling, and signal gradient tracking. Data is relayed back to the cryobot via ultrasound.

Table 6.1: Delta-Wing Concept subsystem volume, power, and mass allocations for a 60 cm^3/unit, 48 unit configuration, plus additional details of interest.

Subsystem (Type)	**Volume** (cm^3)	**Power** (W)	**Energy** (Wh)	**Notes**
Sensing (Ocean Comp.)	2.0	0.10	–	–
Actuation (2x Thrusters)	10.5	2.0	–	Motors from [111]
Actuation (3x Flaps)	2.0	0.5	–	–
Comms. (Ultrasound)	7.0	0.1	–	1 W at 10% duty cycle, 30-35 kHz, $>$ 1 km max range
Compute (2x Microprocessor)	5.0	0.5	–	Redundant processors (Snapdragon or similar)
Power (Li-CF_x Battery)	10.0	–	5.6	600 Wh/L, discharging by 0.5%/year for 15 years
Structure (Epoxy / Foam)	23.5	–	–	20% Epoxy / 80% Syntactic Foam [120]
Total	60	3.2	5.6	1.75 hr run time, 15 years into mission

predominantly be allocated to additional power and/or sensing. Drag should increase relatively minimally, as the vehicle cross-sectional area remains unaffected. As a result:

67.5 cm^3 Configuration – Battery volume increases to 15.3 cm^3 (8.6 Wh), which increases run time to 2.7 hrs (structure increases to 26 cm^3)

75 cm^3 Configuration – Battery volume increases to 20.4 cm^3 (11.4 Wh), which increases run time to 3.6 hrs (structure increases to 28.5 cm^3)

Due to the limited life but large number of robots, the current concept of operations (Fig. 6.1) for the delta-wing robots is to deploy waves of 4-8 robots at a time and operate until the batteries are exhausted (without recharging). Waves of robots are deployed across 1+ full diurnal cycles, with the frequency of deployments to determined in the future by the science team. As the baseline Delta-Wing concept has all robots sharing a uniform set of sensors, the micro-swimmer swarm is able to collect temporally- and spatially-distributed measurements of a consistent set of ocean properties and chemical compositions.

The one major limitation on this concept is that individual robots are likely negatively buoyant, due to per-robot volume constraints that limit the amount of syntactic foam [120] available to generate positive buoyancy. As a result, the robots will be required to operate their thrusters at all times to generate sufficient lift to maintain proper depth. One (small) advantage of negative buoyancy is that the delta-wing robots can also be used as depth probes near the end of life – intentionally operating in a sensing- and communication-only mode (without thrust) while drifting into the depths and collecting a vertical water column profile until reaching crush-depth or exceeding communication range.

Sensing – Our **baseline scientific sensor package** consists of a suite of MEMS ocean composition sensors, including: temperature, pressure, salinity, redox, and pH.

Additionally, our **baseline state estimation sensor(s)** enables robot localization via dead-reckoning (using a 9-DoF IMU with MEMS accelerometer, gyroscope, and magnetometer), possibly supplemented with a flow sensor for improved accuracy.

Total volume for the combined scientific / state estimation sensor package is predicted to be ~1-2 cm^3, depending on the number

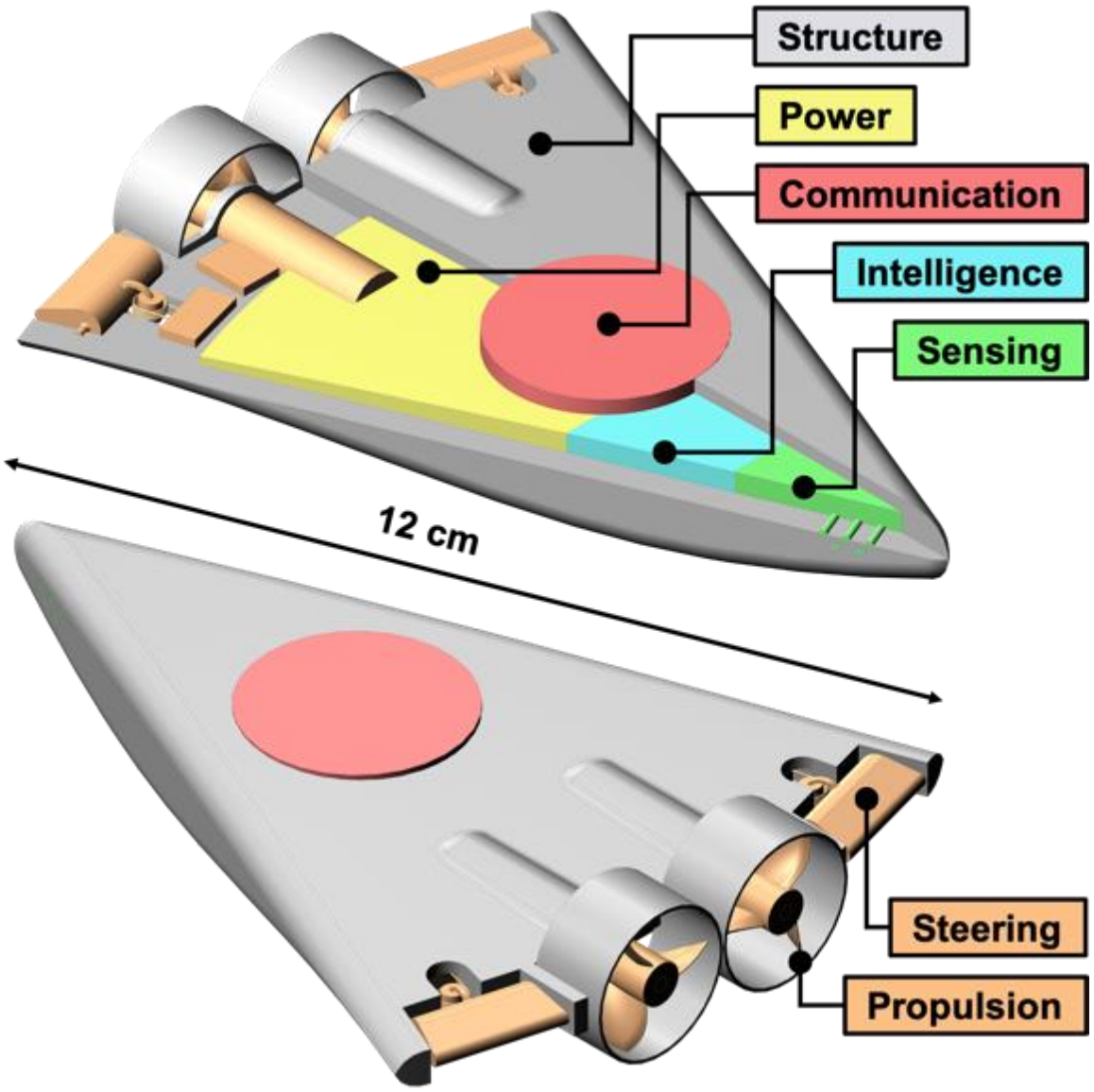

Fig. 6.2: Delta-Wing Robot Concept, including 2x propellers / motors for redundant thrust, 2x elevator flaps, and 1x rudder flap (below vehicle, not shown).

of components co-fabricated / co-packaged on a single wafer, and total power is estimated to be ~100 mW (based on current sensor performance).

We would also like to leverage the delta-wing's onboard ultrasound transducer (used for 2-way communication) as a sonar beacon for ranging (i.e. estimating distance to cryobot) – a long baseline (LBL) acoustic positioning system could be deployed from the PRIME cryobot to further refine micro-swimmer position localization. Doppler velocity logs (DVL) are ideal for improving state estimation and measuring flow velocity, but current DVLs are 100-250 cm^3 [108], which is one order of magnitude too large for the Delta-Wing concept.

Mobility / Control – Our baseline robot design (Fig. 6.2) will employ 2 motors with propellers for redundant thrust, and 2 horizontal elevator flaps / 1 rudder flap (not shown, on robot underside) for steering.

For thrusters, we identified miniature brushless DC (BLDC) motors of the correct form-factor for a 100 cm^3-scale microswimmer (∅ 8 mm x 23 mm length [111]) that are included in the illustrated Delta-Wing model (Fig. 6.2). As discussed in Sec. 4.2.1, we developed a model to calculate per-motor thrust vs. power and the robot velocity vs. motor power in water (Fig. 4.1). This model uses wedge drag coefficients of ~0.18, two robot characteristic beam lengths (L_b = 4, 8 cm), and a pair of motors

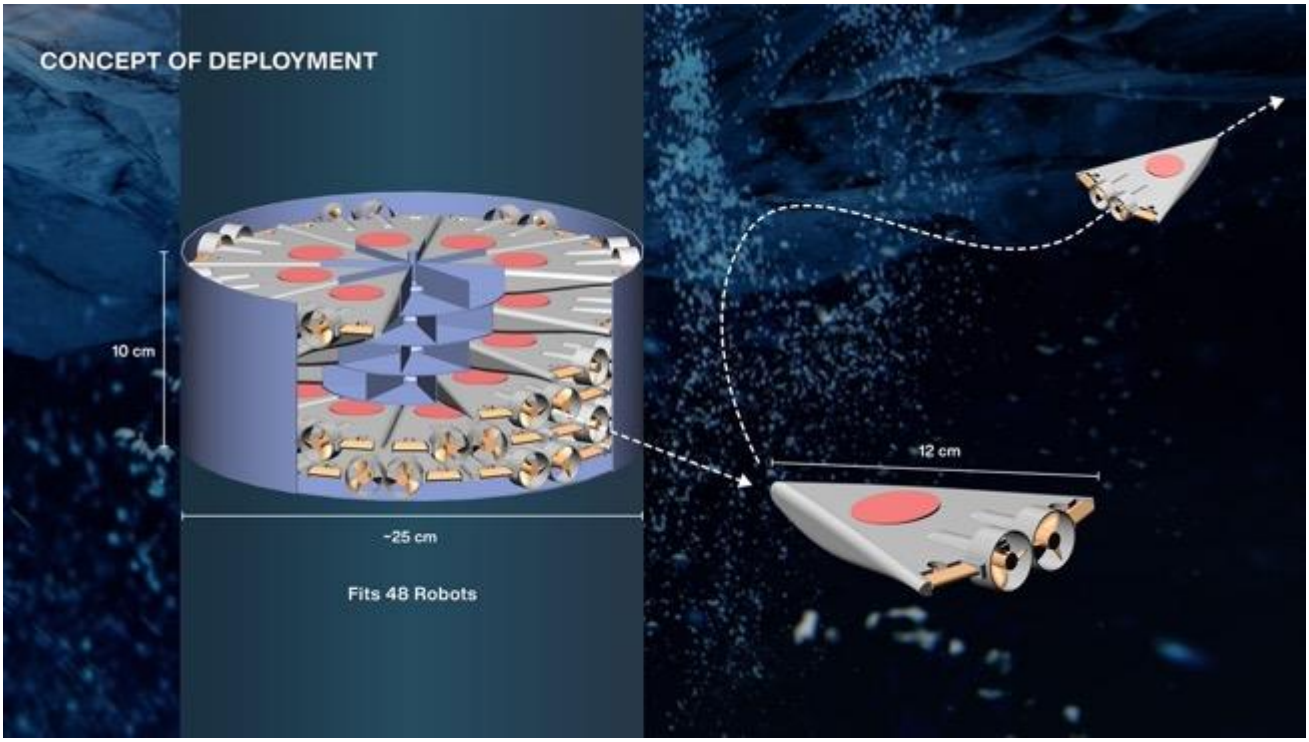

Fig. 6.3: Delta-Wing Robot Concept of Deployment, where 48 robots can be stored in circular arrays within the PRIME cryobot (6 layers with 8 robots per layer). Robots reverse out backwards from the cryobot payload chamber before navigating off on a mission.

for thrust with two possible propeller diameters (D_p = 1, 5 cm). In all plotted configurations (which **bound current viable designs** for the delta-wing concept), these commercial motors generate sufficient thrust to swim at multiple times the 1 m/s predicted Europan ocean velocity while remaining below the motors power requirements. Finally, while the modelled motors [111] are not waterproof, other commercial BLDC motors at 2-3x sizes are waterproof [146], and future work will study necessary steps to fabricate waterproof motors at our desired sizes.

If we are able to operate at the predicted performance levels, then each robot has an endurance of ~6.3 km over 1.75 hours of operation at 2 m/s (maneuvering constantly at 1 m/s into the 1 m/s maximum predicted current).

For steering, we are currently baselining the use of solenoid actuators for controlling deflection of the flaps. This technology has been successfully demonstrated on the BlueSwarm robotic fish [38], [39], [147] to actuate fins for both thrust and steering, and proves to be highly reliable, compact, have large stroke-lengths, are easy to water-proof, and are easy to control. Other mechanical actuation technologies are viable, but less attractive: servomotors are bulky and harder to waterproof, piezoelectric actuators require high voltages and have small stroke lengths, and dielectric elastomer actuators have similar issues to piezoelectric actuators, plus risk long-term material degradation.

Communication – Our preliminary design operates a 30 kHz free-flooded ring transducer (⌀ 4.5 cm x 2.5 cm), that transmits 9.6-16.6 kbps while employing FSK modulation for high error robustness [148]. This design provides >1-2 km theoretical range at < 1 W electrical power, and already exists as a commercial transducer. We are also considering operating a 50 kHz free-flooded ring transducer, which allows us to shrink the transducer size to ⌀ < 2 cm while still maintaining > 1 km range at similar electrical power. These designs provide sufficient data rates (for the baseline ocean composition sensor modules) with high robustness to Europan ocean noise / environmental effects.

If we do opt for a subset of "mapping / imaging" delta-wing robots with multi-spectral imaging sensors, then those robots would also require a wireless optical communication system or fiber-optic tether that is not well-defined or baselined in the design at this time.

Power – Our baseline design uses Lithium-CFx primary batteries in pouch-cell format for power. Within a 60 cm^3 delta-wing

robot, allocating 10 cm^3 (17% of total volume) to this battery provides sufficient power for ~1.75 hours of operation per robot. This also accounts for the ~92.7% remaining state of charge in the battery, assuming 0.5% decay per year, if deployed after a 15-year delay from manufacturing [115].

Our decision to use primary battery cells is based on two key advantages:

- Primary cells have greater volumetric energy density than secondary cells, even after partially discharging over 15 years
- Primary cells avoid the operational challenges of recharging a swarm of robots, either onboard PRIME or once deployed into the ocean

This also enables us to avoid use of a **Tether**, which would present considerable challenges / entanglement hazards in a large swarm of active robots.

Integration / Deployment – 48 delta-wing robots enable efficient packing in circular arrays within the PRIME cryobot (6 layers with 8 robots per layer) on a central spindle, and secured to this spindle with launch-locks until ready for deployment. The storage chamber is designed to be at equilibrium with the external environment throughout the cruise / descent phases of the mission. At least one panel / door on the side of the cryobot is required to drop away in order for the robots to maneuver out into the ocean.

Several launch-locking mechanisms are under consideration, including a solenoid, burn-wire, or shape-memory alloy latch, which are used to secure each robot's nose to the cryobot. Additionally, the spindle onto which the delta-wing robots are packed requires a motor (or other form of actuation) in order to rotate and align individual robots with one of the open doors on the cryobot ahead of deployment. Once properly aligned and released, the delta-wing robots reverse out backwards from the cryobot payload chamber under their own thruster power before navigating off on a mission.

Reliability – A number of potential mission risks are reduced or eliminated through the use of highly-redundant delta-wing robots:

Actuators stop working? Individual micro-swimmers have redundant pairs of thrusters to maintain thrust even if an individual motor fails. Combination of 2 thrusters, 2 elevation flaps, and 1 rudder flap (yaw) allows these robots to maintain some degree of controllability even if a single flap actuator fails.

No current? Mobility on the micro-swimmer is baselined for spatial exploration.

Faulted State on Cryobot? Individual robots have sufficient onboard intelligence, autonomy, and localization capabilities to maintain positions near the cryobot until it recovers.

A single Delta-Wing stops working? Individual robots have limited redundancy, but all other robots will continue to work if a single one fails (or is swept away). Robots have 48x redundancy with identical sensor payloads, so loss of a single robot limits total mission life and number of deployable robots, but doesn't eliminate any science / exploration capabilities of the mission. Swarm control algorithms will also be explored that can gracefully adapt to loss of individual robot agents (or deploy new robots to replace lost ones).

Novelty – This concept demonstrates a feasible design for miniature, untethered robots for swarm-based exploration of ocean worlds. The micro-swimmers are also designed for efficient packing and simple deployment from the cryobot, and strike a balance between per-robot capabilities and large number of robots.

Remaining Trades –

- Final actuator component selection for thrust and steering, etc.
- Final localization sensor package, including method for velocity measurement, possible cameras (Optical Flow, Event cameras) with lights for mapping / feature detection, and possibility of forward- / upward-looking sonar for collision detection.
- Final scientific sensor package
- Exact nature of micro-swimmer activation and mechanical release for deployment.
- Devising a strategy for simultaneously communicating with multiple micro-swimmers.

6.2 Dragon Kite Concept

The "Dragon Kite" Concept (Fig. 6.4) consists of powered, steerable, active sensing nodes that are connected in series by a tether. Each node contains a moderate volume allocation for science payload, and actuated hydrodynamic control surfaces (i.e. wings).

Tether – Carries mechanical load, comms., and power, through a combination of 2x fiber optic cables and 2x copper wires all wrapped in a protective sheath. With no active elements in any one node required to forward any tether services (mechanical, comm, power) to the next node, the cost of failure of an individual node is limited. A tether with a built-in sampling tube is potentially possible, but adds significant complexity and is not included as part of the baseline design.

Sensing – Each node has sensing for state estimation (IMU, sonar, fluid velocity) and a small 1 cm^3 ocean composition payload. Each node also has one 'big' 10 cm^3 payload slot, to be used for a propeller (in the case of the first / distal node), or one of the more sophisticated imaging (camera / microscope) / analysis science sensors for subsequent nodes. The localization problem is highly constrained (easier to solve) due to the presence of the tether. Optical gratings installed along the length of the tether could allow sensing equipment in the cryobot to measure the shape of the tether (although this is still primarily a research-grade capability).

Control – The "Dragon Kite" concept does not simply rely on a string of passive sensing nodes along the length of a tether; each node actively shapes the tether in the down-stream flow by actuating / steering at many points along the length of the tether. Actuation via hydrodynamic control surfaces means high energy efficiency, because the primary motive forces come from the flow. Furthermore, designing the control surfaces with features like trim tabs would reduce the force (i.e. actuator mass and volume) and power required to move control surfaces, and potentially reduce power required to hold a control surface in position to zero. Shaping the tether at many points along its length allows the system to explore in ways that a "single kite" system could not – around obstacles, performing spatial sweeps, etc. Without the aid of the 1st node's propeller, the system is likely constrained to exploring up to +/-45 deg away from the downstream flow direction. With the aid of the end propeller, the explorable workspace increases – potentially significantly, although it is challenging to estimate at this time. The three fins on each node allow the system to instantaneously apply a force to the tether in the 2D plane orthogonal to the tether direction (e.g. no Jacobian singularity, like an airplane has where it needs to roll to direct lift forces sideways), and apply a moment about the tether axis (preventing

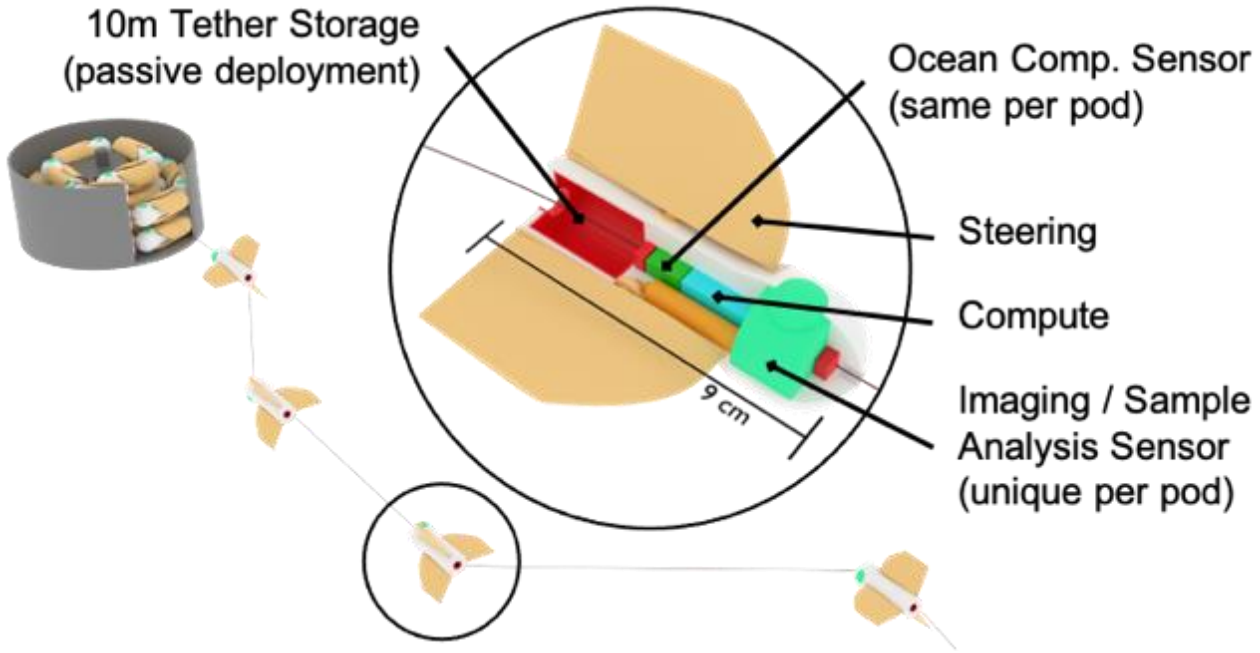

Fig. 6.4: Dragon Kite Robot Concept, including a partially-deployed spool of kites, and a magnified view of one node on the kite.

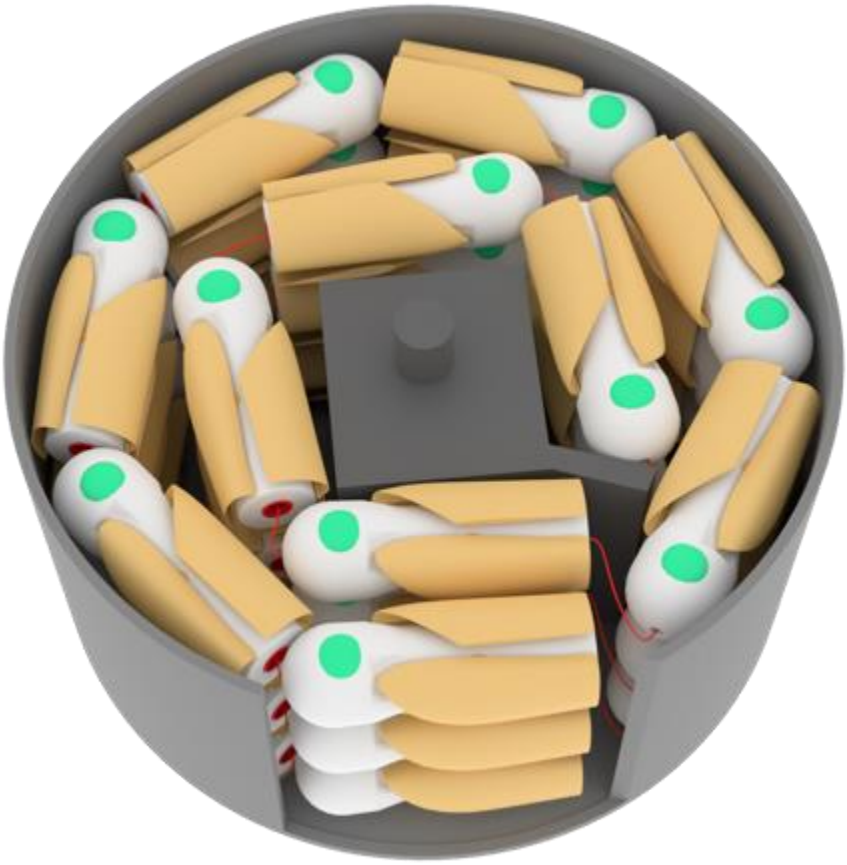

Fig. 6.5: Dragon Kite Robot Concept, including packaging within the cryobot mothercraft.

uncontrolled twisting of the tether). These flexible fins (i.e. polyimide) are wrapped tightly against the node body during transport, and expand on an underlying frame (e.g. nitinol wire) once deployed.

Passive Behaviors – Each node and the tether would be slightly negatively buoyant. This creates a low-energy fallback state where the system simply hangs vertically down the water column. Fins are positioned to the rear of each node to place the center of pressure behind the center of mass and tether connection; the "arrow principle" ensures that the nodes passively align with flow direction when the control surfaces are not actuated.

Deployment – 39 nodes are packed into the cryobot payload volume, in three independent strings of 13 nodes, as shown in Fig. 6.5. Each string is stored in a spiral fashion (head-to-tail), with the most distal node towards the exterior of the cryobot. To deploy, as shown in Fig. 6.6, the payload volume is rotated to orient the first node correctly relative to ocean current, then the first node in a string is released by a spring / pin-puller mechanism. The first (most distal) node in each string doesn't have an imaging sensor payload, but instead has a small motor and propeller to assist with mobility if required. As drag (and the propeller from node 1) pull node N backward, the tether is passively pulled from node N+1 (e.g. torpedo or ball-of-yarn style) until none remains. Then, the drag force pulls node N+1 from the cryobot storage. The single payload bay rotating motor is actuated to maintain a useful orientation for downstream / drag forces to pull nodes free. The connection between the last (most proximal) node and the cryobot payload volume passes through a cable cutter. Nominal operations call for deployment of only a single string at a time, then in the case of a catastrophic failure of a string, it is cut free and the next string is deployed. The total active mechanism count is 7 – 3 initial release pin-pullers, 3 cable cutters, and 1 payload bay rotating actuator.

Reliability – The sole type single point, non-graceful-degradation failure is if there is a complete break in the proximal end of the tether. This is mitigated by being able to cut away a damaged string and deploy two backups kites. For most other failure modes, there is a graceful degradation of performance:

(a) Packaging of 3 Dragon Kites (each layer is 1 kite)

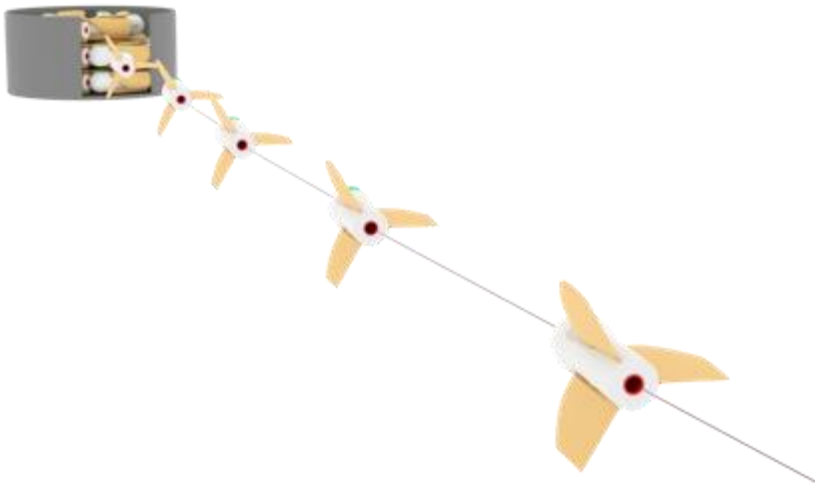

(b) Initial Deployment of Top Dragon Kite (each kite contains 11 nodes connected in series)

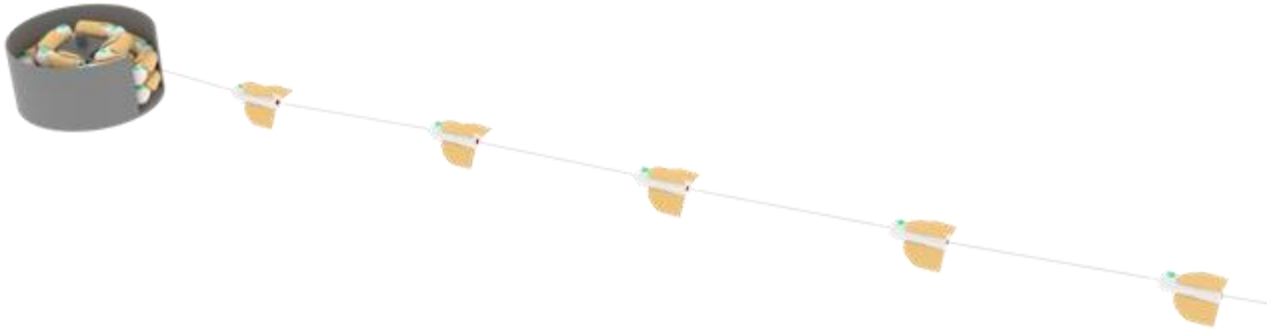

(c) Continued Deployment of Nodes in Top Layer

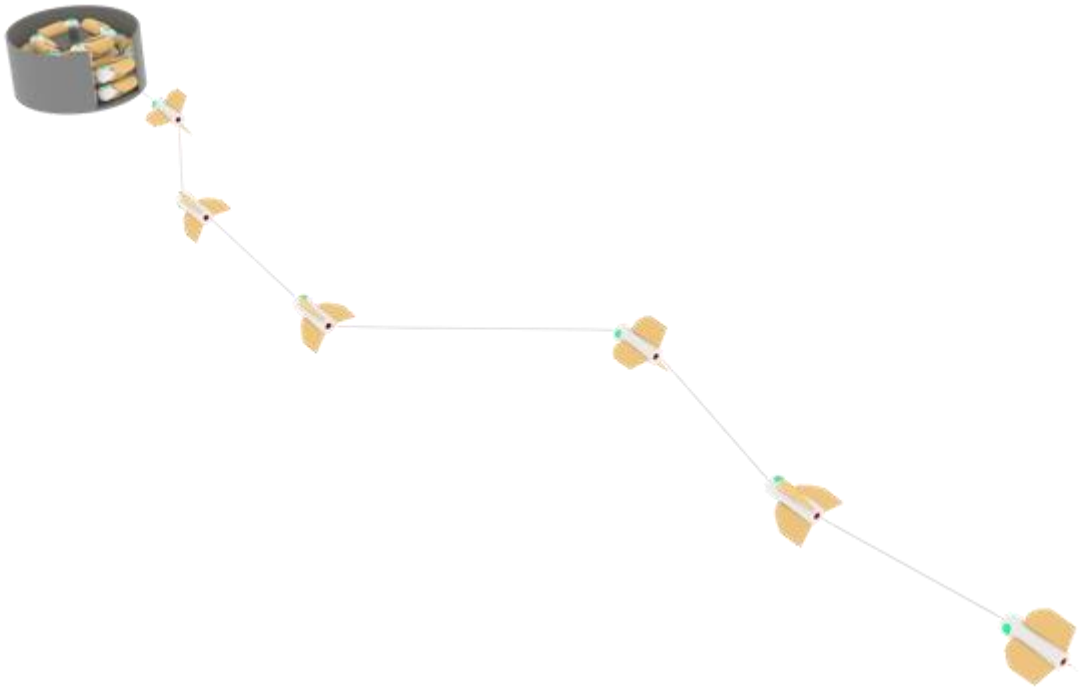

(d) Actuation / Steering of Individual Nodes in Deployed Kite

Fig. 6.6: Dragon Kite Robot Concept, showing packaging within the cryobot mothercraft and deployment from the cryobot mothercraft for operations (in 3 stages).

A single node stops working? The others will continue to work. That node's passive hydrodynamic characteristics still contribute to creating drag to spread out the tether.

Actuators stop working? Passive hydrodynamics still maintain some spatial distribution. It's possible that correctly configured control surfaces would create an oscillatory mode, to continue some spatial sweeps even without

No current? Nodes hang straight down and you get a vertical science profile. Spin up the propeller and you may get some spatial exploration ability.

Faulted State? For fault response, a "turn motors off and let CPU think for a while safe mode" is safe (unlike other concepts that might rise/fall/drift/tangle out of range if you simply do nothing) since the kite behavior the low energy state.

Something horrible happens to a single string? Cut it off, deploy the next string (3 total).

The common theme here is that even if there is a systemic problem with some of the advanced features, the passive characteristics enable the performance to degrade to something that could provide partial mission success.

Novelty – The "Dragon Kite" concept isn't just a standard tether with sensing nodes along its length. Fins at each node along the kite's length allow the kite to actively control its shape and where it explores. Unlike most snakelike robots that have many bulky actuators (and require complex planning and careful coordination to move), operating the Dragon Kite is more analogous to the passive "go-with-the-flow" grace of flying a kite.

Remaining Trades –

- Exact nature of the tether. All-in-one (mechanical + electrical + comms + sample return) seems ideal on paper, but there is a family of valid kite concepts with each different variation of tether.
- Exact design of the control surfaces and their actuation method.
- Exact packing of nodes into payload volume. More strings, more nodes per string or some combination may be possible.
- Architecture of the string – simply a set of serial nodes, or various branching options? Loops? The serial approach is simple and lower-risk, but other options might provide greater sensor coverage.

6.3 Twister Pods Concept

The "Twister Pods" Concept (Fig. 6.7) consists of three powered, steerable, active robot drones that are connected back to the cryobot mothercraft by a tether. Each of the three robot drones further contains ~27 passive "twister pod" sensor nodes that can be controllably deployed by the drone, and each pod contains a small volume allocations for science payload (pressure, temperature, etc.), an ultrasound transducer (for wireless communication), and a battery (power). This concept is inspired by and named after the tornado-sensing pods used in the "Twister" movie (1996).

The Twister pods are also encapsulated in syntactic foam [120], to achieve desired buoyancy (e.g. positive, neutral, negative) when passively floating in the ocean currents: positive buoyancy enables measurements at the ice-ocean interface, neutral buoyancy enables measurements in the free-stream current, and negative buoyancy enables vertical profiling of the water column at controlled rates (until the pod is out of range or exceeds its depth rating).

During nominal operations, a tethered, actively controlled robot drone detaches from the cryobot and carries a group of 27 passive "Twister" style robotic Pods to a region of interest, where they are released to collect sensor data and relay back to the cryobot through the tethered robot. This hybrid approach of active robot drone with passive sensor pods allows for large-volume distributed sensing while utilizing relatively few actively controlled robots.

Sensing – Each Pod contains a MEMS sensor payload that provides state estimation (IMU, fluid velocity) and standardized suite of ocean composition measurements (pressure, temperature, salinity, pH, etc.). Data is collected at 1 Hz to extend battery life.

Each Drone carries the same MEMS sensor payload found on the Pods, to provide state estimation (IMU, fluid velocity) and ocean composition measurements, as well as one 'big payload' spot, to be used for detailed multi-spectral imaging / mapping sensor package.

Power – Each Pod contains a battery cell with sufficient energy for 1 hour of operating life. This battery is baselined as a primary battery, which mitigates needs for a pre-deployment recharging mechanism while the Pods are still stored within the

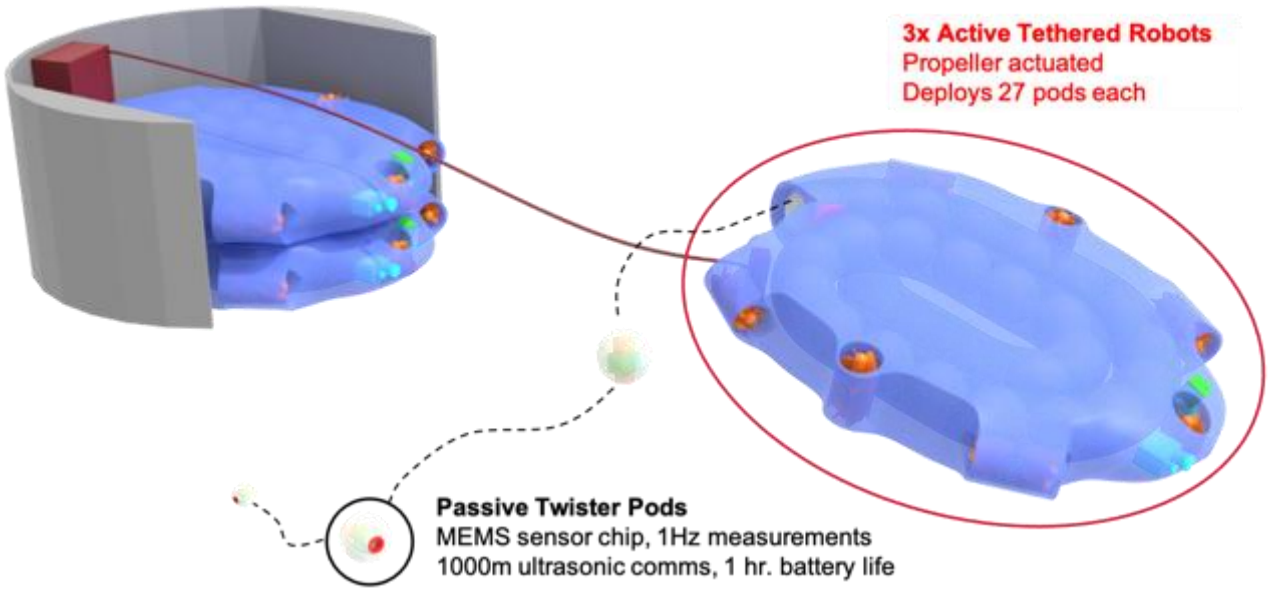

Fig. 6.7: Twister Pods Robot Concept, including three active, tethered robots that each contain 27 passive Twister pods for remote, untethered sensing.

Table 6.2: Twister Pods Concept initial estimates for subsystem volume, power, and mass allocations. Each Pod has 29 mm diameter and operates for 1 hour under battery power, including all sensing / computation / communication.

Subsystem	**Volume (cc)**	**Mass (g)**	**Power (W)**	**Notes**
Sensor	1.0	2	0.05	Ocean composition
Sensor	0.1	2	0.041	IMU
Comms.	0.4	2	0.28	7% duty cycle at 1 Hz
Compute	0.3	1	0.01	SCμM chip or similar [114]
Battery	0.65	1	–	Li-CFx primary cell at 400 Whr/kg
Foam	11	5.5	–	Syntactic foam at 500kg/m^3
Net	13.4	13.5	0.38	1 hr operation, neutrally buoyant

Drones. Various wireless techniques can be used to power-on the Pods just before release, including: magnetic latches, physical switches, and an ultrasound pulse to trigger a transistor.

Each Drone is powered directly through the tether, sourcing abundant power from the cryobot, eliminating the need for onboard batteries, and eliminating power as a constraint on the operating life of the Drones. This allows the Drones to continue exploring and collecting scientifically-valuable data even after all Pods are deployed and run out of power.

Mobility / Control – Each Pod is uncontrolled and passively floats in the ocean currents. Pods can be designed to have positive, neutral, or negative buoyancy by varying the volume of the encapsulating Syntactic foam, and thus have pre-determined rates of descent / ascent, as well as a pre-defined method for dispersing Pods into the ocean currents.

Each Drone contains 7 pairs of counter-rotating thrusters in the current baseline design, which provides omni-directional mobility, including direct vertical translation. The thruster pairs also provide operational redundancy in case one fails.

Communication – Each Pod contains a 1-way ultrasound transducer with ~1000 m range, to wirelessly relay data back to the

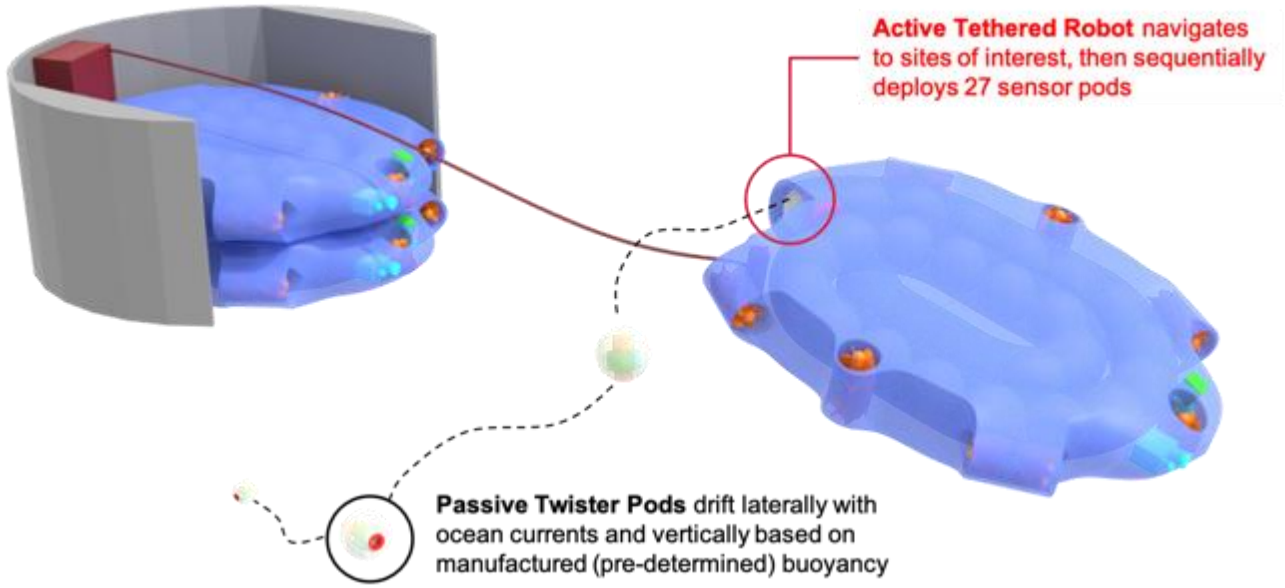

(a) Deployment of Top Drone and several Twister Pods (each drone contains 27 passive pods)

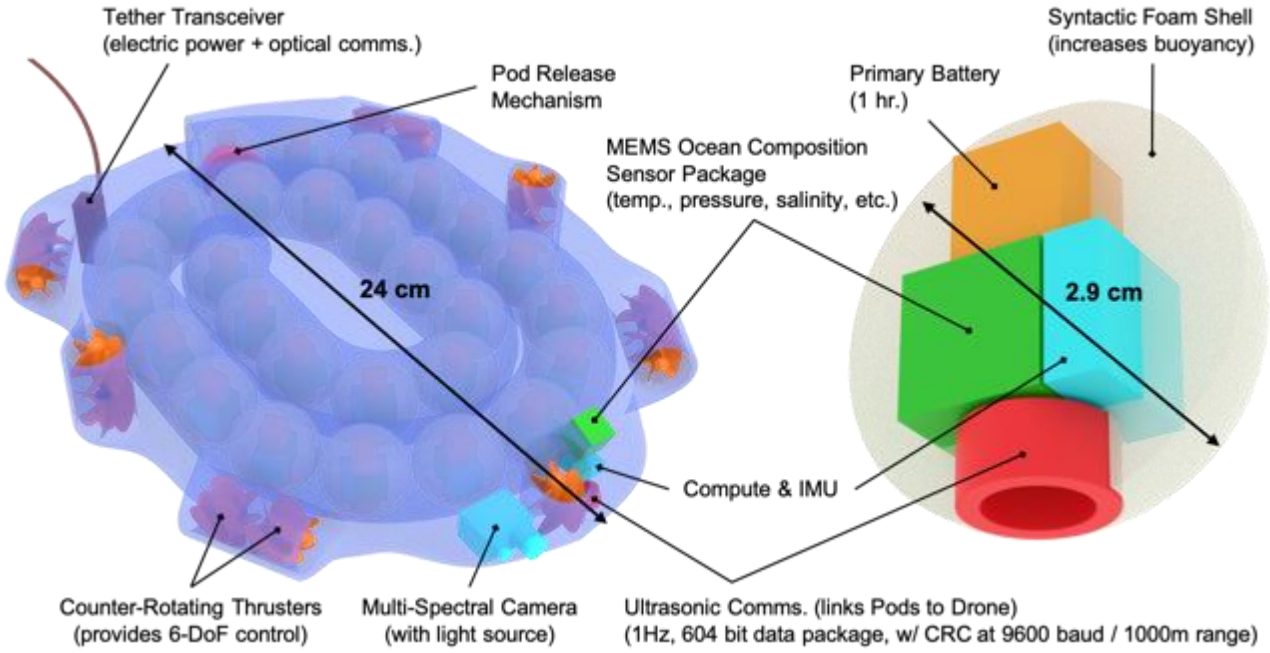

(b) Detail of Tethered Drone (left) and Twister Pod (right)

Fig. 6.8: Twister Pods Robot Concept, showing drone packaging within the cryobot mothercraft, pod packaging within the drone, drone deployment from the cryobot mothercraft for operations, pod deployment from the drone, and component details on both the drone and pods.

Drones / Cryobot. Based on the currently baselined sensor package, 15 Pods can communicate a 1 Hz, 604-bit data packet that includes a cyclic redundancy check for error-correction (matching data acquisition rate) using 9600 baud communication rate, without overlapping.

Data can be collected by any active drone or the Cryobot itself, so long as they all share the appropriately-tuned ultrasound transducer. Additionally, measuring the arrival times of data packets at multiple receivers can be leveraged to improve the localization (position / velocity) estimates of the sensor Pods themselves.

Each Drone then relays data back to the Cryobot using the tether. This supports substantially higher data rates (~Gbps), which allows transfer of aggregated sensor data from the sensor Pods along with image data collected by the Drone itself.

Integration / Deployment – 27 Pods are stored in a spiral chamber within the Drone, and designed to be sequentially deployed from the Drone. Several deployment mechanisms are under consideration, including a solenoid or shape-memory alloy latch (at the exit) and spring-loaded or shape-memory alloy element (to generate force that pushes the pods towards the exit).

3 Drones are stacked within the the Cryobot, and secured with launch-locks until ready for deployment. The storage chamber is designed to be at equilibrium with the external environment throughout the cruise / descent phases of the mission. One panel on the side of the cryobot is required to drop away in order for the drones to maneuver out into the ocean under their own thruster power.

Reliability – A number of potential mission risks are reduced or eliminated through the use of redundant robot Drones that each carry large numbers of deployable Pods:

A single Pod / Drone stops working? Individual Pods have significant redundancy, and all other Pods will continue to work if a single one fails (or is swept away). Individual Drones have 3x redundancy, so loss of a single Drone limits total mission life and number of deployable Pods, but doesn't eliminate any science / exploration capabilities of the mission.

Actuators stop working? Individual Drones have redundant pairs of thrusters on all axes to maintain control even if individual motors fail. Passive ocean hydrodynamics still maintain some spatial distribution of deployed Pods that are subsequently released, even if all Drone actuation fails.

No current? Pods will float up / down / remain in place (depending on buoyancy) and still provide a vertical science profile. Mobility on the Drones still enables spatial exploration.

Faulted State? Tether can maintain connection to the Drone even while the Drone or Cryobot is faulted, allowing for a semi-graceful recovery.

Something horrible happens to a single tether / Drone? Cut it off, deploy the next Drone (3 total).

Overall, the "Twister Pods" concept provides similar levels of redundancy to the "Dragon Kite" concept, with three primary vehicles, but adds additional free-floating sensor pods to expand the number of simultaneous measurements. These additional pods provide extra sensor redundancy without requiring individual actuation.

Novelty – This concept is inspired by the movie "Twister" and in many ways remains the most faithful to the original concept of true cm-scale micro-robots for Ocean World exploration, but leverage the larger Drones to place sensor Pods at scientifically-interesting locations that would not be reachable if they were ejected directly from the cryobot mothercraft.

Remaining Trades –

- Exact nature of the tether integration / deployment (including whether it is passively / actively deployed, and whether the tether spool is mounted on the cryobot or drone) as well as the exact composition of the tether (number / size of optical fibers / wires)
- Exact nature of Pod activation and spring-loaded deployment.
- Devising a strategy for simultaneously communicating with >15 Pods.

6.4 Ultrasound Swimmer Concept

The "Ultrasound Swimmer" Concept (Fig. 6.9) was the original concept for SWIM, and consisted of hundreds to thousands of ~1 cm^3, 3D-printed robots.

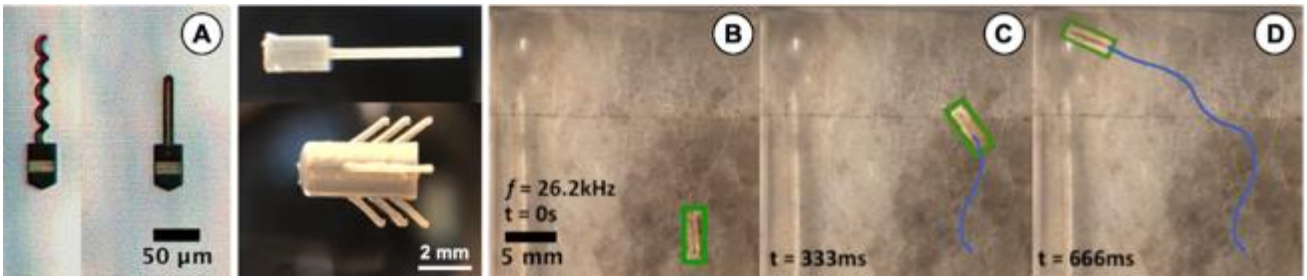

Fig. 6.9: Ultrasound Swimmer Robot Concept, including: (A) sample 3D-printed micro-swimmers; (B-D) Time frames / trajectory of a 3D-printed micro-swimmer, swimming in water via external ultrasound power at up to 53 mm/s (16 body lengths / sec).

Specific concept innovations include using micro-swimmers 3D-printed at true ~cm^3-scales (with μm-scale features) with no external moving parts (monolithic design for planetary protection) and remotely controlled / powered by ultrasound (repurposing existing Cryobot ultrasound hardware used for forward-looking sonar and communication with the lander). Additional novel design aspects that were considered in the trade study include:

1) Multi-frequency ultrasound on the mothercraft to power, steer, and talk with individual swimmers, and passively measure backscattered signals to log swimmer sensor data
2) Micro-swimmer fins that each have unique resonant frequencies to allow 3D steering
3) Micro-swimmer sensors that are wirelessly powered by a resonant circuit and report data by varying that resonant frequency (e.g. backscattering) to minimize onboard electronics [149]
4) Ultrasound beamforming to deliver 2x power compared to an unfocused beam [24]

The smallest ~1 cm^3 micro-swimmer concepts will focus on 3D-printed robots that are propelled by legs / fins, each engineered with resonant modes at unique frequencies (Fig. 6.9). Critically, the shape / motion of the micro-swimmer legs in certain resonant modes have been shown to produce drag force asymmetry – necessary for swimming at low Reynolds numbers [12]. Ultrasound transducers onboard the mothercraft then transmit multi-frequency signals through the water to excite oscillations in one or more micro-swimmer legs / fins at the same time, for remote-controllable, untethered propulsion in 3D.

3D-printed micro-swimmers have previously been fabricated by our team at both sub-mm and cm-scales (Fig. 6.9A). One such micro-swimmer, with ∅ 400 μm × 400 μm cylindrical body and a ∅ 200 μm × 3 mm flexible tail, is shown operating in water (Fig. 6.9B-D), actuated wirelessly by a COTS piezoelectric (PZT) shaker. At a precise frequency (26.2 kHz), the robot swam at 53 mm/s (~16 body lengths per second) for 4 cm until reaching the tank edge.

These true micro-robots are propelled by legs / fins that resonate at unique frequencies and are remotely actuated by ultrasound transducers on the mothercraft. Unfortunately they are too slow (53 mm/s) and have insufficient range (ultrasound power attenuates beyond 1-10 meters) to meet science-driven mission requirements established in the Phase I work. Given these limitations, the design concept was not pursued further.

6.5 Concept Comparison / Scoring

The three main robot concepts were evaluated according to the scoring guidelines outlined in Table 6.3.

Results of this scoring rubric for the the “Delta-Wing,” “Dragon-Kite,” and “Twister Pods” SWIM robot concepts is presented in Table 6.4. The 60-75 cm^3-scale “Delta Wing” concept is the highest rated of the three and provides the best balance of redundancy, unconstrainted mobility, active exploration, and targeted sensing.

Table 6.3: Scoring Guidelines for the SWIM robot concepts.

Concept	Weight	Ranking Instructions
Science	**40%**	
Mission Duration	10%	5 = operate for full PRIME ocean mission; 4.5 = operate for >1 diurnal at full capability; 3 = operate for 1 diurnal at full capability; 2 = operate for <1 diurnal at full capability; 1 = operate for <1 diurnal at partial capability.
Explored Ocean Volume	10%	5 = ability to explore 100m radius x >5m deep volume during mission life, at 2.5m intervals; de-rate to % accessible over mission
Exploration Limitations	10%	5 = unrestricted access >100m from cryobot; -1 for terrain restrictions; -1 for navigation restrictions near ice; -1 for down-stream only restriction
# Science Objectives / Investigations Addressed	10%	5 = provide measurements for all 3 science objectives; -2 per missing Objective or -0.25 per missing Investigation
Cost / Complexity	**15%**	
TRL of Subsystems (COTS vs. new technology)	5%	5 = all COTS components; -1 per low-TRL subsystem (e.g. sensors / comms. / waterproof motors / actuators / etc. at desired size scale)
Cost of Components	5%	5 = all COTS components; -1 per low-TRL subsystem (e.g. sensors at desired size scale)
Cost of V&V, Flight Build, etc.	5%	5 = low quantity or high-redundancy; -1 for >10 units / -2 for >100 units; -1 for each non-redundancy to test; -1 for each item that can't be fully per-unit tested during V&V (e.g. passive tether unspooling); -1 for other V&V complexity
Complexity of ConOps (e.g. robot control)	5%	5 = simple, per-unit control with limited map of environment; -1 if detailed map required; -2 if degraded performance difficult to identify / control; -1 if communication challenges
Survivability / Failure Modes	**15%**	
Does system degrade gracefully?	7.5%	5 = able to fully continue mission after anomaly; -1 for partial loss of capability; -2 for major loss of capability
How many single-point failures? vs. how much redundancy?	7.5%	5 = no single-point failures; -0.5 per subsystem with single-point failures that causes degraded performance; -1 per subsystem with single-point failures that causes
Adaptability	**20%**	
Pre-launch System Adaptability (e.g. to changing cryobot dimensions, payload volume, etc.)	5%	5 = fully-adjustable system size / volume allocation; -1 per restriction on dimension adjustments; -1 per restriction on interface adjustments
Pre-deployment adaptability (e.g. new data collected in orbit or during descent changes mission objectives)	5%	5 = fully-adaptable to ConOps changes during pre-deployment (e.g. new target like a sub-surface lake); -1 per restriction
Mission adaptability (e.g. new data collected at the ocean changes science / environmental reqs., or requires extra measurements at new targets)	10%	5 = fully-adaptable to ConOps changes during mission (e.g. new target like a sub-surface lake); -1 per restriction
Concept Novelty	**10%**	
What aspects are novel, interesting, and push beyond current state-of-the-art for this technology?	10%	2 = average novelty; +0.5 per unique aspect
Total	**100%**	

Table 6.4: Scoring Results for the "Delta-Wing," "Dragon-Kite," and "Twister Pods" SWIM robot concepts.

Concept	Weight	Delta Wing		Dragon Kite		Twister Pods	
		Score	Comments	Score	Comments	Score	Comments
Science	**40%**	**4.4**	**Medium science; high exploration**	**3.2**	**High science; low exploration**	**4.4**	**Medium / high science; medium / high exploration**
Mission Duration	10%	4.5	Deployed in groups to operate over at least 1 diurnal; anchoring can increase per-robot life	5.0	Operates for full PRIME mission	4.5	Drones operate for full PRIME mission; Pods have life limited by comm-range if swept away.
Explored Ocean Volume	10%	5.0	Sized to explore necessary volume	1.3	Limited to ~90 deg cone downstream	5.0	Drones are not power limited for exploration, but Pods limited by total number to deploy
Exploration Limitations	10%	5.0	No limitations	2.0	Limited near terrain, near ice, at fixed intervals along tether, and to down-stream only	4.0	Drones limited by tether near terrain
# Science Objectives / Investigations Addressed	10%	3.0	4 if multi-spectral camera on some robots (requires optical comm. too); 3 if no camera	4.5	Ocean composition + multi-spec. camera or other instrument (on Nodes)	4.0	Ocean composition (on Pods) + multi-spec. camera (on Drone)
Cost / Complexity	**15%**	**4.5**		**3.3**		**3.5**	
TRL of Subsystems (COTS vs. new technology)	5%	4.0	Miniaturized waterproof flooded motors, custom sensor board, DLV needs miniaturization (if used)	4.0	Mature tether technology and kite controls; needs	4.0	Need Pod deployment mechanism; rest are COTS parts and larger motors
Cost of Components	5%	5.0	High redundancy across units; almost all COTS components	4.0	Medium redundancy across Nodes, but higher variation in sensors across units	3.0	High redundancy across Pods / Drones, but need large quantities, and higher Drone complexity
Cost of V&V, Flight Build, etc.	5%	4.0	High redundancy across units; all components can be tested in V&V	2.0	Some non-redundant sensors; challenging V&V (unspooling); can't per-unit test unspooling	3.0	High redundancy across units; many units to test; can't test unspooling
Complexity of ConOps (e.g. robot control)	5%	5.0	Mobility is single-fault redundant; robots are robust to limited environmental info; deploy robots within comms bandwidth	3.0	Need to avoid terrain; control may be hard if tether snags / certain nodes fail / reduced control on some nodes	4.0	Hard to communicate / localize many Pods simultaneously
Survivability / Failure Modes	**15%**	**4.0**		**3.5**		**3.8**	
Does system degrade gracefully?	7.5%	4.0	Redundancy through many identical units; can re-task / deploy other robots if a single robot fails. Robots (slowly) swept downstream if ocean current exceeds design thrust	4.0	Steering loss on individual Nodes limits mobility; fouled tether highly reduces mobility; damaged tether affects down-stream nodes; but 2-3 tethers provides recovery from major anomaly and safing to passive drifting mode with negative buoyancy still collects ocean data	3.0	Significant loss for each non-mobile Drone; minimal loss for each non-working Pod, but quick loss of all Pods in high currents
How many single-point failures? vs. how much redundancy?	7.5%	4.0	Per-Unit – single-point failure tolerant on mobility; no back-up to comms / sensing / processor. Redundancy through many identical robots.	3.0	HV converter if sending power down tether (electrical shorting risk); Tether is major single-point failure; Node mobility failures degrade performance.	4.5	Per-Unit – single-point failure tolerant on mobility; back-up comms (tether + ultrasound) at lower data rate; minimal power back-up
Adaptability	**20%**	**4.5**		**3.5**		**3.5**	
Pre-launch System Adaptability (e.g. to changing cryobot dimensions, payload volume, etc.)	5%	5.0	Can scale size / number of robots; mechanical interface to PRIME only	4.0	Can scale number of nodes / tethers; but need mechanical + tether interface	4.0	Can scale number of Pods per Drone; but needs mechanical + tether interface
Pre-deployment adaptability (e.g. new data collected in orbit or during descent changes mission objectives)	5%	5.0	Unrestricted mobility in alternate environments	4.0	Motorized Node can adapt if no flow; but range limited by tether	4.0	Pod behavior may change, but should still work; range limited by tether
Mission adaptability (e.g. new data collected at the ocean changes science / environmental reqs., or requires extra measurements at new targets)	10%	4.0	Can re-task any active / future robots to new targets; higher-than-designed-for currents limit mobility	3.0	Can't go upstream if interesting signal found in flow	3.0	Can re-task any Drones to new targets; but no control over deployed Pods; high currents sweep away Pods quickly
Concept Novelty	**10%**	**3.5**		**3.0**		**2.5**	
What aspects are novel, interesting, and push beyond current state-of-the-art for this technology?	5%	3.5	Small + untethered + swarm control	3.0	Multi-body smart tether (bonus if you sample too)	2.5	Drone + deployable pods explored before (bonus if smart tether / sampling tether)
Total	**100%**	**4.28**		**3.29**		**3.79**	

7 CONCLUSION

Realizing an operational SWIM system requires developing and operating swarms of untethered, swimming, 100 cm^3-scale micro-robots at ~100 of meter distances from a cryobot mothercraft, under Europan conditions and after a 9-14 year journey to the ocean.

In Phase I, we established the fundamental feasibility of this SWIM concept, through a mission-driven system design trade study supported by simulations / models to define performance envelopes of relevant robot subsystems. Our models focus on 5 areas (communication, propulsion, power, thermal, and swarm exploration) and provide baseline scaling laws to estimate robot performance, range, and power consumption on Europa, across a range of robot designs and ocean velocities. In combination, this work allowed us to close our highest-priority questions:

Sensing – we identified a "wish-list" of existing commercial- / research-grade instruments that scientists can use to study the ice-ocean interface; some need to be miniaturized, and then integrated into a single payload.

Communication – existing, commercial ultrasound sensors are sufficiently compact (1–20 mm radius, depending on frequency) to fit in our candidate robots, and can provide one-way communication at >500 meter ranges and ~10 kbps with <1 W power.

Propulsion – existing, commercial brushless DC motors / propellers generate sufficient thrust to exceed predicted Europan ocean velocities, in viable form-factors; BLDC motors have also been shown to operate underwater in a flooded configuration.

At the end of Phase I, the primary open questions / mission risks have evolved to focus on the challenges associated with performing reliable underwater autonomy and oceanographic measurements in robots at least an order of magnitude smaller than current state-of-the-art, specifically:

- Performing autonomous underwater localization / control of a distributed robot swarm, to enable efficient exploration and characterization of the ice-ocean interface.
- Defining the technological roadmap for miniaturized components, especially sensors (e.g. redox sensors and doppler velocity logs) and thrusters (flooded, brushless motors) that operate in high-pressure underwater environments.

7.1 Potential Future Impact

Current Europa Lander plans target landing in 2032, so the first ocean-access mission may occur later in the 2030s. Now is the time to perform the necessary concept study and technology development to ensure that a mature, swimming micro-robot platform is ready for infusion into an ocean-access mission. NASA has seen novel capabilities enabled through miniaturized cubesat / rover / helicopter platforms – and similar advantages can be found in swimming robots. Miniaturized actuation, sensing, processing, communication, and other MEMS technologies have all advanced dramatically in the past decade. Now is the time to evaluate how they can be leveraged to increase the science return of first-generation ocean-access missions on worlds like Europa.

NASA has invested significant resources to develop and mature meter-scale field-deployable oceanographic robots (through PSTAR) and ocean-access cryobots (through SESAME), yet there has not been a commensurate investment in swimming micro-robots. As a result, the successful development of the SWIM concept will enable a great leap in distributed, untethered, sub-surface ocean exploration capabilities for NASA and the greater oceanographic community. Specifically, work on SWIM advances NASA's state-of-the-art capabilities in submersible micro-robots, underwater autonomy, swarm autonomy, and underwater ultrasound communication technologies. These technologies are widely applicable for future NASA missions to ocean worlds, as well as NASA collaborations with researchers and private industry on Earth.

On Earth, SWIM can be deployed as a new oceanography tool for distributed sensing under ice sheets in the Arctic and Antarctic oceans, below glacial moulins, or in deep hypersaline anoxic basin environments – enhancing scientists' understanding of melting ocean ice (due to global climate change) and the ecosystems that they support by quickly, and affordably, measuring temperature

/ salinity / pressure / pH changes in these environments. SWIM robots could be deployed at the ocean-ice interface by melt-probes, or an autonomous underwater vehicle (AUV) that maintains a safe stand-off distance under the ice. SWIM can also be deployed for distributed sensing at hydrothermal vents – where monitoring is currently performed by stationary probes (expensive to deploy, and lack the mobility to adapt to a dynamic environment) or by instruments on large, expensive AUVs (that lack distributed sensing, and have short deployment periods). In this context, SWIM robots could deploy and recharge from an anchored base-station, to provide persistent, distributed mobile sensing that complements existing stationary probes.

REFERENCES

[1] B. Schmidt, K. Craft, T. Cwik, K. Zacny, B. Stone, F. Bryson, C. Chivers, S. Pierson, J. Lawrence, T. Plattner, E. Spiers, A. Mullen, J. Buffo, N. Daniel, A. Hanna, G. Lightsey, M. Meister, M. Nassif, D. Dichek, and A. Spears, "Dive, Dive, Dive: Accessing the Subsurface of Ocean Worlds," *Whitepaper – Decadal Survey in Planetary Science and Astrobiology*, 2020.

[2] S. M. Howell, W. C. Stone, K. Craft, C. German, A. Murray, A. Rhoden, and K. Arrigo, "Ocean Worlds Exploration and the Search for Life," *Whitepaper – Decadal Survey in Planetary Science and Astrobiology*, 2020. [Online]. Available: http://arxiv.org/abs/2006.15803

[3] B. Schmidt, S. S. Johnson, T. Hoehler, H. Graham, J. Bowman, S. Som, L. Barge, A. Pavlov, A. Pontefract, B. Orcutt, and B. Nunn, "Enabling Progress Towards Life Detection on NASA Missions," *Whitepaper – Decadal Survey in Planetary Science and Astrobiology*, 2020.

[4] M. L. Cable, S. Mackenzie, M. Neveu, T. M. Hoehler, A. R. Hendrix, J. Eigenbrode, L. Spilker, A. E. Hofmann, C. R. Glein, A. Mcewen, J. H. Waite, P. Wurz, A. Anbar, J.-p. D. Vera, F. Postberg, and F. U. Berlin, "The Case for a Return to Enceladus," *Whitepaper – Decadal Survey in Planetary Science and Astrobiology*, 2020.

[5] A. R. Hendrix, T. A. Hurford, L. M. Barge, M. T. Bland, J. S. Bowman, W. Brinckerhoff, B. J. Buratti, M. L. Cable, J. Castillo-Rogez, G. C. Collins, S. Diniega, C. R. German, A. G. Hayes, T. Hoehler, S. Hosseini, C. J. Howett, A. S. McEwen, C. D. Neish, M. Neveu, T. A. Nordheim, G. W. Patterson, D. A. Patthoff, C. Phillips, A. Rhoden, B. E. Schmidt, K. N. Singer, J. M. Soderblom, and S. D. Vance, "The NASA Roadmap to Ocean Worlds," *Astrobiology*, vol. 19, no. 1, pp. 1–27, 1 2019. [Online]. Available: https://www.liebertpub.com/doi/10.1089/ast.2018.1955

[6] S. M. Howell and R. T. Pappalardo, "NASA's Europa Clipper—a mission to a potentially habitable ocean world," *Nature Communications*, vol. 11, no. 1, pp. 9–12, 2020. [Online]. Available: http://dx.doi.org/10.1038/s41467-020-15160-9

[7] NASA Glen Research Center, "Scientific Exploration Subsurface Access Mechanism for Europa (SESAME)," 2019. [Online]. Available: https://www1.grc.nasa.gov/space/pesto/space-vehicle-technologies-current/scientific-exploration-subsurface-access-mechanism-for-europa-sesame/

[8] T. Cwik, W. Zimmerman, A. Gray, B. Nesmith, R. P. Casillas, J. Muller, D. Bell, S. Bryant, A. Karapetian, R. Otis, K. Hand, M. Brandt, K. Zacny, and A. Sengupta, "A Technology Architecture for Accessing the Oceans of Icy Worlds," in *69th International Astronautical Congress (IAC)*, vol. 69.
Bremen, Germany: International Astronautical Federation (IAF), 10 2018, p. 10. [Online]. Available: https://trs.jpl.nasa.gov/bitstream/handle/2014/48794

[9] T. Cwik, W. Zimmerman, and M. Smith, "An Architecture for a Nuclear Powered Cryobot to Access the Oceans of Icy Worlds," *Nuclear and Emerging Technologies for Space*, p. 4, 2019. [Online]. Available: http://anstd.ans.org/NETS-2019-Papers/Track-2--Mission-Concepts-and-Logistics/ abstract-122-0.pdf

[10] J.-P. Fleurial, S. M. Howell, and M. W. Smith, "Probe using radioisotopes for icy moons exploration," 2020. [Online]. Available: https://spacetech.jpl.nasa.gov/downloads/next/Labwide PRIME 2020Jun09.pdf

[11] S. Howell, C. Sotin, K. Carpenter, J.-P. Fleurial, K. Hand, and A. Klesh, "Diving into Ocean Worlds," *ECO Magazine (Environment Coastal & Offshore)*, pp. 27–29, 2020. [Online]. Available: http://digital.ecomagazine.com/publication/?m=9890&i=659148&p=28&ver=html5

[12] J. Liu and H. Ruan, "Modeling of an acoustically actuated artificial micro-swimmer," *Bioinspiration and Biomimetics*, vol. 15, no. 3, 2020.

[13] Y. Chen, H. Wang, E. F. Helbling, N. T. Jafferis, R. Zufferey, A. Ong, K. Ma, N. Gravish, P. Chirarattananon, M. Kovac, and R. J. Wood, "A biologically inspired, flapping-wing, hybrid aerial-aquatic microrobot," *Science Robotics*, vol. 2, no. 11, p. eaao5619, 10 2017. [Online]. Available: http://robotics.sciencemag.org/https://robotics.sciencemag.org/lookup/doi/10.1126/scirobotics.aao5619

[14] P. Bhushan and C. Tomlin, "Untethered Microrobots of the Rolling, Jumping & Flying kinds," Ph.D. dissertation, University of California, Berkeley, Berkeley, 8 2019. [Online]. Available: http://www2.eecs.berkeley.edu/Pubs/TechRpts/2019/EECS-2019-128.html

[15] J. Zhu, C. White, D. K. Wainwright, V. Di Santo, G. V. Lauder, and H. Bart-Smith, "Tuna robotics: A high-frequency experimental platform exploring the performance space of swimming fishes," *Science Robotics*, vol. 4, no. 34, p. 4615, 9 2019. [Online]. Available: http://robotics.sciencemag.org/

[16] W. H. Lee, J.-H. Lee, W.-H. Choi, A. A. Hosni, I. Papautsky, and P. L. Bishop, "Needle-type environmental microsensors: design, construction and uses of microelectrodes and multi-analyte MEMS sensor arrays," *Measurement Science and Technology*, vol. 22, no. 4, p. 042001, 4 2011. [Online]. Available: https://iopscience.iop.org/article/10.1088/0957-0233/22/4/042001

[17] "LPS22HH – High-performance MEMS nano pressure sensor," STMicroelectronics, Tech. Rep., 2019. [Online]. Available: https://www.st.com/resource/en/datasheet/lps22hh.pdf

[18] "STTS751 – 2.25 V low-voltage local digital temperature sensor," STMicroelectronics, Tech. Rep., 2019. [Online]. Available: https://www.st.com/resource/en/datasheet/stts751.pdf

[19] "LIS2DTW12 – MEMS digital output dual motion and temperature sensor," STMicroelectronics, Tech. Rep., 2019. [Online]. Available: https://www.st.com/resource/en/datasheet/lis2dtw12.pdf

[20] A. Hyldgard, I. Olafsdottir, M. Olesen, T. Hedegaard, O. Hansen, and E. Thomsen, "FISH & CHIPS: Four Electrode Conductivity / Salinity Sensor on a Silicon Multi-Sensor Chip for Fisheries Research," in *IEEE Sensors, 2005.*, vol. 2005. IEEE, 2005, pp. 1124–1127. [Online]. Available: http://ieeexplore.ieee.org/document/1597902/

[21] R. R. A. Syms and S. Wright, "MEMS mass spectrometers: the next wave of miniaturization," *Journal of Micromechanics and Microengineering*, vol. 26, no. 023001, p. 29, 1 2016. [Online]. Available: https://iopscience.iop.org/article/10.1088/0960-1317/26/2/023001/pdf

[22] P. Szyszka, T. Grzebyk, A. Gorecka-Drzazga, and J. A. Dziuban, "A Concept of MEMS Mass Spectrometer," in *2018 15th International Scientific Conference on Optoelectronic and Electronic Sensors, COE 2018*. Institute of Electrical and Electronics Engineers Inc., 8 2018, p. 4. [Online]. Available: https://www.researchgate.net/publication/327063202 A Concept of MEMS Mass Spectrometer

[23] J. P. Hauschild, E. Wapelhorst, and J. Muller, "Mass spectra measured by a fully integrated MEMS mass spectrometer,"" *International Journal of Mass Spectrometry*, vol. 264, no. 1, pp. 53–60, 6 2007. [Online]. Available: https://www.sciencedirect.com/science/article/pii/S1387380607001583

[24] H. J. Lee, M. Badescu, Y. Bar-Cohen, X. Bao, S. P. Jackson, and S. Sherrit, "Piezoelectric charging and wireless communication," *Proc. SPIE 10598, Sensors and Smart Structures Technologies for Civil, Mechanical, and Aerospace Systems*, vol. 1059810, no. May, p. 34, 2018.

[25] H. Kaushal and G. Kaddoum, "Underwater Optical Wireless Communication," *IEEE Access*, vol. 4, pp. 1518–1547, 2016. [Online]. Available: https://ieeexplore.ieee.org/document/7450595/

[26] D. Seo, "Neural Dust: Ultrasonic Biological Interface," Ph.D. dissertation, University of California, Berkeley, Berkeley, 12 2018. [Online]. Available: https://www2.eecs.berkeley.edu/Pubs/TechRpts/2018/EECS-2018-146.html

[27] Microchip, "Rad-Tolerant / Rad-Hard Integrated Circuits." [Online]. Available: https://ww1.microchip.com/downloads/en/DeviceDoc/00002200C.pdf

[28] A. Good, "Origami-inspired Robot Can Hitch a Ride with a Rover," 3 2017. [Online]. Available: http://www.nasa.gov/feature/jpl/origami-inspired-robot-can-hitch-a-ride-with-a-rover

[29] J. Balaram, M. M. Aung, and M. P. Golombek, "The Ingenuity Helicopter on the Perseverance Rover," *Space Science Reviews*, vol. 217, no. 4, pp. 1–11, 6 2021. [Online]. Available: https://link.springer.com/article/10.1007/s11214-021-00815-w

[30] D. Woerner, S. Johnson, J.-P. Fleurial, S. Howell, B. Bairstow, and M. Smith, "Radioisotope Heat Sources and Power Systems Enabling Ocean Worlds Subsurface and Ocean Access Missions," *Bulletin of the AAS*, vol. 53, no. 4, 3 2021. [Online]. Available: https://baas.aas.org/pub/2021n4i322

[31] K. Carpenter and M. Cable, "Exobiology Extant Life Surveyor (EELS) Robotic Architecture," 7 2019. [Online]. Available: https://www.kiss.caltech.edu/lectures/2019 EELS.html

[32] ——, "Exobiology Extant Life Surveyor (EELS)," 2020. [Online]. Available: https://spacetech.jpl.nasa.gov/downloads/next/EELS June 9b Distribute.pdf

[33] M. Ono, "Enceladus Vent Explorer," 4 2020. [Online]. Available: http://www.nasa.gov/directorates/spacetech/niac/2020 Phase I Phase II/Enceladus Vent Explorer

[34] "Outer Planets Assessment Group (OPAG)." [Online]. Available: https://www.lpi.usra.edu/opag/

[35] "Network for Ocean Worlds." [Online]. Available: https://oceanworlds.space/

[36] Woods Hole Oceanographic Institution, "Orpheus AUV." [Online]. Available: https://www.whoi.edu/what-we-do/explore/underwater-vehicles/auvs/orpheus/

[37] A. Samuelson, "Aquatic Rover Goes for a Drive Under the Ice," 11 2019. [Online]. Available: https://www.jpl.nasa.gov/news/news.php?feature=7543

[38] F. Berlinger, M. Gauci, and R. Nagpal, "Implicit coordination for 3D underwater collective behaviors in a fish-inspired robot swarm," *Science Robotics*, vol. 6, no. 50, p. eabd8668, 2021. [Online]. Available: https://www.science.org/doi/abs/10.1126/scirobotics.abd8668

[39] F. Berlinger, J. Dusek, M. Gauci, and R. Nagpal, "Robust Maneuverability of a Miniature, Low-Cost Underwater Robot Using Multiple Fin Actuation," *IEEE Robotics and Automation Letters*, vol. 3, no. 1, pp. 140–147, 2018.

[40] B. Schmidt, "ICEFIN – Small, Under-Ice, Robotic Oceanographer," 2020. [Online]. Available: https://schmidt.eas.gatech.edu/icefin/

[41] "Ocean Robots: Glider." [Online]. Available: https://www.whoi.edu/oceanrobots/robots/glider-phone.html

[42] "Slocum Glider." [Online]. Available: https://www.whoi.edu/what-we-do/explore/underwater-vehicles/auvs/slocum-glider/

[43] "Spray Glider." [Online]. Available: https://www.whoi.edu/what-we-do/explore/underwater-vehicles/auvs/spray-glider/

[44] P. Brodsky and J. Luby, "Final Report Flight Software Development for the Liberdade Flying Wing Glider," Office of Naval Research, Tech. Rep., 2013. [Online]. Available: https://apps.dtic.mil/sti/pdfs/ADA602311.pdf

[45] Woods Hole Oceanographic Institution, "REMUS 100 – Oceanographic Systems Lab." [Online]. Available: https://www2.whoi.edu/site/osl/vehicles/remus-100/

[46] Hydroid, "Remus 100 - Advanced Autonomous Underwater Vehicle," Tech. Rep. [Online]. Available: https://auvac.org/uploads/platform pdf/ Remus-100-Brochure.pdf

[47] General Dynamics Mission Systems, "Bluefin-9 UUV (Unmanned Underwater Vehicle)." [Online]. Available: https://gdmissionsystems.com/products/underwater-vehicles/bluefin-9-autonomous-underwater-vehicle

[48] Aquabotix, "SwarmDiver," 2018. [Online]. Available: https://www.aquabotix.com/uploads/5/1/7/3/51732055/swarmdiver technical specifications.pdf

[49] Northeastern University Field Robotics Lab, "SeaBED (Puma, Jaguar)." [Online]. Available: https://fieldroboticslab.ece.northeastern.edu/seabed/

[50] Woods Hole Oceanographic Institution and National Deep Submergence Facility, "SENTRY AUV," Tech. Rep. [Online]. Available: ndsf.whoi.edu/sentry

[51] Woods Hole Oceanographic Institution, "Mesobot." [Online]. Available: https://www.whoi.edu/what-we-do/explore/underwater-vehicles/auvs/mesobot/

[52] ——, "HROV Nereid Under Ice - Specifications." [Online]. Available: https://www.whoi.edu/what-we-do/explore/underwater-vehicles/hybrid-vehicles/nereid-under-ice/nereid-under-ice-specifications/

[53] General Dynamics Mission Systems, "Bluefin HAUV (Hovering Autonomous Underwater Vehicle)." [Online]. Available: https://gdmissionsystems.com/products/underwater-vehicles/bluefin-hauv

[54] Woods Hole Oceanographic Institution, "REMUS 3000 – Oceanographic Systems Lab." [Online]. Available: https://www2.whoi.edu/site/osl/vehicles/remus-3000/

[55] ——, "REMUS 600 – Oceanographic Systems Lab." [Online]. Available: https://www2.whoi.edu/site/osl/vehicles/remus-600/

[56] ——, "REMUS 6000 – Oceanographic Systems Lab." [Online]. Available: https://www2.whoi.edu/site/osl/vehicles/remus-6000/

[57] E. Lubofsky, "The Rise of Orpheus," 10 2019. [Online]. Available: https://www.whoi.edu/news-insights/content/the-rise-of-orpheus-2/

[58] L. Ren, N. Nama, J. M. McNeill, F. Soto, Z. Yan, W. Liu, W. Wang, J. Wang, and T. E. Mallouk, "3D steerable, acoustically powered microswimmers for single-particle manipulation," *Science Advances*, vol. 5, no. 10, p. eaax3084, 2019. [Online]. Available: https://www.science.org/doi/abs/10.1126/sciadv.aax3084

[59] Z. Ren, W. Hu, X. Dong, and M. Sitti, "Multi-functional soft-bodied jellyfish-like swimming," *Nature Communications*, vol. 10, no. 2703, 2019. [Online]. Available: https://www.nature.com/articles/s41467-019-10549-7

[60] B. C. Johnson, K. Shen, D. Piech, M. M. Ghanbari, K. Y. Li, R. Neely, J. M. Carmena, M. M. Maharbiz, and R. Muller, "StimDust: A 6.5mm¡sup¿3¡/sup¿, wireless ultrasonic peripheral nerve stimulator with 82{\%} peak chip efficiency," in *2018 IEEE Custom Integrated Circuits Conference (CICC)*, 2018, pp. 1–4.

[61] K. Suzumori, S. Endo, T. Kanda, N. Kato, and H. Suzuki, "A Bending Pneumatic Rubber Actuator Realizing Soft-bodied Manta Swimming Robot," in *Proceedings 2007 IEEE International Conference on Robotics and Automation*, 2007, pp. 4975–4980.

[62] T. Bujard, F. Giorgio-Serchi, and G. Weymouth, "A resonant squid-inspired robot unlocks biological propulsive efficiency," *Science Robotics*, vol. 6, no. 50, 2021. [Online]. Available: https://eprints.soton.ac.uk/446581/

[63] G. D. Weymouth, V. Subramaniam, and M. S. Triantafyllou, "Ultra-fast escape maneuver of an octopus-inspired robot," *Bioinspiration {\&} Biomimetics*, vol. 10, no. 1, p. 16016, 2015. [Online]. Available: https://doi.org/10.1088/1748-3190/10/1/016016

[64] L. Cen and A. Erturk, "Fish-Like Self Propulsion Using Flexible Piezoelectric Composites," *Volume 2: Mechanics and Behavior of Active Materials; Integrated System Design and Implementation; Bio-Inspired Materials and Systems; Energy Harvesting*, 2012.

[65] C. Christianson, N. N. Goldberg, D. D. Deheyn, S. Cai, and M. T. Tolley, "Translucent soft robots driven by frameless fluid electrode dielectric elastomer actuators," *Science Robotics*, vol. 3, no. 17, p. eaat1893, 2018. [Online]. Available: https://www.science.org/doi/abs/10.1126/scirobotics.aat1893

[66] G. Li, X. Chen, F. Zhou, and et al, "Self-powered soft robot in the Mariana Trench," *Nature*, vol. 591, no. 7848, pp. 66–71, 2021. [Online]. Available: https://doi.org/10.1038/s41586-020-03153-z

[67] A. Zhu, J. Song, Y. Li, M. Wu, and X. Zhang, "Small Cluster Underwater Robot design with Variable Pitch Propeller," in *2018 15th International Conference on Ubiquitous Robots (UR)*, 2018, pp. 235–240.

[68] S. Imai, H. Mizoguchi, and E. Inagakii, "Proposition of new control method of Eel-like swimming robot for swimming in narrow water ways," in *2008 10th International Conference on Control, Automation, Robotics and Vision*, 2008, pp. 681–684.

[69] T. Paschal, J. Shintake, S. Mintchev, and D. Floreano, "Development of bio-inspired underwater robot with adaptive morphology capable of multiple swimming modes," in *2017 IEEE/RSJ International Conference on Intelligent Robots and Systems (IROS)*, 2017, pp. 4197–4202.

[70] G. Picardi, M. Chellapurath, S. Iacoponi, S. Stefanni, C. Laschi, and M. Calisti, "Bioinspired underwater legged robot for seabed exploration with low environmental disturbance," *Science Robotics*, vol. 5, no. 42, p. eaaz1012, 2020. [Online]. Available: https://www.science.org/doi/abs/10.1126/scirobotics.aaz1012

[71] Forestry Sciences Laboratory, "Fish Length and Swim Speeds." [Online]. Available: http://www.fsl.orst.edu/geowater/FX3/help/9 _Fish Performance/ Fish Length and Swim Speeds.htm

[72] C. Cano-Barbacil, J. Radinger, M. Argudo, F. Rubio-Gracia, A. Vila-Gispert, and E. Garc´ıa-Berthou, "Key factors explaining critical swimming speed in freshwater fish: a review and statistical analysis for Iberian species," 2020. [Online]. Available: https://doi.org/10.1038/s41598-020-75974-x

[73] J. Zhu, C. White, D. K. Wainwright, V. Di Santo, G. V. Lauder, and H. Bart-Smith, "Tuna robotics: A high-frequency experimental platform exploring the performance space of swimming fishes," *Science Robotics*, vol. 4, no. 34, 2019.

[74] K. L. Ekinci, Y. T. Yang, and M. L. Roukes, "Ultimate limits to inertial mass sensing based upon nanoelectromechanical systems," *Journal of Applied Physics*, vol. 95, p. 2682, 2004. [Online]. Available: https://doi.org/10.1063/1.1642738

[75] M. S. Hanay, S. Kelber, A. K. Naik, D. Chi, S. Hentz, E. C. Bullard, E. Colinet, L. Duraffourg, and M. L. Roukes, "Single-protein nanomechanical mass spectrometry in real time," *Nature Nanotechnology 2012 7:9*, vol. 7, no. 9, pp. 602–608, 8 2012. [Online]. Available: https://www.nature.com/articles/nnano.2012.119

[76] A. K. Naik, M. S. Hanay, W. K. Hiebert, X. L. Feng, and M. L. Roukes, "Towards single-molecule nanomechanical mass spectrometry," *Nature Nanotechnology 2009 4:7*, vol. 4, no. 7, pp. 445–450, 6 2009. [Online]. Available: https://www.nature.com/articles/nnano.2009.152

[77] Y. T. Yang, C. Callegari, X. L. Feng, K. L. Ekinci, and M. L. Roukes, "Zeptogram-Scale Nanomechanical Mass Sensing," *Nano Letters*, vol. 6, no. 4, pp. 583–586, 4 2006. [Online]. Available: https://pubs.acs.org/doi/full/10.1021/nl052134m

[78] Thermo Fisher Scientific, "Overview of Mass Spectrometry." [Online]. Available: https://www.thermofisher.com/us/en/home/life-science/protein-biology/ protein-biology-learning-center/protein-biology-resource-library/pierce-protein-methods/overview-mass-spectrometry.html

[79] J. L. Arlett, E. B. Myers, and M. L. Roukes, "Comparative advantages of mechanical biosensors," *Nature Nanotechnology 2011 6:4*, vol. 6, no. 4, pp. 203–215, 3 2011. [Online]. Available: https://www.nature.com/articles/nnano.2011.44

[80] M. Mansooor and et al, "An SOI CMOS-Based Multi-Sensor MEMS Chip for Fluidic Applications," *Sensors*, vol. 16, p. 1608, 2016.

[81] D. W. Allen, M. Jones, L. Mccue, C. Woolsey, and W. B. Moore, "Europa: Exploration of Under-Ice Regions with Ocean Profiling Agents," Virginia Polytechnic Institute and State University, Tech. Rep., 7 2013. [Online]. Available: https://www.nasa.gov/sites/default/files/atoms/files/niac _2012 phasei mccue europa tagged.pdf

[82] DigiKey, "TMP35FT9." [Online]. Available: https://www.digikey.com/en/products/detail/analog-devices-inc/TMP35FT9/12127000

[83] ——, "TMP12FP." [Online]. Available: https://www.digikey.com/en/products/detail/analog-devices-inc/TMP12FP/12127447

[84] ——, "AD590KRZ-RL." [Online]. Available: https://www.digikey.com/en/products/detail/analog-devices-inc/AD590KRZ-RL/994559

[85] ——, "BNO055." [Online]. Available: https://www.digikey.com/en/products/detail/bosch-sensortec/BNO055/6136301

[86] ——, "LSM9DS1." [Online]. Available: https://www.digikey.com/en/products/detail/stmicroelectronics/LSM9DS1TR

[87] ArduCam, "PZT Camera Specifications." [Online]. Available: https://www.arducam.com/docs/cameras-for-raspberry-pi/ptz-camera/specification/

[88] Z. P. Tech, "pH Sensors." [Online]. Available: https://www.zimmerpeacocktech.com/products/electrochemical-sensors/ph-sensor/

[89] Sensorex, "pH1400 Light Duty Glass pH Electrode." [Online]. Available: https://sensorex.com/product/ph1400-general-use-glass-ph-probe/

[90] PASCO, "PASPORT Salinity Sensor PS-2195." [Online]. Available: https://www.pasco.com/products/sensors/pasport/ps-2195

[91] TE.com, "89-05KA-0U 5K PSIA Media Isolated mV Output Pressure Sensors." [Online]. Available: https://www.te.com/usa-en/product-89-05KA-0U.datasheet.pdf

[92] R. T. Wood, A. Bannazadeh, N. Q. Nguyen, and L. G. Bushnell, "A salinity sensor for long-term data collection in estuary studies," in *OCEANS 2010 MTS/IEEE SEATTLE*. IEEE, 9 2010, pp. 1–6. [Online]. Available: http://ieeexplore.ieee.org/document/5664602/

[93] C. Sonar, "Doppler Velocity Log (DVL-75)." [Online]. Available: https://ceruleansonar.com/products/dvl-75

[94] C. M. Jha, G. Bahl, R. Melamud, S. A. Chandorkar, M. A. Hopcroft, B. Kim, M. Agarwal, J. Salvia, H. Mehta, and T. W. Kenny, "Cmos-Compatible Dual-Resonator MEMS Temperature Sensor with Milli-Degree Accuracy," in *TRANSDUCERS 2007 - 2007 International Solid-State Sensors, Actuators and Microsystems Conference*. IEEE, 2007, pp. 229–232. [Online]. Available: http://ieeexplore.ieee.org/document/4300111/

[95] M. Shamsul Arefin, M. Bulut Coskun, T. Alan, A. Neild, J.-M. Redoute, and M. R. Yuce, "A MEMS capacitive pH sensor for high acidic and basic solutions," in *IEEE SENSORS 2014 Proceedings*. IEEE, 11 2014, pp. 1792–1794. [Online]. Available: https://ieeexplore.ieee.org/document/6985373

[96] A. R. Hendrix, T. A. Hurford, L. M. Barge, M. T. Bland, J. S. Bowman, W. Brinckerhoff, B. J. Buratti, M. L. Cable, J. Castillo-Rogez, and G. C. Collins, "The NASA Roadmap to Ocean Worlds," *Astrobiology*, vol. 19, no. 1, pp. 1–27, 2019.

[97] M. G. Kivelson, K. K. Khurana, C. T. Russell, M. Volwerk, R. J. Walker, and C. Zimmer, "Galileo magnetometer measurements: A stronger case for a subsurface ocean at Europa," *Science*, vol. 289, no. 5483, pp. 1340–1343, 2000, iSBN: 0036-8075 Publisher: American Association for the Advancement of Science.

[98] X. Jia, M. G. Kivelson, K. K. Khurana, and W. S. Kurth, "Evidence of a plume on Europa from Galileo magnetic and plasma wave signatures," *Nature Astronomy*, vol. 2, no. 6, pp. 459–464, Jun. 2018. [Online]. Available: https://www.nature.com/articles/s41550-018-0450-z

[99] K. P. Hand, C. F. Chyba, J. C. Priscu, R. W. Carlson, and K. H. Nealson, "Astrobiology and the Potential for Life on Europa," in *Europa*, ser. The University of Arizona space science series, R. T. Pappalardo, W. B. McKinnon, and K. Khurana, Eds. Tucson: University of Arizona Press, 2009, p. p. 589.

[100] S. M. Howell and R. T. Pappalardo, "Band Formation and Ocean-Surface Interaction on Europa and Ganymede," *Geophysical Research Letters*, vol. 0, no. 0, 2018. [Online]. Available: https://agupubs.onlinelibrary.wiley.com/doi/abs/10.1029/2018GL077594

[101] S. A. Kattenhorn and L. M. Prockter, "Evidence for subduction in the ice shell of Europa," *Nature Geosci*, vol. 7, pp. 762–767, 2014.

[102] T. A. Cwik, M. W. Smith, J.-P. Fleurial, K. Zacny, and D. P. Winebrenner, "A Cryobot for Melting, Cutting and Water-jetting through the Icy Crust of Ocean Worlds." AGU, Dec. 2019. [Online]. Available: https://agu.confex.com/agu/fm19/meetingapp.cgi/Paper/550565

[103] J.-P. Fleurial, S. Howell, D. Woerner, D. Landau, J. Gayle, M. Smith, J. Mueller, T. Hendricks, S. Roberts, and B. Nesmith, "Notional Concept of Operations and System Capability Definition for Enabling Scientific Ocean Access Missions on Icy Worlds," *EPSC*, vol. 2019, pp. EPSC–DPS2019, 2019.

[104] B. G. Clement, J.-P. Fleurial, S. M. Howell, T. J. Hendricks, E. Klonicki, and D. Woerner, "Planetary Protection for accessing the oceans of icy satellites," in *AGU Fall Meeting 2019*. AGU, 2019.

[105] E. Klonicki, B. G. Clement, R. Kidd, M. Gonzalez, J.-P. Fleurial, D. Woerner, T. J. Hendricks, and S. M. Howell, "Evaluation and Integration of Potential Instruments for Subsurface Ocean Worlds Missions," *AGUFM*, vol. 2019, pp. P51B–05, 2019.

[106] S. D. Vance, L. M. Barge, S. S. S. Cardoso, and J. H. E. Cartwright, "Self-Assembling Ice Membranes on Europa: Brinicle Properties, Field Examples, and Possible Energetic Systems in Icy Ocean Worlds." [Online]. Available: www.liebertpub.com

[107] Woods Hole Oceanographic Institution, "Conductivity, Temperature, Depth (CTD) Sensors ." [Online]. Available: https://www.whoi.edu/what-we-do/explore/instruments/instruments-sensors-samplers/conductivity-temperature-depth-ctd-sensors/

[108] WaterLinked, "WaterLinked – DVL A50 & A125." [Online]. Available: https://www.waterlinked.com/dvl

[109] J. N. Newman and K. (Firm), *Marine Hydrodynamics*. MIT Press, 1977. [Online]. Available: https://books.google.com/books?id=nj-k%5ClAmaBYC

[110] S. F. Hoerner, *Fluid-Dynamic Drag*, 1965.

[111] Maxon Motors, "ECX SPEED 8M," 2021. [Online]. Available: https://www.maxongroup.us/medias/sys master/root/8882127142942/EN-21-186.pdf

[112] "Perseverance Rover Brains." [Online]. Available: https://mars.nasa.gov/mars2020/spacecraft/rover/brains/

[113] Xilinx, "Touchdown! NASA's Perseverance Rover Lands on Mars with Xilinx FPGAs On Board," 2021. [Online]. Available: https://www.xilinx.com/about/blogs/xilinx-xclusive-blog/2021/rover-lands-on-mars-with-xilinx-fpgas-on-board.html

[114] A. Moreno, F. Maksimovic, L. Lee, B. Kilberg, C. Schindler, H. Gomez, D. Teal, D. Acker-James, A. Fearing, K. Pister, B. Sensor, A. Center, J. S. Rentmeister, and J. Stauth, "Single-Chip micro-Mote for Microrobotic Platforms," 2019.

[115] R. Surampudi, J. Elliott, J. Blosiu, K. Bugga, P. Beauchamp, and J. Cutts, "Advanced Energy Storage Technologies for Future NASA Planetary Science Mission Concepts," NASA Jet Propulsion Laboratory, Tech. Rep., 2018. [Online]. Available: https://www.lpi.usra.edu/opag/meetings/feb2018/presentations/Surampudi.pdf

[116] E. Sahraei, J. Meier, and T. Wierzbicki, "Characterizing and modeling mechanical properties and onset of short circuit for three types of lithium-ion pouch cells," *Journal of Power Sources*, vol. 247, pp. 503–516, 2 2014. [Online]. Available: http://dx.doi.org/10.1016/j.jpowsour.2013.08.056https://linkinghub.elsevier.com/retrieve/pii/S0378775313014043

[117] Linden Photonics, "2021 Cable Catalog (Fiber Optic, Hybrid, Copper)," 2021. [Online]. Available: http://www.lindenphotonics.com/documents/ Linden-Catalog2021.pdf

[118] R. Feistel and E. Hagen, "On the GIBBS thermodynamic potential of seawater," *Progress in Oceanography*, vol. 36, no. 4, pp. 249–327, 1 1995. [Online]. Available: https://linkinghub.elsevier.com/retrieve/pii/0079661196000018

[119] J. W. P. Schmelzer, E. D. Zanotto, and V. M. Fokin, "Pressure dependence of viscosity," *The Journal of Chemical Physics*, vol. 122, no. 7, p. 074511, 2 2005. [Online]. Available: http://aip.scitation.org/doi/10.1063/1.1851510

[120] Engineered Syntactic Systems, "Microsphere Syntactic Foam." [Online]. Available: www.esyntactic.com

[121] B. N. Biswas, S. Chatterjee, S. P. Mukherjee, and S. Pal, "A discussion on Euler method: a review," *Electronic Journal of Mathematical Analysis and Applications*, vol. 1, no. 2, pp. 2090–2792, 2013.

[122] C. W. Reynolds, "Flocks, herds and schools: A distributed behavioral model," in *Proceedings of the 14th annual conference on Computer graphics and interactive techniques*, 1987, pp. 25–34.

[123] M. Brambilla, E. Ferrante, M. Birattari, and M. Dorigo, "Swarm robotics: a review from the swarm engineering perspective," *Swarm Intelligence*, vol. 7, no. 1, pp. 1–41, 2013.

[124] R. Olfati-Saber, "Flocking for multi-agent dynamic systems: Algorithms and theory," *IEEE Transactions on automatic control*, vol. 51, no. 3, pp. 401–420, 2006.

[125] T. Vicsek, A. Czirok, E. Ben-Jacob, I. Cohen, and O. Shochet, "Novel type of phase transition in a system of self-driven particles,"′ *Physical review letters*, vol. 75, no. 6, p. 1226, 1995.

[126] J. Toner and Y. Tu, "Flocks, herds, and schools: A quantitative theory of flocking," *Physical review E*, vol. 58, no. 4, p. 4828, 1998.

[127] D. Helbing, I. Farkas, and T. Vicsek, "Simulating dynamical features of escape panic," *Nature*, vol. 407, no. 6803, pp. 487–490, 2000.

[128] Q. Du, V. Faber, and M. Gunzburger, "Centroidal Voronoi tessellations: Applications and algorithms," *SIAM review*, vol. 41, no. 4, pp. 637–676, 1999.

[129] J. Cortes, S. Martinez, T. Karatas, and F. Bullo, "Coverage control for mobile sensing networks," *IEEE Transactions on robotics and Automation*, vol. 20, no. 2, pp. 243–255, 2004.

[130] S. Lloyd, "Least squares quantization in PCM," *IEEE transactions on information theory*, vol. 28, no. 2, pp. 129–137, 1982.

[131] M. Santos, S. Mayya, G. Notomista, and M. Egerstedt, "Decentralized minimum-energy coverage control for time-varying density functions," in *2019 International Symposium on Multi-Robot and Multi-Agent Systems (MRS)*. IEEE, 2019, pp. 155–161.

[132] S. G. Lee, Y. Diaz-Mercado, and M. Egerstedt, "Multirobot control using time-varying density functions," *IEEE Transactions on Robotics*, vol. 31, no. 2, pp. 489–493, 2015.

[133] B. Pang, Y. Song, C. Zhang, H. Wang, and R. Yang, "A swarm robotic exploration strategy based on an improved random walk method," *Journal of Robotics*, vol. 2019, 2019.

[134] B. B. Mandelbrot and B. B. Mandelbrot, *The fractal geometry of nature*. WH freeman New York, 1982, vol. 1.

[135] T. Itami, "Brownian Motion Applied to Macroscopic Group Robots Without Mutual Communication," in *Recent Advances in Natural Computing*. Springer, 2016, pp. 51–70.

[136] I. A. Wagner, M. Lindenbaum, and A. M. Bruckstein, "Robotic exploration, brownian motion and electrical resistance," in *International Workshop on Randomization and Approximation Techniques in Computer Science*. Springer, 1998, pp. 116–130.

[137] H. Hakl\i and H. U\uguz, "A novel particle swarm optimization algorithm with Levy flight," *Applied Soft Computing*, vol. 23, pp. 333–345, 2014.

[138] R. Fujisawa and S. Dobata, "Levy walk enhances efficiency of group foraging in pheromone-communicating swarm robots," in´ *Proceedings of the 2013 IEEE/SICE International Symposium on System Integration*. IEEE, 2013, pp. 808–813.

[139] A. Schroeder, S. Ramakrishnan, M. Kumar, and B. Trease, "Efficient spatial coverage by a robot swarm based on an ant foraging model and the Levy´ distribution," *Swarm Intelligence*, vol. 11, no. 1, pp. 39–69, 2017.

[140] D. K. Sutantyo, S. Kernbach, P. Levi, and V. A. Nepomnyashchikh, "Multi-robot searching algorithm using Levy flight and artificial potential field,"´ in *2010 IEEE Safety Security and Rescue Robotics*. IEEE, 2010, pp. 1–6.

[141] R. Fujisawa, S. Dobata, K. Sugawara, and F. Matsuno, "Designing pheromone communication in swarm robotics: Group foraging behavior mediated by chemical substance," *Swarm Intelligence*, vol. 8, no. 3, pp. 227–246, 2014.

[142] K.-K. Oh, M.-C. Park, and H.-S. Ahn, "A survey of multi-agent formation control," *Automatica*, vol. 53, pp. 424–440, 2015.

[143] M. Egerstedt and X. Hu, "Formation constrained multi-agent control," *IEEE transactions on robotics and automation*, vol. 17, no. 6, pp. 947–951, 2001.

[144] B. D. O. Anderson, C. Yu, B. Fidan, and J. M. Hendrickx, "Rigid graph control architectures for autonomous formations," *IEEE Control Systems Magazine*, vol. 28, no. 6, pp. 48–63, 2008.

[145] M. Mesbahi and M. Egerstedt, *Graph theoretic methods in multiagent networks*. Princeton University Press, 2010.

[146] RCJuice, "HobbyStar 2435 4-Pole Brushless Motor." [Online]. Available: https://www.rcjuice.com/motor-esc/brushless-car-motors/small-scale-other/hobbystar-2435-4-pole-sensorless-brushless-motor-waterproof.html

[147] F. Berlinger, M. Saadat, H. Haj-Hariri, G. V. Lauder, and R. Nagpal, "Fish-like three-dimensional swimming with an autonomous, multi-fin, and biomimetic robot," *Bioinspiration & Biomimetics*, vol. 16, no. 2, p. 026018, 3 2021. [Online]. Available: https://doi.org/10.1088/1748-3190/abd013https://iopscience.iop.org/article/10.1088/1748-3190/abd013

[148] Sensortech, "Sensortech – Products." [Online]. Available: https://sensortechcanada.com/products/

[149] D. Seo, "Neural Dust: Ultrasonic Biological Interface," Ph.D. dissertation, University of California, Berkeley, Berkeley, 12 2018. [Online]. Available: http://www2.eecs.berkeley.edu/Pubs/TechRpts/2018/EECS-2018-146.html

BIBLIOGRAPHIES

Ethan W. Schaler, Ph.D. (NASA JPL) Dr. Ethan Schaler is a member of the Robotic Actuation and Sensing group, within the Mobility and Robotic Systems section at NASA JPL, where he supports both research and flight tasks. As a Robotic Systems Engineer on the Mars 2020 project, he currently supports tactical and strategic sampling operations of the Perseverance rover's robotic arm and sample caching subsystem on Mars. Previously, he has performed planning, commissioning, testing (V&V), and analysis of the rover's Robotic Arm and integrated force / torque sensor. As a researcher, he has also supported multiple DARPA and DOD research tasks, involving construction of legged robots, flexible grippers, and more.

He is an expert in designing unique meso-scale robotic systems – particularly those that integrate flexible structures, actuators, adhesives, and sensors. He manufactures these systems using a combination of macro-scale (3D printing, machining, etching) and micro-scale techniques (deposition, micromachining).

Dr. Schaler received a B.S. in Mechanical Engineering from the University of Maryland, College Park in 2011, an M.Phil. in Micro- / Nano-Technology Enterprise from the University of Cambridge in 2012, and a Ph.D. in Electrical Engineering from the University of California, Berkeley in 2018. He has previously been awarded a Churchill Scholarship, Goldwater Scholarship, NSF GRFP Fellowship, and NDSEG Fellowship. Dr. Schaler is a 2-time NIAC fellow.

Azadeh Ansari, Ph.D. (Georgia Institute of Technology) Dr. Azadeh Ansari received the B.S. degree in Electrical Engineering from Sharif University of Technology, Iran in 2010. She earned the M.S and Ph.D. degrees in Electrical Engineering from University of Michigan, Ann Arbor in 2013 and 2016 respectively, focusing upon III-V semiconductor and MEMS devices and microsystems for RF applications. Prior to joining the ECE faculty at Georgia Tech, she was a postdoctoral scholar in the Physics Department at Caltech from 2016 to 2017.

Dr. Ansari is the recipient of a 2017 ProQuest Distinguished Dissertation Award from the University of Michigan for her research on "Gallium Nitride integrated microsystems for RF applications." She received the University of Michigan Richard and Eleanor Towner Prize for outstanding Ph.D. research in 2016. She is a member of IEEE, IEEE Sensor's young professional committee and serves as a technical program committee member of IEEE IFCS 2018.

Samuel Howell, Ph.D. (NASA JPL) Dr. Samuel Howell is an Ocean Worlds Scientist in the Planetary Interiors and Geophysics Group at JPL. He primarily works on constraining geologic processes on Ocean Worlds and the connection from their icy surfaces to interiors. Additionally, he supports the Europa Clipper mission as a Project Staff Scientist, and is the Deputy Principle Investigator and Lead Scientist for JPL's PRIME, a technology concept to explore the interior oceans of Ocean Worlds.

Dr. Howell obtained his B.S. in Engineering Physics from the Rose-Hulman Institute of Technology in 2010, with a concentration in Mechanical Engineering and minor in Thermal Fluid Mechanics. He obtained his M.S. and PhD in Geology and Geophysics University of Hawai'i at Manoa in 2013 and 2017, respectively, where he explored planetary-scale process through studies of local surface features. His research on Earth, the first-discovered Ocean World, focused on the simple understanding that observable features are fingerprints of the planetary processes at depth: failure, flow, melting, mixing, and material transport. Samuel's graduate research garnered national attention, including a 2016 Popular Mechanics Breakthrough Award for innovation detecting and predicting motions on the San Andreas Fault.

Samuel's current and proposed research concerns the mechanisms and timescales of ocean world material mixing and evolution, as well as the exchange of materials between interior oceans and outer ice shells. His recent research linking tectonic processes on Europa and Ganymede to the surface exposure of fossilized ocean material received NASA-wide coverage and the 2017 JPL Outstanding Postdoctoral Research Award in Planetary Science and Astrobiology.

Hyeong Jae Lee, Ph.D. (NASA JPL) Dr. Hyeong Jae Lee is a member of the technical staff in the Jet Propulsion Laboratory's Electroactive Technologies Group. He has over 10 years' experience related to piezoelectric technologies, including the piezoelectric material developments and applications, such as energy harvesting, acoustic energy/power transfer, acoustic mass sensors, ultrasonic drilling, ultrasonic motors, acoustic communications, structural health monitoring system and ice elastic wave analyzer. He is specifically an expert in the piezoelectric material development that can withstand extremely harsh environmental conditions. He designs and performs modeling of piezoelectric systems, materials selection for extreme dynamic loads, as well as developing tools and sampling system.

Prior to joining JPL, he has worked on the development of piezoelectric transducers, including high frequency ¿20kHz relaxor-PT single crystal piezocomposites for medical imaging, and high power ultrasonic transducers for underwater sonar transducers during his Ph.D degree. He currently holds 4 U.S. patents related to piezoelectric technologies.

Dr. Lee received a B.S., M.S., and Ph.D. in Materials Science and Engineering from Pennsylvania State University in 2007, 2010, and 2012, respectively.

Miles Smith, Ph.D. (NASA JPL) Dr. Miles Smith has played a critical role in the development of several planetary mission concepts, including serving as the Surface Phase Lead for the Europa Lander mission and the Project Manager for PRIME, a concept to access the Europan Ocean using a thermal ice probe. He brings an understanding of the driving constraints for accommodating the SWIM technology into an ice probe and the overall mission architecture.

Dr. Smith received a B.S. in Physics from Monash University in 1992, an M.S. in Applied Mathematics from the University of Cambridge in 1994, an M.S. and Ph.D. in Physics from the University of Washington in 1997 and 2002, respectively. He is the recipient of the JPL Voyager and Mariner awards, a Breakthrough Prize in Physics and numerous other NASA / JPL awards for mission formulation, development, and operation.

Luis Phillipe Tosi, Ph.D. (NASA JPL) Dr. Phillipe Tosi is a mechanical and aerospace engineer working in the extreme environment robotics group at JPL. He obtained his masters and PhD from Caltech in 2015 and 2018, respectively, where his dissertation work focused on fluid-structure interaction instabilities, particularly for the design of robust flow energy harvesters. Phillipe graduated with a Bachelor's in mechanical and aerospace engineering in 2009 and masters in aerospace in 2010, both from Cornell University.

His work focused on the design of a passive attitude control system for a satellite-on-a-chip. Phillipe worked for Chevron Corporation from 2010-2018 as a Completions Engineer and Project Manager, and as a Research Engineer while pursing his PhD. His family moved to the US from Brazil in 1998, where he still tries to spend most of the year-end holidays.

Adarsh Rajguru, (NASA JPL) Mr. Adarsh Rajguru is a mechanical and aerospace engineer working in the Architecture and Formulation Group within the Mechanical Systems Engineering Section at JPL. He obtained his M.S. in Astronautical Engineering from the University of Southern California. He has participated in a variety of robotic exploration concept formulation studies, including for asteroid mappers / hoppers, and ocean worlds cryobot probes, and led research tasks on radioisotope thermo-photovoltaic power systems.